Fall 12-20-2019

Towards a Unified Disease Mechanism for tRNA Synthetase-Mediated Peripheral Neuropathy

Emily L. Spaulding
The Jackson Laboratory, elspaulding@gmail.com

TOWARDS A UNIFIED DISEASE MECHANISM FOR TRNA SYNTHETASE-MEDIATED PERIPHERAL NEUROPATHY

By

Emily Louisa Spaulding

B.S. Gordon College, 2005

M.Ed. Gordon College, 2010

A DISSERTATION

Submitted in Partial Fulfillment of the

Requirements for the Degree of

Doctor of Philosophy

(in Biomedical Sciences)

The Graduate School

The University of Maine

December 2019

Advisory Committee:

Robert Burgess, Professor of Biomedical Science, Advisor

Susan Ackerman, Professor of Cellular and Molecular Medicine

Gregory Cox, Associate Professor of Biomedical Science

Sandra Rieger, Associate Professor of Biology

Roger Sher, Research Associate Professor of Neurobiology

TOWARDS A UNIFIED DISEASE MECHANISM FOR TRNA SYNTHETASE-MEDIATED PERIPHERAL NEUROPATHY

By Emily Louisa Spaulding

Dissertation Advisor: Dr. Robert Burgess

An Abstract of the Dissertation Presented
in Partial Fulfillment of the Requirements for the
Degree of Doctor of Philosophy
(in Biomedical Science)
December 2019

Charcot-Marie-Tooth disease (CMT) is a debilitating inherited peripheral neuropathy resulting in progressive distal muscle atrophy and loss of sensation. CMT is genetically heterogeneous, with mutations in over 80 different genes leading to demyelinating or axonal forms. There are genetically similar subgroups, including the largest protein family implicated in the disease, the tRNA synthetases (ARSs). ARSs are responsible for aminoacylation of tRNAs during translation and are therefore ubiquitously expressed and essential proteins. Dominant mutations in at least five ARSs cause axonal forms of CMT. How mutations in ARSs cause CMT is unclear, however, the similar clinical presentation of patients suggests shared disease mechanisms. To investigate peripheral axon sensitivity to dominant mutations in ARSs, we first performed an extensive examination of motor axon terminals in two mouse models of CMT type 2D, caused by mutations in glycyl-ARS (*GARS*). Our findings reveal a progressive, presynaptic dysfunction at the mutant neuromuscular junction that correlates with fewer acetylcholine vesicles, release sites, and mitochondria. One of the proposed disease mechanisms of mutant ARSs is through gain-of-function impairments in translation. Because all ARSs participate in translation, impairment in this process is an attractive disease mechanism to test in mammalian models of ARS-associated CMT. To this end we have profiled translation and transcription in motor neurons of three CMT2D mouse models. This profiling has revealed global impairments in translation in mutant *Gars* motor neurons. Identification of the integrated stress response

(ISR) only in the largest motor and sensory peripheral neurons has further refined our understanding of the cell type-specificity of CMT2D. Activation of the ISR occurs in these cells through the translational homeostasis-sensing kinase, GCN2, indicating that GCN2 is responding to impairments in translation. Genetic removal of GCN2 alleviates mutant *Gars* neuropathy, suggesting that chronic activation of the ISR contributes to CMT2D. The ISR is also activated in motor neurons of mice with dominant mutations in *Yars*, a model of CMT type C. These data support impairments in translation as a disease mechanism in mice with dominant mutations in *Gars* and *Yars* and have increased our understanding of the cellular and molecular pathways leading to motor axon degeneration.

ACKNOWLEDGEMENTS

I would like to sincerely thank Dr. Robert Burgess, my advisor, for welcoming me into his laboratory and providing unfailing support and guidance throughout my doctoral research. I would also like to thank the members of my thesis committee including Drs. Greg Cox, Susan Ackerman, Sandra Rieger, and Roger Sher for their participation in my training and valuable scientific advice. I would like to thank current and past members of the Burgess lab for their friendship and scientific support, including Drs. Kevin Seburn, Andrew Garrett, Abby Tadenev, Kathy Morelli, and Tim Hines, as well as Kate Miers. The Graduate School of Biomedical Science and Engineering at the University of Maine, especially former head Dr. David Neivandt and administrative assistant Tammy Crosby for always putting what is in the best interest of the students first. The Jackson Laboratory for the excellent training environment, especially Dr. Carrie Cowan and members of the scientific services. Finally, I would like to thank my parents, Danny and Katherine Allen, and my husband, Jeff Spaulding, for providing encouragement and support throughout my graduate career.

TABLE OF CONTENTS

LIST OF TABLES

LIST OF FIGURES

LIST OF ABBREVIATIONS
(in order of appearance)

Chapter 1

CMT	Charcot-Marie-Tooth disease
ARS	aminoacyl tRNA synthetase
mRNA	messenger RNA
tRNA	transfer RNA
Glu-Pro-ARS	glutamyl-prolyl tRNA synthetase
GARS	glycyl tRNA synthetase
KARS	lysyl tRNA synthetase
AARS	alanyl tRNA synthetase
ANKRD16	ankyrin repeat domain 16
eEF1A	eukaryotic elongation factor 1A
ARS2	mitochondrial tRNA synthetase
DARS2	mitochondrial aspartyl tRNA synthetase
EARS2	mitochondrial glutamyl tRNA synthetase
AARS2	mitochondrial alanyl tRNA synthetase
HARS	histidyl tRNA synthetase
DI-CMTC	Dominant-Intermediate CMT type C
WARS	tryptophanyl tRNA synthetase
MARS	methionyl tRNA synthetase
Nrp1	neuropillin 1
VEGF	vascular endothelial growth factor
Trk	tropomyosin receptor kinase
HDAC6	histone deacetylase 6
TRIM28	tripartite motif containing 28

ER	endoplasmic reticulum
BDNF	brain derived neurotrophic factor
rRNA	ribosomal RNA
miR	micro RNA
COXIV	cytochrome c oxidase IV
SCG	Superior cervical ganglia
NMNAT2	Nucleotide adeylyltransferase 2
SMN1	spinal muscular atrophy 1
TRAP	translating ribosome affinity purification
RPL22	ribosomal protein 22
RGC	retinal ganglion cells
GO	gene ontology
NMJ	neuromuscular junction
CMT2D	Charcot-Marie-Tooth disease type 2D
FUNCAT	fluorescent non-canonical amino acid tagging
IPA	Ingenuity Pathway Analysis
ISR	integrated stress response
GCN2	general control nonderepressible 2
tRNA-gly	tRNA-glycine

Chapter 2

LAL	levator auris longus
MEPC	miniature endplate current
EPC	end plate current
3,4-DAP	3,4- diaminopyridine
MFN2	mitofusin 2

Chapter 3

ATF4	activating transcription factor 4
ANL	azidonorleucine
ChAT	choline acetyltransferase
Chodl	chondrolectin
Nefh	neurofilament heavy chain
Nefm	neurofilament medium chain
Nefl	neurofilament light chain
GFAP	glial fibrillary acid protein
Mog	myelin oligodendrocyte protein
Mag	myelin associated protein
Sprr1a	small proline-rich repeat protein 1A
Atf3	activating transcription factor 3
Npy	neuropeptide tyrosine
Fgf21	fibroblast growth factor 21
Gdf15	growth differentiation factor 15
Amd2	adrenomedullin 2
Cdsn	corneodesmosin
B4galnt2	Beta-1,4-N-Acetyl-Galactosaminyltransferase 2
Err3	estrogen related receptor 3
Prph	peripherin
Pvalb	parvalbumin
PKR	protein kinase R
PERK	PKR-like endoplasmic reticulum kinase
HRI	heme-regulated inhibitor
APP/PS1	amyloid precursor protein/presinilin 1

Gtpbp2	GTP binding protein 2

Chapter 4

mTOR	mammalian target of rapamycin
mTORC1	mammalian target of rapamycin complex 1
4E-BP1	eukaryotic initiation factor 4E-binding protein 1
eIF4E	eukaryotic initiation factor 4E
eIF4G	eukaryotic initiation factor 4G
S6K1	S6 kinase 1
AD	Alzheimer's disease
eIF2	eukaryotic initiation factor 2
eIF2B	eukaryotic initiation factor 2B
GDP	guanosine diphosphate
GTP	guanosine triphosphate
Met	Methionine
uORF	upstream open reading frame
UTR	untranslated region
ORF	open reading frame
CHOP	C/EBP homologous protein
PP1	protein phosphatase I
GADD34	growth arrest and DNA-damage inducible protein
CReP	constitutive repressor of eIF2α phosphorylation
5XFAD	5X familial Alzheimer's disease
eEF1A	eukaryotic elongation factor 1A
CNS	central nervous system
tRNA-arg	tRNA-arginine

ZNF598	E3 ubiquitin-protein ligase ZNF598
Dom34	duplication of multilocus region
Hbs1	Hsp70 subfamily B suppressor
ABCE1	ATP-binding cassette, sub-family E
Rli1	RNase L inhibitor
Ltn1	listerin
Nemf	nuclear export mediator factor
Cdc48	cell division cycle 48
SPR	surface plasmon resonance
ICV	intracerebroventricular
BONCAT	biorthogonal non-canonical amino acid-tagging
ATAC	assay for transposable accessible chromatin
qPCR	quantitative polymerase chain reaction
AAV9	adeno-associated virus 9

CHAPTER 1

TRNA SYNTHETASE-MEDIATED PERIPHERAL NEUROPATHY

Introduction

Peripheral neuropathy impacts an estimated 1 in 5 adults in the United States, and can be the result of an inherited mutation, exposure to neurotoxic agents, or another primary disease. All forms cause the specific degeneration of peripheral axons. Both the wide array of causes and the technical challenge of studying this unique cell compartment *in vivo* contribute to the lack of a cure. Among the many types of peripheral neuropathies, Charcot-Marie-Tooth (CMT) is the most common inherited form (Saporta and Shy 2013a; Skre 1974a). While CMT is genetically heterogeneous, dominant mutations in at least five aminoacyl tRNA synthetases (ARSs) have been firmly linked to the disease (Antonellis and Green 2008). The first report of the involvement of an ARS in CMT came as a surprise to the field (Antonellis et al. 2003b). How could mutations in a ubiquitously expressed housekeeping gene cause such a cell type-specific disease? As the list of ARSs implicated in CMT grew, an additional question surfaced; do all forms of ARS-mediated peripheral neuropathy share a common disease mechanism? For almost the past two decades the search for a unified disease mechanism that helps to explain the extreme tissue specificity of the disease has been a major goal of the field. Gene therapy approaches to treat this group of dominantly-inherited CMTs show great promise. However, determining how ARSs cause disease will broaden the therapeutic landscape for patients and allow for a better understanding of the basic biology of ARSs and their role in peripheral neuron health.

Biology of Aminoacyl tRNA Synthetases

Canonical Role of tRNA Synthetases in Translation

The delicate balance of cellular homeostasis depends on the correct expression of the genetic code as a complex repertoire of protein. Many factors influence the fidelity of translation, the process of decoding mRNA into protein. Among these factors are the ARSs,

essential enzymes that charge tRNA molecules with amino acids. The aminoacylation reaction is carried out in two steps: (1) ARSs bind to their respective amino acid and ATP to catalyze the formation of an enzyme-bound aminoacyl-adenylate, and (2) the aminoacyl-adenylate then reacts with the correct tRNA. In both human and mouse cells there are 19 members of the ARS family, each responsible for one of the 20 amino acids, with the exception of the bifunctional Glutamyl-Prolyl-ARS (GLU-PRO-ARS). Two separate ARSs are usually used for cytosolic and mitochondrial translation, except for glcyl-ARS (GARS) and lysyl-ARS (KARS), which are dual-localized. Most ARSs contain catalytic and anticodon binding domains, and a number of ARSs contain additional domains for dimerization, editing, or other unknown functions. Based on the architecture of the catalytic domain and the mechanism of tRNA binding and activation, ARSs are equally divided into class I and class II enzymes (Eriani et al. 1990; Ribas de Pouplana and Schimmel 2001).

The importance of ARS functional accuracy cannot be overstated; misacylation of tRNAs will result in a faulty proteome. Thus, mistakes made by ARSs are just as detrimental to cellular homeostasis as a mutation at the DNA level. An accurate aminoacylation reaction depends on recognition of the correct amino acid and the correct tRNA by the ARS. The tertiary structure of some, but not all, ARSs limits the incorrect binding of larger amino acids through steric hindrance. However, occasional misincorporations of smaller amino acids or of those that are structurally similar to the cognate amino acid do occur, in which case ARSs have to rely on mechanisms other than steric exclusion. These mechanisms together form the “triple sieve” of proofreading, and involve the ARS active site, separate editing domains, and free-standing “trans” proteins. Half of all ARSs possess direct editing abilities that are divided into two forms: (1) pre-transfer editing occurs at the active site when the incorrect aminoacyl adenylate produced in the first part of the reaction is removed, and (2) post-transfer editing involves hydrolysis of misacylated tRNA at a separate editing domain. Some class II ARSs also employ the help of *trans* editing factors which catalyze the post-transfer hydrolysis of misacylated tRNA

after its release from the ARS (Perona and Gruic-Sovulj 2014). The importance of the editing abilities of ARSs in maintaining a stable cellular proteome is evident in mice that contain a defective editing domain in alanyl-ARS (AARS). In these mice, mutant AARS has reduced ability to edit misincorporated serine, resulting in accumulation of misfolded proteins, activation of the unfolded protein response, and degeneration of Purkinje neurons (Lee et al. 2006). Accumulation of misfolded proteins and neurodegeneration is alleviated by an editing co-factor, ANKRD16, which binds directly to the catalytic domain of AARS and captures misactivated serine. Intriguingly, low levels of ANKRD16 expression in Purkinje cells speaks to the cell type-specificity of neurodegeneration due to mutations in *Aars*, a ubiquitously expressed gene (Vo et al. 2018). This provides a compelling example of how expression levels of genes that work in parallel to the gene with the neurodegenerative-associated mutation can modulate the severity and tissue specificity of phenotypes.

Similar to amino acid binding to the ARS, accurate and efficient tRNA binding is also crucial. At physiological pH, the association of ARSs with tRNAs is much weaker than most protein-DNA interactions, with dissociation constants several orders of magnitude larger. This feature of the ARS-tRNA physical interaction allows for the rapid turnover of the aminoacylation reaction which feeds the translational burden of a cell (Schimmel and Soll 1979). Therefore, equally important as the accurate creation of the aminoacylated tRNA is its timely release from the ARS. Upon release from the ARS, proper shuttling of the aminoacylated tRNA to the ribosome by translation elongation factors is also a key step in maintaining the required speed of translation. In fact, evidence suggests that the movements of tRNA occur not through diffusion, but rather by a “processive mechanism,” meaning the tRNA is directly transferred from one translation component to the next in a highly regulated manner. Early evidence suggested that tRNAs never freely diffuse throughout mammalian cells and are always bound to components of the translation machinery under normal physiological conditions (Negrutskii and Deutscher 1992; Stapulionis and Deutscher 1995). This “tRNA cycle” includes (1) association with the

ARS, (2) direct handoff to the translation elongation factor eEF1A, (3) transfer from eEF1A to the ribosome, and finally (4) release from the ribosome and a renewed association with the ARS (Mirande 2010). The constant supervision of tRNA molecules by translation factors strongly suggests that the efficient cycling of tRNA is critical to translational homeostasis.

Non-canonical Functions of tRNA Synthetases

In light of their fundamental role in protein synthesis, the finding that most ARSs have novel and essential functions in higher organisms came as a surprise to the field. These functions are spread throughout the cytoplasm and nucleus, and even extend beyond the boundary of the cell. Some of the earliest suggestions of a role for ARSs beyond aminoacylation came from work in bacteria and lower eukaryotes. This work revealed that some ARSs are involved in regulating their own transcription and translation. For example, mRNA sequences of ARSs can encode short sequences that fold to mimic their cognate tRNAs. When the ARS protein is in excess, binding of this tRNA mimic blocks translation of the full ARS mRNA, thereby limiting its expression within the cell (Ryckelynck, Giege, and Frugier 2005). At the transcriptional level, *E. coli* AARS binds to its own gene promotor and represses its expression (Putney and Schimmel 1981).

In members of the animal kingdom, the evolution of new domains of ARSs have greatly expanded the possibility of non-translational functions. Early in the structural analysis of higher eukaryotic ARSs, it was found that in addition to the catalytic core of the enzyme were regions completely dispensable to the aminoacylation reaction. This suggested that ARSs might have other roles within cells that are unrelated to the canonical aminoacylation function (Schimmel 1987). Indeed, a plethora of biological functions have now been assigned to some ARSs including (1) glucose and amino acid metabolism, (2) tissue and organ development, (3) control of angiogenesis, (4) inflammation, (5) tumorigenesis, and (6) regulation of the immune response. Proteolysis or alternative splicing of ARSs can also create truncated protein

fragments that lack aminoacylation activity but are endowed with novel biological functions (Guo and Schimmel 2013).

The early finding that at least 7 tRNA synthetase enzymes formed a very specific multisynthetase complex (MSC) in two different rabbit and sheep tissues strongly suggested biological relevance, perhaps relating to translation or denoting a completely novel function (Mirande et al. 1982; Kellermann et al. 1982). It is now known that in higher eukaryotes 9 ARSs and 3 scaffold proteins comprise this large complex. The complex is thought to facilitate efficient translation, but other unknown functions are quite possible, especially because the 3 MSC scaffold proteins participate in diverse, non-translational biological processes (Guo and Schimmel 2013).

tRNA Synthetases and Human Neurological Disease

Recessive Loss of Function Mutations Cause Multi-Systemic Syndromes

Autosomal recessive mutations in cytosolic (*ARS*) and mitochondrial tRNA synthetases (*ARS2*) presumably impair translation, and cause a broad range of syndromes. Recessive loss of function mutations in every single *ARS2* gene have been linked to human disease, and cause phenotypes that are often severe and most prominent in tissues with high metabolic demand. For example, virtually all of these mutations result in central nervous system dysfunction, with the most common clinical presentation being leukoencephalopathy with brainstem and spinal cord or thalamus involvement due to mutations in mt-aspartyl-ARS (*DARS2)* and mt-glutamyl-ARS (*EARS2)*. In contrast, mt-alanyl-ARS (*AARS2)* mutations either cause neurological problems with late onset ovarian failure or infantile mitochondrial cardiomyopathy. These diseases present with a large degree of clinical heterogeneity and may also include developmental delays (Boczonadi, Jennings, and Horvath 2018).

Recessive mutations in 16 cytoplasmic *ARSs* cause human disease and affect an even broader range of organ systems than mutations in *ARS2* genes. Symptoms are extremely variable even among mutations within a single *ARS* gene, but can include microcephaly,

epileptic encephalopathy, hearing loss, developmental delay, liver dysfunction, or lung disease (Boczonadi, Jennings, and Horvath 2018). Despite the ubiquitous nature of ARSs and the universal need for protein synthesis, some tissues are uniquely sensitive to mutations in specific ARSs. For example, retinitis pigmentosa is only found in patients with bi-allelic *histidyl-ARS* (*HARS)* mutations (Puffenberger et al. 2012). Likely, some of the tissue specificity of mutations can be attributed to the many tissue-specific, non-translational functions of cytosolic ARSs.

Patients with recessive ARS-associated disease are usually homozygous for missense mutations, compound heterozygous for missense mutations, or compound heterozygous for one missense mutation and one null allele. Based on work in mice, homozygosity for null alleles would be incompatible with life (Seburn et al. 2006). There is strong evidence that recessive *ARS* mutations that cause human disease work through a loss-of-function mechanism. For example, ARS protein levels are decreased and/or the mutant enzyme shows significant decrease in enzymatic activity. In addition, studies in zebrafish and *C. elegans* demonstrate that knocking down the *ARS* gene recapitulates hallmark phenotypes of the human disorders (Meyer-Schuman and Antonellis 2017).

Dominant Mutations in a Subset of tRNA Synthetases Cause Peripheral Neuropathy

The first human disease linked to an ARS was the neurodegenerative condition, Charcot-Marie-Tooth disease (CMT). Dominant mutations in *GARS* were found to cause the length-dependent degeneration of peripheral motor and sensory axons, resulting in patient weakness, motor impairment, and sensory loss (Antonellis et al. 2003b). CMT can be divided into two classes: the demyelinating type 1, in which a gene mutation affects the integrity of the myelin sheath surrounding peripheral axons, or the axonal type 2, in which the mutation affects the health of the peripheral axon directly. All ARS-associated forms of CMT fall into the type 2 axonal class (or are considered an intermediate form), indicating a special sensitivity of motor and sensory axons to dominant mutations in *ARS* genes. Despite the genetic heterogeneity of CMT as a whole, the ARS protein family is the largest implicated in the disease. Dominant

mutations in at least five different ARSs cause CMT. Because patients with these mutations present with similar clinical symptoms, shared disease mechanisms are thought to be likely (Wei, Zhang, and Yang 2019).

Glycyl tRNA-synthetase (GARS).

At least 19 dominant mutations in *GARS* have been associated with CMT type 2D (CMT2D). These mutations are spread across every domain of the protein. The majority are found in the class II catalytic domain, but others are located in the anticodon binding domain and in the metazoan-specific helix-turn-helix WHEP domain of unknown function. GARS is the only bifunctional tRNA-synthetase associated with CMT (Wei, Zhang, and Yang 2019).

Tyrosyl tRNA-synthetase (YARS).

YARS is a class I aaRS with evolutionarily conserved catalytic and anticodon binding domains and a C-terminal EMAP-II-like-domain first found in insects. 5 dominant mutations have been linked to Dominant-Intermediate CMT type C (DI-CMTC), which contains features of both demyelinating and axonal forms. All 5 mutations are found in the catalytic domain of the protein (Wei, Zhang, and Yang 2019).

Histidyl tRNA-synthetase (HARS).

Similar to GARS, the HARS enzyme contains a class II catalytic domain, an anticodon binding domain, and the WHEP domain. Thus far, 8 different dominant mutations are associated with CMT type 2W (CMT2W) and all are located in the catalytic domain of the protein (Wei, Zhang, and Yang 2019).

Tryptophanyl tRNA-synthetase (WARS).

WARS has an N-terminal WHEP domain, a class I catalytic domain, and an anticodon binding domain. Only one mutation, located in the catalytic domain, has been reported in CMT patients, but it has been found in multiple families with a clear inheritance pattern (Wei, Zhang, and Yang 2019).

Alanyl tRNA-synthetase (AARS).

AARS is a structurally unique cytoplasmic tRNA synthetase in that it has not acquired any new domains during evolution. It also stands out among the other CMT-associated ARS in that it lacks an anticodon binding domain but has an editing domain and a special C terminal domain. In total, 9 mutations in *AARS* are linked to CMT type 2N (CMT2N), with the majority in the catalytic domain, but a few in the editing domain and the C terminal domain (Wei, Zhang, and Yang 2019).

Methionyl tRNA-synthetase (MARS).

MARS contains a class I catalytic domain, an anticodon binding domain, an N-terminal domain to anchor it to the MSC, and a WHEP domain. MARS is unique among the other CMT-linked ARSs both in participating in the MSC and in not forming a dimer. 3 mutations all found in the anticodon binding domain have been linked to CMT type 2U (CMT2U), but are currently lacking enough human genetic evidence to unequivocally classify them as CMT-causing (Wei, Zhang, and Yang 2019).

Animal Models of tRNA Synthetase-Mediated Peripheral Neuropathy

The first mammalian model of an ARS-associated CMT arose from a spontaneous mutation in the mouse *Gars* gene at The Jackson Laboratory (P278KY). These mice display several characteristics of human CMT2D, including overt muscle weakness and atrophy, reduced nerve conduction velocity, motor and sensory axon loss, and synaptic dysfunction (Seburn et al. 2006; Spaulding et al. 2016). The second mouse model of CMT2D was a product of a mutagen-induced mutation (C201R), which results in a similar but milder phenotype compared to P278KY (Achilli et al. 2009a). The third model of CMT2D includes a 12 base pair deletion introduced into exon 8 of the *Gars* gene, as found in a human patient (deltaETAQ) (Morelli et al., submitted). These mice present with similar phenotypes as compared to P278KY and C201R, with a severity falling in the middle of the spectrum.

D. melanogaster has been another successful experimental system in which to study ARS-associated CMT, largely through the forced expression of mutant forms of human GARS and YARS enzymes. This expression causes overt motor deficits, neuronal dysfunction, and axon degeneration (Niehues et al. 2015; Ermanoska et al. 2014). *C. elegans* has been used to demonstrate the dominant toxicity of mutations in *HARS*. Transgenic overexpression of mutant *C. elegans hars-1* in a cell type equivalent to motor neurons causes severe morphological phenotypes (Vester et al. 2013). Finally, zebrafish have been used for the demonstration of genetic causation of *AARS* mutations found in three families with features of a dominant axonal form of CMT. Injection of mRNAs of three different AARS mutants, but not wild-type AARS, resulted in neuronal abnormalities in fish (Weterman et al. 2018).

Potential Disease Mechanisms of Dominant Mutations in tRNA Synthetases

Loss of Function or Gain of Function?

When dominant mutations in *ARSs* were first linked to CMT, an obvious disease mechanism to test was loss of aminoacylation function. However, human disease phenotypes, mouse genetics, and fly experiments strongly suggest that loss of aminoacylation activity is not the cause of CMT neuropathy. A few years after GARS was implicated in CMT2D, it became clear that homozygous recessive or bi-allelic mutations in *ARS* or *ARS2* genes caused severe multi-system syndromes in humans. Although some of these syndromes included peripheral neuropathy, only dominant mutations in *ARS* genes cause pure axonal CMT.

Just as bi-allelic mutations were first being associated with a different type of human disease, genetic experiments in mice began to suggest that neuropathy was caused by a toxic gain of function mechanism. Mice with a heterozygous gene trap allele in the *Gars* gene show mRNA expression levels around 50% of wild-type. These mice showed no signs of peripheral neuropathy, suggesting that a heterozygous loss of function allele would not be sufficient to cause CMT (Seburn et al. 2006). If CMT2D neuropathy was caused by a heterozygous loss of function mutation, overexpression of wild-type *GARS* should improve the phenotype. In

contrast, if neuropathy is caused by a toxic gain of function, increasing wild-type GARS levels would not improve the phenotype. Consistent with the second possibility, ubiquitous overexpression of wild-type GARS at levels resulting in a greater than 10-fold increase in aminoacylation activity failed to rescue neuropathy in two different mutant *Gars* mouse models (Motley et al. 2011b).

Lack of viability of homozygous *Gars* mutants suggests some impairments in aminoacylation activity *in vivo*. Interestingly, overexpression of wild-type GARS on homozygous backgrounds fully rescued viability, but resulted in a much more severe neuropathy. These results indicate that the transgene is effective at restoring aminoacylation to the mutant protein and at the same time, show that increased dosage of the mutant protein leads to greater toxicity in peripheral motor and sensory neurons (Motley et al. 2011b).

Overexpression of human forms of mutant *GARS* (with wild-type *drosophila-Gars* present at normal levels) is inherently toxic to motor neurons in flies, as demonstrated by impaired performance on a negative geotaxis climbing assay and cell morphology defects. Dose-dependent motor neuron toxicity was observed with overexpression in motor neurons, just as was observed in mouse models. Interestingly, ubiquitous overexpression of mutant *GARS* results in developmental lethality in flies, suggesting that mutant GARS proteins can become toxic to cell types other than peripheral neurons when present at high enough levels. All human mutant forms of GARS tested were found to have normal subcellular localization, and aminoacylation activity was not diminished in any of the mutant lines (Niehues et al. 2015). Taken together, evidence from humans, mice, and flies strongly suggest that CMT2D neuropathy is not caused by loss of aminoacylation activity, but rather by an unknown toxic gain of function of mutant forms of GARS.

Aberrant Protein-Protein Interactions

Hydrogen-deuterium exchange and small-angle X-ray scattering have demonstrated that several human *GARS* and *YARS* mutations, as well as the mouse P278KY, result in a

conformational change in the proteins (He et al. 2011; Blocquel et al. 2017; He et al. 2015). Protein domains normally buried in the wild-type enzyme become open to the surface, potentially available for aberrant binding to other proteins. In support of this, several interactions between mutant GARS and YARS and other proteins important to peripheral axon health seem to contribute to CMT phenotypes.

Neuropilin 1 (Nrp1) is a cell-surface receptor that binds to various signaling proteins, including the semaphorins and vascular endothelial growth factor (VEGF). Several human mutant forms of GARS, and the mouse P278KY and C201R mutants, all bind to Nrp1, whereas wild-type does not. Mutant GARS competes with VEGF-A for Nrp1 binding, and is proposed to result in motor axon degeneration through attenuation of this signaling pathway (He et al. 2015; Sleigh, Gomez-Martin, et al. 2017). Heterozygous removal of Nrp1 from P278KY mice worsens neuropathy, and overexpression of VEGF-A results in a mild improvement in motor performance. Effects of VEGF-A on neuromuscular junction innervation, nerve conduction velocity, or axon number/size are not reported. However, at least one human mutant form of GARS (deltaETAQ) that causes a severe form of CMT2D, has very low levels of Nrp1 binding (Morelli et al., submitted). In addition, disruption of VEGF signaling is known to affect vascular development, but mouse CMT2D tissues including the muscle, retina, sciatic nerve, and hindbrain show no defects in blood vessel number or morphology (Sleigh, Gomez-Martin, et al. 2017; Fantin et al. 2014). There is also no evidence linking aberrant VEGF-A signaling to sensory neuron degeneration, which is a component of neuropathy in mouse models and some patients. Thus, although aberrant GARS-Nrp1 interactions may contribute to motor neuropathy in some animal models and patients, this mechanism is unlikely to be the major cause of CMT2D neuropathy.

Tropomyosin receptor kinase (Trk) receptors, essential for sensory neuron development, have also been shown to aberrantly interact with some human mutant forms of GARS *in vitro*. Both P278KY and C201R mouse models have perturbed sensory neuron differentiation, with a

smaller proportion of large-fiber sensory neurons in dorsal root ganglia and a corresponding greater proportion of small-fiber neurons. C201R mice show altered performance on several sensory tests, supporting the abnormalities in sensory subtypes (Sleigh, Dawes, et al. 2017). Sensory neuron identity may be altered at birth in CMT2D mice, but in the severe P278KY model, sensory axon degeneration occurs well after birth. Thus, there must be additional disease mechanisms at play long after development of sensory neurons is complete. Interestingly, motor neuron fate is not disturbed in CMT2D mice. Motor neurons are arguably the primary cell type affected in CMT2D patients and undergo the most severe degeneration. This work demonstrates that altered peripheral neuron fate underlies some sensory components of CMT2D neuropathy, but is unlikely to play a major role in disease progression, especially of motor phenotypes.

Histone deacetylase 6 (HDAC6) has also been shown to interact with several human GARS mutants. One of the main targets of HDAC6 is α-tubulin, a component of microtubules and essential for axonal transport. Binding of mutant GARS to HDAC6 is hypothesized to enhance its activity, resulting in decreased acetylation of α-tubulin and impaired transport. Indeed, cultured P278KY sensory axons show impaired transport, which is improved with the HDAC6 inhibitor, Tubastatin. *In vivo* administration of Tubastatin to P278KY mice slightly improves motor function, but effects on additional well-established measures of neuropathy are not reported (Mo et al. 2018). Because motor and sensory neurons have such a specialized morphology, with extremely long axon projections, it is easy to imagine how impaired axonal transport could result in axon degeneration. It is also easy to imagine that generally increasing axonal transport speed through HDAC6 inhibition could result in enhanced motor function, whether or not impairments in transport have a primary role in disease.

While most aberrant interactions have been studied in relation to mutant forms of GARS, mutant YARS has been shown to form aberrant interactions related to its seemingly non-

translational function within the nucleus. Three YARS mutants were found to form stronger interactions with the scaffolding protein, TRIM28, compared to wild-type. TRIM28 functions in a complex with HDAC1 to suppress acetylation and activity of transcription factors. Enhanced interaction with mutant YARS apparently leads to the overactivation of these transcription factors and broad transcriptional dysregulation (Blocquel et al. 2017).

Clearly, the structural effects of dominant mutations in *GARS* and *YARS* are relevant to CMT pathology, although it remains to be seen how structural changes in MARS, AARS, or WARS might relate to disease. So far, the aberrant ARS-protein interactions that have been reported are either cell type-, mutation-, or ARS-specific. Thus, although each of these interactions may be playing a role in some tissues or some patients, and in that way may help to explain phenotypic diversity, they are unlikely to represent the major underlying cause of CMT neuropathy. Because patients with ARS-linked CMT present similarly in the clinic, disease mechanisms shared by all patients, and perhaps even in all affected cell types, are thought to be likely. A disease mechanism that can universally explain the large number of ARSs involved, the progressive nature of the disease, and the shared sensitivity of both motor and sensory peripheral axons is needed.

Toxic Gain of Function Impairments in Translation

The one thing that all ARSs have in common is their participation in protein synthesis. Although loss of aminoacylation is not thought to be the cause of neuropathy, toxic gain of function impairments in translation could still be the root cause of disease. With this hypothesis, a study using *Drosophila* models of ARS-associated CMT set out to measure translation in relevant cell types. Expression of three different forms of human mutant GARS in motor and sensory neurons causes axon degeneration and significantly reduces translation rates, as measured by non-canonical amino acid-tagging. Defects in translation cannot be attributed to impaired aminoacylation or mislocalization of mutant GARS and cannot be rescued by overexpression of *Drosophila Gars*, supporting translational slowdown through a toxic gain-of-

function mechanism. In addition, genetically reducing translation in motor and sensory neurons is sufficient to cause similar neuropathy. Translation defects are not limited to peripheral neurons, as ubiquitous overexpression of mutant GARS also reduces global translation, as measured by ^{35}S-methionine incorporation. Finally, overexpression of human mutant YARS, which causes Dominant Intermediated CMT Type 2C (CMTDIC), also results in reduced translation in peripheral neurons. These results lend strong support to the possibility of a translation-related disease mechanism shared by at least two CMT-linked ARS mutants (Niehues et al. 2015). A comprehensive *in vivo* analysis of translation in the primary tissue affected by the disease, the mammalian peripheral neuron, would strengthen this hypothesis. Because CMT2D causes an axonal neuropathy, assessment of translation specifically in the axonal compartment is also relevant.

Accumulating Evidence for Axonal Translation in Neuronal Homeostasis

Toxic gain of function impairments in translation could be occurring everywhere in the peripheral neuron, or they could be specific to the axonal compartment. The largest and longest axons are primarily affected in human and animal models of ARS-mediated peripheral neuropathy, and specific impairments in axonal translation could explain this trend. The specialized structure of the largest peripheral neurons requires that homeostasis is sustained over the meter or more that may separate a cell body from its axonal terminus. Given this impressive distance and an axonal volume that is many times that of the cell body, how is such a compartment grown during development, re-grown after injury, and maintained throughout adulthood? While early answers to these questions focused on the local environment or the cell soma as supplying the needs of the axon, it is now well-established that the axon has some unique needs that can only be met from within. Decades of research have revealed local translation as an indispensable mechanism of axonal homeostasis during development and regeneration in both invertebrates and vertebrates. In contrast, the extent to which the adult,

mammalian axonal proteome is maintained through local translation remains unclear and controversial.

Somal Provision of the Axonal Proteome.

In the early twentieth century popular opinion stated that the axon drew the majority of its nutrients from the local environment. Classic experiments by Weiss and Hiscoe challenged this idea by providing observable evidence for the directed movement of material from the neuronal soma to the axon terminal (Weiss and Hiscoe 1948). Rat peripheral nerves were crushed, ligated, and allowed to regenerate. Within days, the axon segment just proximal to the ligation became swollen and enlarged. Upon removal of the ligation, the accumulated axoplasm moved from the soma to the axon, suggesting the presence of a dynamic communication system between the cell body and the axon and establishing the field of axonal transport.

Soon the idea that the neuronal soma supplied the axonal proteome prevailed. Radiolabeled amino acids systemically injected into rats were incorporated into new proteins in the soma and at the base of large dendrites within minutes of injection, but were observed in the axon hillock 1 day after injection, in the ventral root 2 days after injection, and 20mm down the sciatic nerve 16 days after injection (Droz and Leblond 1963). It was concluded that proteins are continuously synthesized in the cell body and at the base of large dendritic spines, and are subsequently transported into distal dendrites and axons. Although background from supporting cells would have made it difficult to observe low signals in axons, this evidence supported the idea that would dominate the field for the next several decades; translation does not occur in axons.

Axons Possess Translation Machinery.

Dendrites soon became an established site for local translation, supported by the presence of polyribosomes, mRNA, and the seminal finding that it is required for synaptic plasticity in the mammalian hippocampus (Steward and Levy 1982; Steward 1983; Caceres et al. 1988; Kang and Schuman 1996). Despite the biological importance of dendritic translation, the apparent absence of polyribosomes and rRNA in the axon still made the possibility of axonal translation

seem unlikely (Lasek, Dabrowski, and Nordlander 1973). Nevertheless, a series of *in vitro* metabolic labeling studies were carried out in goldfish, squid, and rabbit. These experiments established that proteins can be synthesized in invertebrate and vertebrate axons (Koenig 1967; Giuditta, Dettbarn, and Brzin 1968; Edstrom and Sjostrand 1969). Eventually, more sensitive techniques enabled the identification of rRNA, mRNA, and actively translating polysomes in squid giant axons (Giuditta, Cupello, and Lazzarini 1980; Giuditta, Hunt, and Santella 1986; Giuditta et al. 1991). In mammalian axons, ribosomes were identified at embryonic stages both in culture and *in vivo* (Tennyson 1970; Bunge 1973; Bassell et al. 1998). Polyribosomes were observed by electron microscopy in the axonal initial segment of mature mammalian central nervous system (CNS) neurons, although not in myelinated sections. Polyribosomes were tightly associated with synapses, suggesting that axonal translation may occur during times of extensive synaptic growth, such as development (Steward and Ribak 1986).

Electron microscopy failed to detect rough ER or golgi apparatus in vertebrate axons, raising the question of whether or not axons have the ability to process or secrete locally synthesized proteins (Tennyson 1970; Bunge 1973). However, the Twiss lab addressed this question using cultured rat sensory neurons. Their extensive studies have shown that (1) ER and golgi components needed for classical protein synthesis and secretion are present in the axon, (2) ER chaperone proteins can be axonally translated, and (3) axons can target locally synthesized proteins to the membrane (Willis et al. 2005; Merianda et al. 2009). This evidence strongly suggests that neurons can post-translationally modify and secrete axonally synthesized proteins, although the associated machinery may exist in very small quantities or adopt unique morphologies in the axon, perhaps explaining how the axon is able to maintain the energetic burden of translation machinery.

Axonal Translation Occurs During Nervous System Development.

Given that axonal ribosomes are present in embryonic axons and preferentially associated with synapses, many of the earliest studies in the field of axonal translation were related to its

role in neuronal development. Axonal mRNA localization was revealed as a general mechanism of protein sorting and proteome management in the developing axon (Jung, Yoon, and Holt 2012). In growing neurons, mRNA is sorted to neuronal processes in granules that also contain ribosomal subunits and translation factors (Knowles et al. 1996; Olink-Coux and Hollenbeck 1996). β-actin was among the first such mRNA species to be identified as enriched within growth cones and axonal processes of developing neurons, and the axonal synthesis of actin protein in embryonic neurons was established soon after (Bassell et al. 1998; Eng, Lund, and Campenot 1999).

It is now known that axonal translation is important for many aspects of neuronal development. Some neurotrophins can induce growth cones to turn toward their source in an actin-dependent manner (Zheng, Wan, and Poo 1996; Ming, Lohof, and Zheng 1997). The finding that β-actin mRNA is translated in the axon made this mechanism a good candidate for how axons can quickly and independently modulate the cytoskeleton for growth cone turning during development. Confirming this hypothesis, stimulation of either embryonic or adult neurons with neutrotrophins increases the transport of β-actin mRNA into the axon (Zhang, Singer, and Bassell 1999; Zhang et al. 2001; Willis et al. 2005). A directional gradient of netrin-1 induces translation of β-actin that directly precedes attractive growth cone turning (Leung et al. 2006). Repulsion is just as important as attraction for axonal pathfinding during development, and axonal translation contributes to this phenomenon as well. The guidance cue Semaphorin 3A results in axonal translation of RhoA mRNA and subsequent collapse of the growth cone, preventing the axon from innervating incorrect targets (Wu et al. 2005). Overall neuronal growth and size-sensing is also dependent upon mRNA localization and axonal translation. In growing sensory neurons importin β1 mRNA is anterogradely transported to the axon, where it associates with ribosomes. Perturbation of this localization by 3′ UTR knockout or by sequestration of the importin β1-ribonucleoprotein complex to the cell body results in significantly longer axons (Perry et al. 2016). Finally, axonal protein synthesis is essential for

localized BDNF-induced synaptic potentiation in developing neurons (Zhang and Poo 2002). Thus, axonal translation is a mechanism by which growing neurons correctly pathfind, innervate target tissues, sense their own size, and modulate synaptic strength during development.

Axonal Translation Occurs During Nervous System Regeneration.

Immunohistological studies eventually revealed that mature mammalian axons of the peripheral nervous system contain ribosomal proteins and rRNA, which are irregularly distributed and located close to the plasma membrane, possibly explaining the difficulty in identifying them (Koenig et al. 2000). The importance of axonal translation to neuronal growth during development and the identification of ribosomes in adult peripheral axons raised the possibility that axonal translation plays an additional role during peripheral nerve regeneration. Adult rat dorsal root ganglion (DRG) cells were shown to regenerate neuronal processes *in vitro* after *in vivo* axonal crush by regulating the translation of an existing pool of mRNAs (Twiss et al. 2000). Moreover, translation of these mRNAs within the axon itself is required for normal regeneration in vitro. *In vivo*, rat motor axons of the sciatic nerve isolated 7 days after a crush injury contain translation factors, ribosomal proteins, and rRNA (Zheng et al. 2001). Whether translation components originate from the neuron or from glial cells is still under question. Glia-to-axon transfer of proteins occurs in squid giant axons transected from their cell bodies (Lasek, Gainer, and Barker 1977). In perfused squid axons cell-to-cell transfer of RNA occurs upon stimulation of glial receptors by axonal neurotransmitters, indicating that signaling from active or injured axons can induce glial cells to provide axonal translation components (Eyman et al. 2007). In mammals, the *in vivo* transfer of ribosomal components from Schwann cells to peripheral axons after injury suggests the presence of a dynamic collaboration between these cell types during regeneration (Court et al. 2008; Court et al. 2011). Independent of the origin of translation machinery in uninjured axons, the glia-axon collaboration during injury conditions, along with increased aggregation of axonal ER components, suggests an increased capacity for

axonal translation, processing, and secretion of newly synthesized proteins during regeneration (Merianda et al. 2009; Court et al. 2011).

Conceptual Arguments for Axonal Translation in Neuronal Homeostasis.

One of the most common conceptual arguments for the role of axonal translation in neuronal maintenance centers around efficiency. Mature, mammalian neurons are the largest cells in the body and are highly compartmentalized. Transport of mRNA to distant locations within a neuron followed by local translation may be more efficient than transportation and storage of proteins. One mRNA molecule can be translated many times, allowing for communication with the use of fewer resources, fewer space restrictions, and less risk of aberrant protein accumulation. In addition, nascent proteins may provide opportunities for unique post-translational processing crucial to specific functions in the mature axonal compartment (Figures 1A,C) (Jung, Yoon, and Holt 2012; Perry and Fainzilber 2014).

Axonal translation could also confer molecular flexibility at individual synapses. This could be especially useful during periods of high synaptic activity, providing synapse-specific, “on demand” adaptations to the proteome. Replenishment of proteins used for neurotransmission may be needed at some synapses after intense use such as during motor activity or learning. An example of this is found in growing axons, in which the membrane-bound receptor DCC physically associates with translation machinery and mediates local protein synthesis upon stimulation with netrin (Tcherkezian et al. 2010). In this example, the availability of extracellular signals coupled with the expression of presynaptic membrane receptors provides translational control at the level of individual synapses (Figure 1B).

Local translation may help axons maintain a healthy supply of functional mitochondria. Mutations that affect either the function or transport of axonal mitochondria result in neurodegeneration (Schwarz 2013; Pease and Segal 2014). Nigrostriatal dopamine neurons have extensive axonal arbors, estimated to form up to 245,000 synapses (Matsuda et al. 2009; Bolam and Pissadaki 2012). Given that mitochondria are enriched at synapses, the cell body

may be unable to synthesize the complete nuclear mitochondrial proteome at a rate sufficient for an uninterrupted supply of axonal mitochondria (Court and Coleman 2012; Schwarz 2013). Proteins of the inner and outer mitochondrial membranes possess different turnover rates, thus, axonally translated mitochondrial proteins may also allow for finer control of mitochondrial replenishment (Beattie 1969). In support of axonal synthesis of nuclear encoded mitochondrial proteins, rat superior cervical ganglia (SCG) axons contain mRNA for several of these proteins and inhibition of axonal protein synthesis decreases mitochondrial membrane potential (Hillefors et al. 2007). SCG axons also contain the micro RNA (miR), miR-338, which is known to post-transcriptionally modulate the expression of cytochrome c oxidase IV (COXIV), a nuclear protein important to oxidative phosphorylation. Overexpression ofmiR-338 in the axon reduces COXIV protein levels, mitochondrial oxygen consumption, and axonal ATP levels (Figure 1D) (Aschrafi et al. 2008).

Finally, axonal translation may provide a local supply of essential axon survival factors. Neurotrophins are important regulators of axonal survival that rely on both transported and locally translated proteins to exert their protective effects. For example, stimulation of axons by neurotrophins coordinates transcription of the antiapoptotic gene *bcl-w* with transport of bcl-w mRNA to the axon and subsequent local translation (Cosker et al. 2013). Because the inhibition of axonal protein synthesis with cycloheximide abolishes the protective effects of neurotrophins, local synthesis of other axonal survival proteins is likely (Pazyra-Murphy et al. 2009; Pease and Segal 2014). A possible example is nicotinamide nucleotide adenylyltransferase 2 (NMNAT2), an essential axon survival factor with a half-life of only 4 h (Gilley and Coleman 2010). Even if NMNAT2 were transported by fast axonal transport, estimated to move cargo at a speed of 400 mm/day, the protein would only travel ~67 mm before 50 percent degradation (Hirokawa, Niwa, and Tanaka 2010). This would result in vanishingly low levels of NMNAT2 in the most distal axons in large mammals, including humans. Distinct neuronal types may require different balances of transported vs. locally translated NMNAT2 (Figure 1).

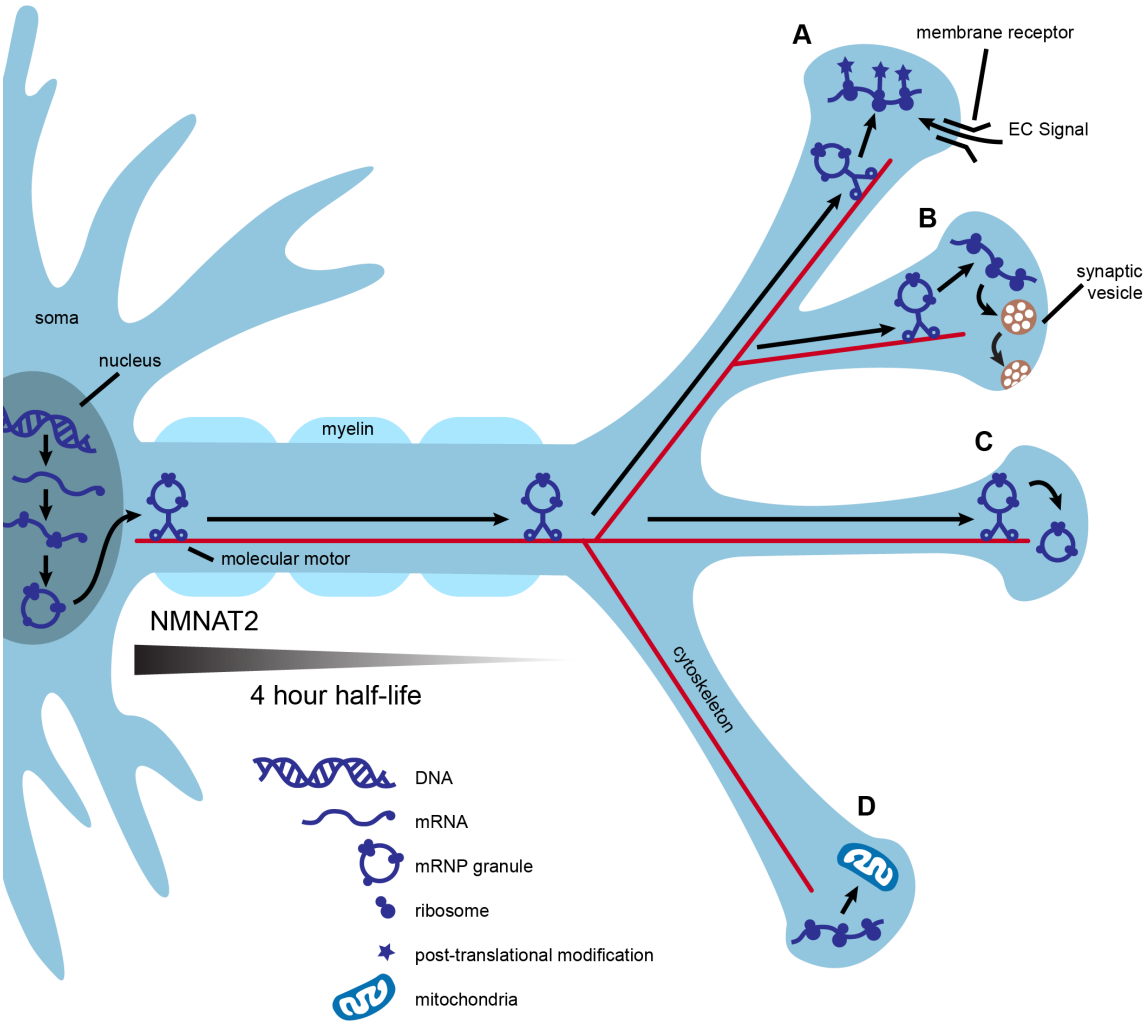

Figure 1: Conceptual Arguments for Axonal Translation in Neuronal Homeostasis
Local translation may contribute to axonal efficiency and compartmentalization. mRNA is transcribed in the nucleus, packaged into mRNP granules, and transported by multiple molecular motors down the axon. Granules are transported into some synapses and mRNA is immediately translated into polypeptides (A and B). Nascent polypeptides may present the opportunity for unique post-translational modification, as in synapse A, or may be used to fulfill specific activity-based needs of individual synapses, as in B. Local translation of some mRNAs may be controlled at the synaptic level by the interaction of local extracellular signals with membrane receptors (A). Alternatively, mRNP granules can be transported into synapses and stored for later use (C), or excluded from other synapses (D). Local translation of mitochondrial proteins could help to maintain a healthy supply of axonal mitochondria (D). Axonal survival factors may also be translated locally. For example, NMNAT2 has a half-life of 4 hours, and even if transported via fast axonal transport, would not make it to the most distance synapses before significant degradation.

Recent Evidence for Local Translation in Adult Mammalian Axons.

Despite these arguments, the physiological significance of axonal translation in nervous system maintenance remains ambiguous. Asymmetrical mRNA localization is a commonly utilized communication strategy for many types of mature polarized cells. (Xing and Bassell 2013). It is tempting to hypothesize that the longest axons *in vivo*, such as mature sensory and motor peripheral axons, may be the most reliant on mRNA transport and local translation for homeostasis. Mature sensory axons possess a complex repertoire of mRNA, and it is suspected that the microtubule stabilizing agent, Paclitaxel, causes sensory neuropathy at least in part by impairing axonal transport (Scripture, Figg, and Sparreboom 2006; Gumy et al. 2011). More direct evidence of neurodegeneration as a result of dysregulation of mRNA transport is found with mutations in the RNA binding protein, SMN1, which cause the severe motor neuron disease, spinal muscular atrophy (Wang et al. 2016). Mutations in at least five ARSs cause the specific degeneration of sensory and motor axons, supporting the idea that local translation of transported mRNA is crucial for axonal maintenance (Antonellis and Green 2008).

A challenge in establishing axonal translation in mature mammalian neurons is studying axons in isolation from their cell bodies and other supporting cell types in vivo. The genetic method, translating ribosome affinity purification (TRAP), now allows for axonally-derived populations of ribosomes and their associated RNA to be analyzed without fear of contamination from other cell types. Shigeoka, et al. used the RiboTag knockin mouse line, in which Cre-mediated recombination results in expression of a triple HA-tagged ribosomal protein, RPL22 (Sanz et al. 2009; Shigeoka et al. 2016). Ribosome-bound mRNAs in retinal ganglion cell (RGC) axons were isolated from their CNS targets in developing and adult mice. Comparison of cell somas in the retina to axons in the brain revealed distinct populations of ribosome-associated mRNAs in axons. Axons at all ages were enriched for the gene ontology (GO) terms “cellular metabolism” and “mitochondrial respiratory chain,” suggesting that mitochondrial proteins are indeed locally translated in developing and adult axons. Analysis of

developmental stages revealed that axonal translation is intimately associated with RGC circuit assembly. In contrast, adult axons are enriched for transcripts related to the maintenance of neurotransmission, including components of the trans-SNARE complex, glutamate receptors, and neurotrophin receptors. NMNAT2 transcript is associated with ribosomes in both developing and adult axons, but more highly enriched at the adult stage. Neurotrophin induced survival signals, including components of the CREB and STAT3 pathways, are also enriched in the adult axon. This study provides key evidence that axonal translation in adult RGCs supports metabolic function, neurotransmission, axon survival, and many other aspects of axonal homeostasis. Although additional work is needed to provide a complete picture of the physiological relevance of translation in adult mammalian axons *in vivo*, it is reasonable to hypothesize that disruption of the intricacies of axonal translation, in whatever capacity, could impair neuronal homeostasis and lead to neurodegeneration.

Moving Forward: Testing for Impairments in Translation in Mouse Models of GARS-Mediated Peripheral Neuropathy (Charcot-Marie-Tooth Disease Type 2D)

Despite the variety of disease mechanisms that have been proposed, how dominant mutations in *GARS* cause CMT2D still remains unclear. In light of the impairment in translation found in *Drosophila* models of CMT2D and CMTDIC, and because of the obvious connection between ARSs and protein synthesis, we viewed gain-of-function impairments in translation to be the strongest candidate as the cause of neuropathy and set out to test this in mammalian models of the diseases.

The clinical presentation of CMT2D patients combined with previous studies of mouse models of CMT2D first led us to investigate synaptic efficacy at the neuromuscular junction (NMJ) (Spaulding et al. 2016). Patients present with progressive distal muscle weakness that is consistent with synaptic impairment. We tested if abnormal synaptic transmission was a feature of neuromuscular junctions in two CMT2D mouse models. Our findings clearly indicate a presynaptic impairment defined by decreased quantal content that correlates with disease

severity and worsens with age. Although transmission machinery was intact in mutant NMJs and there was no single identifiable cause of impairment, a combination of smaller terminals with fewer acetylcholine vesicles and morphological fracturing of the nerve itself probably contribute to synaptic weakness. Intriguingly, our work also identified fewer mitochondria at mutant NMJs. This lack of mitochondria could be because of defects in axonal transport and/or because of a lack of biogenesis related to decreased axonal translation, either cytosolic or mitochondrial. Nevertheless, the clear functional and morphological defects found at mutant axon terminals caused us to hypothesize that specific impairments in axonal translation could be the cause of synaptic weakness and axon degeneration. Impaired axonal translation would also help to account for the cell type-specificity of the disease, as it could be easy to imagine that the largest and longest axons have the greatest dependence on local protein production.

To test the hypothesis of impaired axonal translation, an *in vivo* approach that afforded both cell type- and compartment-specific resolution was needed. We began by assessing translation and transcription in motor neuron cell bodies of two mouse models of CMT2D. *In vivo*, cell type-specific, fluorescent non-canonical amino acid-tagging (FUNCAT) revealed reduced translation in motor neuron cell bodies of mutant *Gars* mice. This early finding caused us to refine our hypothesis and predict impaired translation in the entire motor neuron.

To complement the protein analysis, i*n vivo* ribosome-tagging from mutant *Gars* motor neuron cell bodies was used to identify mRNAs undergoing translation. We found a distinct translation signature in mutant motor neurons that was reproducible among both *Gars* alleles. This signature was also present at the transcriptional level, indicating that it represents broad gene expression changes, and was present with the human mutation, $Gars^{delETAQ/+}$. Using RNAScope *in situ* hybridization, we show that activation of this gene expression signature occurs in alpha motor neurons and does not occur in any other cell types of the spinal cord. The signature is also upregulated in medium-large mechanosensitive and proprioceptive dorsal root ganglion sensory neurons. As a strong indicator of shared disease mechanisms between

CMT2D and CMTDIC, this signature is also upregulated in gamma motor neurons of mice with mutations in *Yars*.

Ingenuity Pathway Analsys (IPA) indicated that the signature was representative of the integrated stress response (ISR). The ISR can be activated by a variety of intrinsic or extrinsic cell stressors, and results in a global decrease in mRNA translation and the upregulation of specific stress response genes. Genetic experiments revealed that the ISR was activated through the protein kinase, GCN2, as its removal shut off expression of ISR genes. Removing GCN2 from mutant *Gars* mice also significantly alleviates neuropathy, resulting in increased body weight, improved grip strength, less denervation at the neuromuscular junction, less motor axon loss, and motor nerve function closer to wild-type mice. Thus, it is likely that some of the reduced translation seen with FUNCAT is a result of activation of the ISR, and removal of this chronic decrease in translation alleviates some, but not all, of the *Gars* phenotype.

Because GCN2 can be directly activated by stalled ribosomes, our data has led us to hypothesize that primary, toxic gain-of-function impairments in translation caused by mutant GARS result in ribosomes stalled at glycine codons (Ishimura et al. 2016; Inglis et al. 2019). In support of this hypothesis, genetic crosses between *Gars* mice and a known model of ribosome stalling result in an exacerbated phenotype (Ishimura et al. 2014). We hypothesize that stalled ribosomes activate GCN2 and the ISR, causing upregulation of the disease signature and decreased global translation. By preventing activation of the ISR and the associated translational slowdown, neuropathy is partially alleviated. We also hypothesize that the remainder of the phenotype is a result of the lingering primary impairment in translation caused by the mutant GARS protein.

We have previously shown that dietary supplementation of glycine does not alleviate *Gars* neuropathy. Besides ATP, the only other substrate of GARS is tRNA-gly, thus, we hypothesize that mutant GARS disrupts efficient cycling of tRNA-gly, and in this way impairs the translation process. This disruption could be because of an increased affinity of mutant GARS for tRNA-

gly, or because of sequestration of the tRNA chaperone protein, eEF1A, or a combination of both. In addition, tRNA-gly cycling impairments could be present in the axon as well as in the cell body, and in that way disrupt local translation at nerve terminals. Cell type-specificity of phenotypes could be a result of local translation defects in large axons and/or because of motor and sensory neuron-specific expression levels of genes directly related to the translation process, including *tRNA-gly*, *GARS*, ribosome recycling factors, or ISR components. Future work includes investigating these potential causes of cell type-specificity, testing for tRNA-gly sequestration, and continuing to strengthen the connection between this potential disease mechanism and other forms of ARS-associated peripheral neuropathy.

CHAPTER 2

SYNAPTIC DEFICITS AT NEUROMUSCULAR JUNCTIONS IN TWO MOUSE MODELS OF CHARCOT-MARIE-TOOTH TYPE 2D

Abstract

Patients with Charcot-Marie-Tooth Type 2D (CMT2D), caused by dominant mutations in Glycl tRNA synthetase (*GARS*), present with progressive weakness, consistently in the hands, but often in the feet also. Electromyography shows denervation, and patients often report that early symptoms include cramps brought on by cold or exertion. Based on reported clinical observations, and studies of mouse models of CMT2D, we sought to determine if weakened synaptic transmission at the neuromuscular junction (NMJ) is an aspect of CMT2D. Quantal analysis of NMJs in two different mouse models of CMT2D ($Gars^{P278KY}$, $Gars^{C201R}$), found synaptic deficits that correlated with disease severity and progressed with age. Results of voltage-clamp revealed presynaptic defects characterized by: 1) decreased frequency of spontaneous release without any change in quantal amplitude (MEPC), 2) reduced amplitude of evoked release (EPC) and quantal content, 3) age-dependent changes in the extent of depression in response to repetitive stimulation and, 4) release failures at some NMJs with higher frequency, longer duration stimulation. Although further work did not reveal a primary mechanism that fully accounts for the reduced quantal content, smaller mutant NMJs with correspondingly fewer vesicles and partial denervation that reduces release sites contribute to the reduction at a proportion of mutant NMJs. However, taken all together, the voltage-clamp data suggest other release processes, while essentially intact, are also likely operating sub-optimally at most NMJs. Drugs that modify synaptic efficacy were tested to see if neuromuscular performance improved. The presynaptic action of 3,4 diaminopyridine (3,4 DAP) was not beneficial, whereas postsynaptic-acting physostigmine did improve performance.

Introduction

Charcot-Marie-Tooth (CMT) disease was described more than a century ago (Charcot and Marie 1886; Tooth 1886.) and encompasses a large group of genetically and phenotypically heterogeneous diseases that affect the peripheral nerve at a worldwide frequency of at least 1/2500 (Skre 1974b). In this study we focus on CMT2D, which is a type 2 axonal CMT (Dyck 1975) caused by autosomal dominant mutations in Glycyl tRNA synthetase (*GARS*) (Antonellis et al. 2003a).

CMT2D patients present with a range of "classic" CMT2 symptoms that include slowly progressive, distal weakness with or without sensory abnormalities. The absence of sensory involvement may result in a diagnosis of distal spinal muscular atrophy type V, which is allelic to CMT2D (Rohkamm et al. 2007; Sivakumar et al. 2005; Antonellis et al. 2003a). Clinical reports on CMT2D and other type 2 CMT patients describe electrophysiological abnormalities including aberrant spontaneous muscle activity, reduced compound muscle action potentials (CMAP), and less commonly, decreased nerve conduction velocities (NCVs) (Saporta and Shy 2013b; Shen et al. 2011; Sivakumar et al. 2005). Some CMT2D patients report early symptoms that included cramping in hands and legs either in response to cold or upon exertion, and transient episodes of weakness and fatigue that slowly worsen with age (Sivakumar et al. 2005). These electrophysiological signatures and other symptoms of type 2 CMTs are typically attributed to axonal degeneration (Sivakumar et al. 2005) but, are also consistent with possible neuromuscular junction (NMJ) dysfunction and transmission failure. To our knowledge, this possibility has not been systematically investigated for type 2 axonal CMTs. If synaptic defects are indeed an unrecognized factor in type 2 CMTs, even as a secondary effect of axonal pathology, it would open a possible new treatment avenue for patients. For example, patients with NMJ defects due to congenital myasthenias, are effectively treated with drugs that

modulate synaptic efficacy (Engel et al. 2015) and if myasthenia-like deficits were a component of type 2 CMT, drugs to improve NMJ transmission could be considered.

The dominantly inherited mutations in Glycyl tRNA Synthetase (*GARS*)(Antonellis et al. 2003a) underlying CMT2D have been successfully modeled through mouse genetics, with the identification of dominant *Gars* alleles that recapitulate most aspects of CMT2D, including axon atrophy and loss, denervation, muscle weakness and consistently more severe symptoms in certain distal muscles than proximal ones (Achilli et al. 2009b; Motley et al. 2011a; Seburn et al. 2006). The severity of CMT2D varies widely among patients due, in part, to the specific *GARS* mutation that an individual carries (Antonellis et al. 2003a; Del Bo et al. 2006; Dubourg et al. 2006; James et al. 2006), and a similar correlation exists for different mutant alleles of *Gars* mice (Achilli et al. 2009b; Seburn et al. 2006; Sleigh et al. 2014). Here we focus on two mutant mouse strains, one referred to as $Gars^{P278KY}$, which develops a severe peripheral neuropathy (Seburn et al. 2006), and the second, $Gars^{C201R}$, which has a milder disease (Achilli et al. 2009b). Both mutant strains are weaker than age-matched wild-types and weakness correlates with disease severity. Differences in muscle strength between the mild and severely affected CMTD2 mice is partly explained by early axon loss (~30%) in the $Gars^{P278KY}$ mice that is not seen in the $Gars^{C201R}$ allele. However, motor axon number in $Gars^{P278KY}$ largely stabilizes after about five weeks of age, whereas there is no reduction in axon number in $Gars^{C201R}$ nerves (Achilli et al. 2009b; Seburn et al. 2006). Despite essentially stable axon counts, both alleles have a persistent, overt tremor that worsens gradually with age (Achilli et al. 2009b; Motley et al. 2011a; Seburn et al. 2006; Sleigh et al. 2014), which could be caused by unreliable neuromuscular transmission at innervated terminals. Consistent with this idea is the previous finding that $Gars^{P278KY}$ muscle showed a more marked decrement in an integrated electromyogram (EMG) during tetanic contraction than wild-type (Seburn et al. 2006). In addition, both *Gars* mutant strains show muscle atrophy and some degree of morphological

abnormality at the NMJ (Motley et al. 2011a; Seburn et al. 2006; Sleigh et al. 2014) that may be indicative of ongoing synaptic dysfunction, but it is currently unknown whether intact NMJs function normally in CMT2D, or any other type 2 axonal CMT.

Results

Proximal LAL Muscles in CMT2D Mice Show Prevalent NMJ Dysmorphology, But Most Terminals Retain Innervation

The proximal LAL muscle has not previously been examined in CMT2D mice, so prior to conducting voltage-clamp experiments we evaluated NMJ morphology and assessed innervation status. Compared to wild-type terminals (Figure 2 A,B) nearly all LAL terminals, in both *Gars*^{P278KY} (Figure 2C-I) and *Gars*^{C201R} (Figire 2 J-L) muscles, have evident dysmorphology that includes more diffuse postsynaptic staining with less distinct guttering as well as thinner axons and presynaptic nerves. As with other previously studied muscles NMJ dysmorphology varies with disease severity (severe *Gars*^{P278KY} > mild*Gars*^{C201R}) and can range from subtle, near normal looking NMJs to clearly fragmented junctions (compare Figure 2J vs. 2K). At low magnification an innervating presynaptic axon is evident at most NMJs in LAL muscles of even the more severely affected *Gars*^{P278KY} mice (Figure 2 C-E), but at higher magnification some of these junctions are found to be only partially innervated even in the mildly affected *Gars*^{C201R} mice (Figure 2 G-I,L). Indeed, the most striking difference in LAL NMJs between CMT2D alleles was the extent of partial denervation (Figure 2 F). In *Gars*^{P278KY} muscles from 2-month-old mice, more than half of the junctions were partially innervated, whereas in muscles of 4-month-old *Gars*^{C201R} mice only ~5% of NMJs had this status. There were also more than three times as many denervated junctions in the *Gars*^{P278KY} than in the *Gars*^{C201R} muscles (6.5 vs. 1.9%) even though the latter were 2 months older. Synaptic function is likely to be compromised at junctions that are not fully occupied by a presynaptic terminal if other processes cannot compensate. Our analysis of the LAL predicts that innervation status could contribute to observed changes in synaptic function at *Gars*^{P278KY} NMJs of 2-month-old mice where ~50% of

NMJs are incompletely innervated. In contrast, because ~95% of NMJs in the *Gars*^{C201R} LAL are fully innervated, even at 4 months, functional changes would be independent of innervation status at most NMJs.

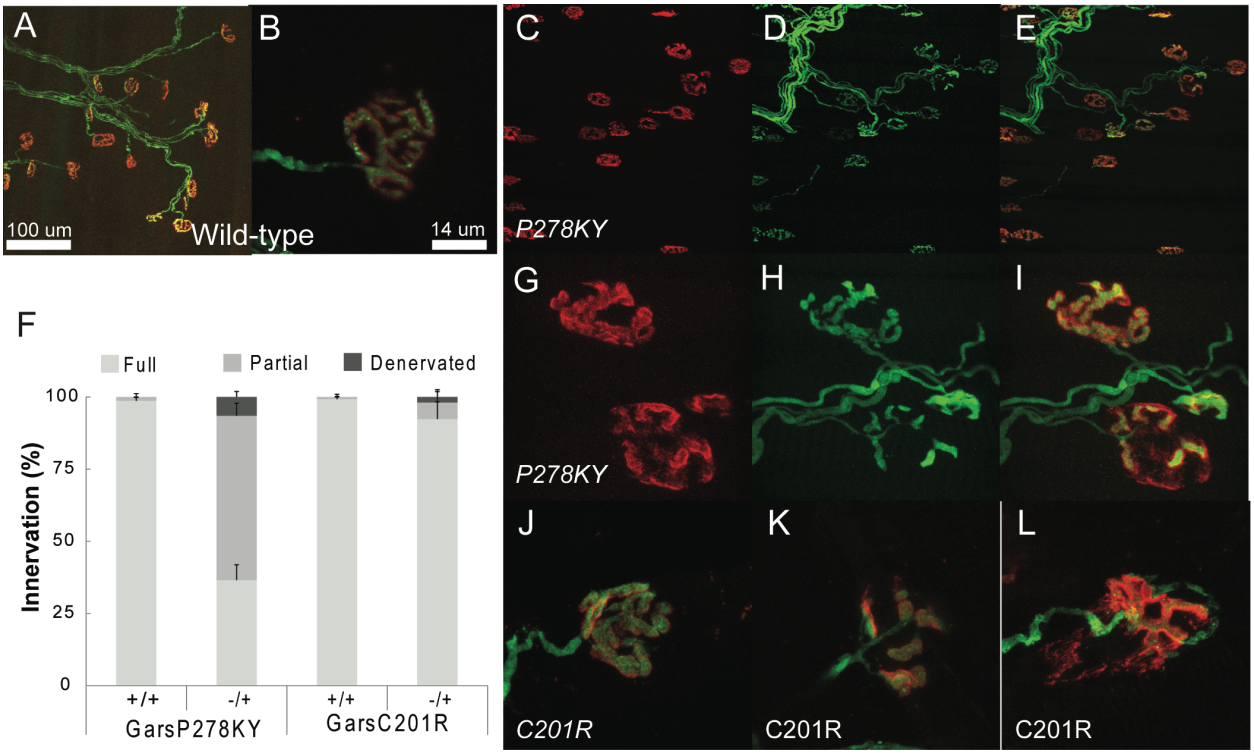

Figure 2. Morphological analysis of LAL muscle in CMT2D mice*:* Images shown are of LAL terminals in 2 month-old (A,B) wild-type, (C-I) *Gars*^{P278KY} and (J-L) 4-month-old *Gars*^{C201R} mice. Red shows α-bungarotoxin stained postsynaptic ACh receptors, green is presynaptic nerve expressing YFP (see Methods). Innervation analysis (F) included examination of ≥100 terminals from each of 3 LAL muscles/genotype. Control wild-type (A,B) terminals show typical complex pretzel-like morphology and postsynaptic receptors are entirely apposed by the presynaptic nerve. *Gars*^{P278KY} terminals. At low magnification (20x) it can be seen that (C-E) *Gars*^{P278KY} terminals retain some innervation, but when viewed at higher magnification (63x) (G-I) nearly all terminals show some dysmorphology (upper and lower terminal G,H,I) and many are only partially innervated (lower terminal G,H,I). Occupancy was analyzed, and ~ 10% of terminals were denervated but more than 50% showed some degree of partial denervation muscles. *Gars*^{C201R} *terminals.* The LAL muscle in *Gars*^{C201R} mice showed a similar phenotype to *Gars*^{P278KY} muscles, with widespread dysmorphology at most terminals with severity ranging from (J) mild, near-normal to (K) fragmented or (L) partially denervated. Overall, consistent with previous findings, *Gars*^{C201R} LAL muscles had many (F) fewer denervated or partially denervated terminals than seen in *Gars*^{P278KY}, but across both alleles at least 80-90% of NMJs retain at least partial innervation.

Quantal Analysis Reveals Abnormal Synaptic Transmission in CMT2D Mice at 2 Months of Age.

Motor endplate current recordings were made under voltage clamp conditions to control for potential changes in passive properties of muscle fibers that could occur with disease-related changes in muscle activity (Lomo and Rosenthal 1972). Our first set of experiments used muscles from 2-month-old *Gars*^{P278KY} and *Gars*^{C201R} mutants and respective wild-type littermate controls. At this age we found qualitatively similar changes in synaptic function for both mutants, but as with other phenotypes, the dysfunction was more pronounced at NMJs of the *Gars*^{P278KY} mice than at synapses of *Gars*^{C201R} mutants with the milder disease.

At 2 months of age, both alleles show no difference in MEPC amplitude (quantal amplitude) (Figure 3 A,G), but the frequency of spontaneous release was consistently and significantly lower than wild-type (Figure 3 B,H). The finding that quantal amplitude at mutant synapses is not different than wild-type indicates that both postsynaptic receptor density and the amount of acetylcholine loaded into individual vesicles is unaffected at CMT2D terminals.

Evoked release was also affected at 2-month-old mutant NMJs, as both alleles showed significant decreases of approximately 25% in EPC amplitude (Figure 3 C,I) and quantal content (Figure 3 D, J). Clinical diagnoses of NMJ dysfunction utilizes response to repetitive stimulation (Rich 2006), so we also examined changes in EPC amplitude in response to a 10 pulse, 50 Hz stimulus train. In addition, changes in facilitation or depression with this protocol can be used to infer changes in release probability (Zucker and Regehr 2002; Kong et al. 2009). Using the ratio of the amplitude of the $10^{th}/1^{st}$ EPC in the train we found that, on average, NMJs of *Gars*^{P278KY} and *Gars*^{C201R} mice showed significantly greater depression (Figure 3, E,K). For healthy synapses greater depression correlates with higher initial probability of release (Zucker and Regehr 2002).

Finally, we examined time-course measures of both MEPCs and EPCs and found no significant changes between mutant and control NMJs at 2 months of age for either allele. (Time

constants in ms: MEPC control vs. mutant – *Gars*^{P278KY}: 0.79±0.24 vs. 0.74±.0.20, *Gars*^{C201R}: 0.75±0.12 vs. 0.73±0.12)(EPC control vs. mutant: *Gars*^{P278KY}: 1.1±0.20 vs. 1.2±.0.24, *Gars*^{C201R}: 1.2±0.14 vs. 1.2±0.17). Additional time course measures (time-to-peak, half-width, 10-90 rise time) also showed no changes at synapses in either *Gars* mutant at 2-months of age.

Together analysis of synaptic measures reveals changes in synaptic transmission in 2-month-old CMT2D mice that are characterized by decreased spontaneous release frequency and evoked release amplitude and greater EPC depression in response to 50Hz stimulation. The absence of any change in MEPC amplitude or time-course measures points to a presynaptic defect. As with other CMT2D phenotypes examined previously, synaptic changes in the CMT2D mice correlate with disease severity associated with different mutant alleles.

Quantal Content is Further Reduced in Gars^{C201R} LAL Terminals Between 2 and 4 Months.

Given the relationship between synaptic dysfunction and disease severity across mutant alleles, we were also interested in determining if synaptic measures changed with age for a given allele. For these experiments we aged an additional cohort of *Gars*^{C201R} mice to 4-months. We chose the milder *Gars*^{C201R} allele for this study because innervation status is near normal even at the older age (Figure 2F).

The additional two-months produced no significant changes in spontaneous release compared to younger mutants. MEPC amplitude recorded at *Gars*^{C201R} NMJs was still not different than control (Figure 3 G,G′), and MEPC frequency remained reduced to approximately the same extent as measured at 2 months (Figure 3 H,H'). Since the reduction in frequency of spontaneous release was such a robust, consistent finding we were interested in determining if a mutant synapse could increase spontaneous release in response to higher extracellular calcium. Raw traces show increased MEPC frequency when recorded from the same LAL synapse (4- month-old, *Gars*^{C201R}) at two different calcium concentrations: 2mM (Figure 3 F, upper), and 4mM (Figure 3 F, lower). Initial release frequency was 0.4 Hz, below the mutant

Gars^{C201R} average (~0.8 Hz; Fig. 2H, H'), but doubling extracellular calcium increased release frequency to 1.0 Hz, within normal range for a wild-type synapse, a comparable relative increase to that reported previously for wild-type mice (e.g.(Plomp et al. 2000)). Average MEPC amplitude also increased from 1.9 to 2.3 mA.

Evoked release at *Gars*^{C201R} synapses showed a further decline, as mean EPC amplitude and quantal content were significantly lower at 4 months compared to 2-month and age-matched wild-type values (Figure 3 I,I',J,J'). Interestingly, the extent of depression in response to 50Hz trains at the older mutant NMJs was significantly less (i.e. >10^{th}/1^{st} ratio) compared to 2-month mutant values, and higher than 4-month wild-type control values (Figure 3 K,K'), indicating a decrease in the probability of release between 2 and 4 months. Examination of time-course measures (MEPC and EPC, not shown) revealed neither an age-related effect of the *Gars*^{C201R} mutation nor any difference from age-matched controls.

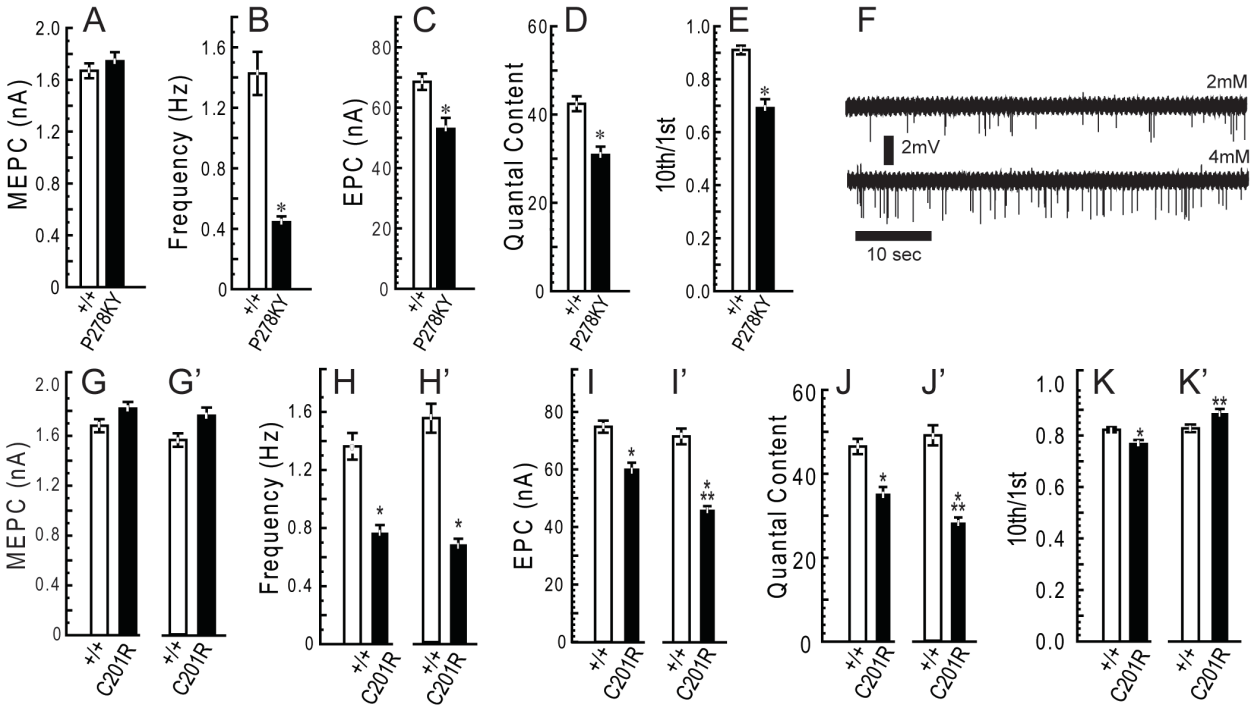

Figure 3. Quantal analysis. Voltage clamp experiments were performed using LAL muscles from 2-month-old *Gars*^{P278KY}, (upper panels) and both 2- and 4-month-old *Gars*^{C201R} mice (lower panel). All recordings were made at a holding potential of -50mV. At 2-months of age, mutant NMJs in both *Gars*^{P278KY} and *Gars*^{C201R} mice showed: no change in MEPC amplitude, (A, G) lower frequency of spontaneous release, (B,H) reduced EPC amplitude and quantal content (C,I,J), and significantly greater depression ($10^{th}/1^{st}$) in response to 50 Hz stimulation (E,K). At 4 months of age *Gars*^{C201R} NMJs show no additional changes in spontaneous release (G',H') but a further reduction in EPC amplitude and quantal content (I',J') while repetitive stimulation produced less depression compared to 2-month mutant NMJs (K'). (F) Increased extracellular calcium successfully increased spontaneous release frequency at 4-month-old mutant *Gars*^{C201R} NMJ. LAL muscles of 6 different mice for each genotype/age were used. In each muscle recordings were made on 3-12 synapses (mean and mode=8) for a total of between 47-58 synapses for each genotype/age. Comparisons made using nested ANOVA. * = $p<0.05$ – mutant vs. wild-type; **= $p<0.05$ – 2 vs. 4 months *Gars*^{C201R}.

Dynamic Frequency-Related Changes in Evoked Release Show Atypical Response at Mutant NMJs.

Observations during the delivery of 50 Hz stimulus trains prompted a more detailed analysis of dynamics during the 10-pulse train. EPC amplitude was measured for each pulse of the train and expressed relative to the amplitude of the first EPC. The typical pattern of the 50 Hz frequency response averaged across wild-type littermate NMJs was similar regardless of age or strain (Figure 4) and is characterized by potentiation of initial EPCs (2-4th response, ~105% initial) followed by moderate depression (85-90% initial). However, this pattern differed between mutant alleles and changed between 2 and 4 months in *Gars*^{C201R} muscles.

At NMJs of 2-month-old CMT2D mice, both *Gars*^{P278KY} (Figure 4 A) and *Gars*^{C201R}, (Figure 4 B) showed near complete absence of potentiation, barely evident only for the second response at NMJs of *Gars*^{C201R} mice. In addition, EPCs at NMJs for both mutant alleles showed a slightly steeper depression relative to respective wild-type (Figure 4 A,B), and the effect is again more marked at *Gars*^{P278KY} NMJs than at *Gars*^{C201R} NMJs (Figure 4 A,B).

Given the additional reduction in quantal content at *Gars*^{C201R} NMJs between 2 and 4 months, we expected the response pattern of 4-month mutant NMJs to appear more like that observed at *Gars*^{P278KY} terminals. To our surprise, the typical early potentiation was now evident and the overall pattern was more similar to wild-type, but with even slightly greater initial potentiation and somewhat less marked depression (decreased probability of release) in later responses (Figure 4 C).

We were also interested in the ability of mutant NMJs to sustain release for periods longer than the 200ms duration of the 10-pulse 50Hz trains. Thus, at NMJs where a sufficiently stable penetration was established we also recorded EPCs in response to 10 consecutive stimulus trains of 1 second duration (70 pulses@70 Hz) delivered once every 2 seconds. Successful recordings, of at least 10 stimulus trains per NMJ, were made in several muscles at 16 different NMJs including 5 wild-type and 11 mutants (2 *Gars*^{P278KY} and 9 *Gars*^{C201R}, 3 and 6 from 2- and

4-month old muscles respectively). Overall, qualitative examinations of 70 Hz raw traces reveal that mutant NMJs do not sustain release during the repeated 1 second stimulus as well as wild-type (Figure 4 D-G). If the response to the 1st train in a series is compared across genotype/age (top panel, D-G) a marked difference is only clearly evident for the severe *Gars*^{P278KY} NMJ, but effects on each mutant NMJ becomes more marked with successive trains such that by the 10th train (bottom panel, D-G) release is clearly more severely reduced at mutant NMJs. In traces shown, release failures occur in the 2nd train at the *Gars*^{P278KY} NMJ (arrows in middle panel E,) and during the 10th train for both *Gars*^{P278KY} and 2-month-old *Gars*^{C201R} NMJs shown (arrows in bottom panels, E, F). We examined all individual 70Hz traces for each NMJ to better evaluate the extent of the failures. Failures never occurred at wild-type NMJs, but at least one failure occurred during at least one stimulus train at 5 of 11 mutant NMJs. Of these 5 two were from *Gars*^{P278KY} muscles and three were recorded in 2-month-old old *Gars*^{C201R} muscles. Failures for both *Gars*^{P278KY} NMJs occurred as early as the second stimulus train and failures also occurred during the initial 10 stimuli of the train, whereas for *Gars*^{C201R} NMJs (2-month), failures did not appear until the 4th train or later and failures were not seen during the initial 10 stimuli of any train. The 50 Hz analysis above suggested a compensatory response between 2 and 4 months for *Gars*^{C201R} NMJs, and in keeping with this, examination of traces for 4-month-old *Gars*^{C201R} NMJs revealed no clear failures, but traces included intermittent, very small EPCs (5-15 nA), not present in any wild-type traces, and these were more common towards the end of individual traces and in later (4-10th) trains.

We also calculated quantal content using the EPC averaged across trains (n=10/NMJ) of the 70th EPC in the trains and compared mutant and wild-type values. Final quantal content at the end of the 70 Hz trains ranged between 21 and 49 for the five wild-type NMJs and between 5 and 22 for the 11 mutant synapses. Including all mutant data, the average mutant quantal content of the final 70Hz EPC (mean 13.2±5) was significantly lower than wild-type (mean

31.4±12) ($t(14)=4.4$, $p=0.01$) and this difference was also significant if the comparison was restricted to 4-month-old *Gars*^{C201R} (mean 13.5±3) and wild-type ($t(9)=3.5$, $p=0.01$).

As a final assessment of the severity of defects at *Gars* NMJs, we reviewed all of our experiments seeking fibers where we were able to record MEPCs (i.e. innervated), but were unable to evoke an EPC (N.B. data not included in Figure 2). This scenario was found in 17 of 179 NMJs (7,6,4 *Gars*^{P278KY} and *Gars*^{C201R}, 2 and 4 month respectively) including 1 or more occurrence (max. = 4) in 9 of the18 mutant muscles (6-12 NMJs recorded per muscle). In contrast, for wild-type this situation arose at only 4 of 184 NMJs in 4 of 18 muscles and never occurred more than once in any experiment (6-11 NMJs/experiment).

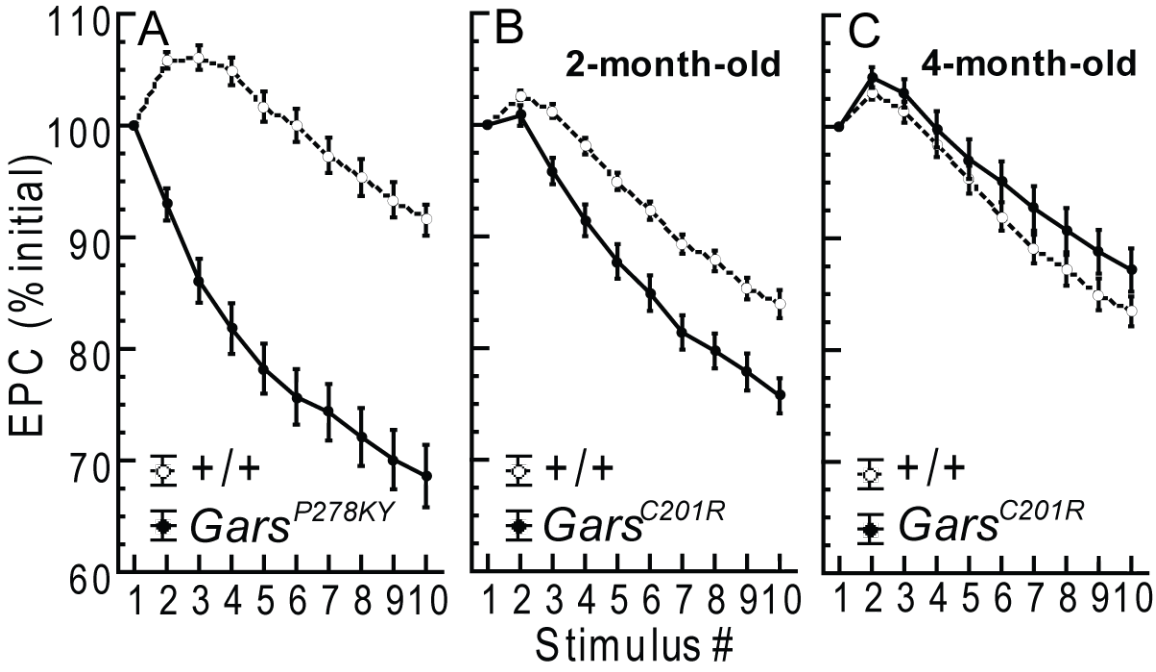

Figure 4. Evoked response to repetitive stimulation. A,B&C show plots of averaged normalized EPC amplitude (± s.e.) for each stimulus of a 10 pulse, 50hz stimulus train (average of 20 trains@0.5Hz for each NMJ). In contrast to wild-type synapses, mutant NMJs in 2-month-old animals showed reduced or absent potentiation of initial EPCs and somewhat steeper depression. At 4-months of age, initial EPCs showed potentiation similar to wild-type. EPC amplitude was measured for each stimulus and plotted relative to the amplitude of the first pulse. Numbers of animals/synapses are the same as for data shown in Fig. 2. Plots in D,E,F&G show the 1st,2nd and 10th raw traces from a series of ten EPC trains recorded in response to a 70 pulse,70hz stimulus (1sec duration), delivered every 2 seconds. Starting quantal content (m) is shown for each of the four NMJs. Mutant NMJs showed marked steadily progressive decrements from the 1st to 10th train while the wild-type decreased and stabilized. The mutant NMJs are easily identified by comparing response to the 10th stimulus train (lower traces) to wild-type. In addition, clear failures of release were evident (arrows) for NMJs from severe and 2-month-old mild *Gars*^{C201R} muscles. Failures were present in at least one train for 5 of 11 mutant NMJs, but were never observed in wild-type. The 1 second duration, 70Hz trains were recorded in 9 different muscles/experiments (n= 5,6,3 and 2 NMJs from 4-month-old wild-type, 4M-*Gars*^{C201R}, 2M-*Gars*^{C201R} and 2M-*Gars*^{P278KY} respectively).

Is the Observed Reduction in Quantal Content Associated with Fewer Active Release Sites?

Voltage-clamp data reveal apparent presynaptic changes that cause a reduced quantal content as well as a reduced capacity for sustained release for mice carrying either *Gars* mutant allele. To investigate whether a reduced number of release sites could account for the lower quantal content and MEPC frequency at mutant NMJs, we stained LAL terminals for Bassoon, a presynaptic protein present at NMJ release sites (tom Dieck et al. 1998) (see Methods for details based on (Nishimune, Sanes, and Carlson 2004)). We used only LAL muscles from 2-month-old *Gars*^{P278KY} mice with the rationale that, if release sites were contributing, it would be clearly evident at synapses of the most severely affected muscles. Wild-type terminals showed complete apposition of YFP-positive presynaptic terminals with postsynaptic receptors and bassoon-stained puncta in association with the presynaptic nerve (Figure 5 A-D). Consistent with the smaller size of the mutant mice/muscles,(Seburn et al. 2006; Achilli et al. 2009b) the mean area of LAL end plates in *Gars*^{P278KY} mice was significantly smaller (compare solid and dashed vertical lines, Figure 5 I). However, the range in counts of the bassoon-stained puncta was similar for wild-type and *Gars*^{P278KY} terminals (solid vs. open, Figure 5 I) and there was no significant change ($p=0.4$) in either the average absolute number (solid and dashed horizontal lines, Fig.4I) or density of release sites ($p \geq 0.17$)(Figure 5 J) compared to wild-type terminals. As expected from the initial morphological analysis of mutant NMJs (Figure 2) 10 of the 34 terminals that were sampled from *Gars*^{P278KY} muscles for this analysis had a portion of postsynaptic receptors not apposed by the presynaptic nerve and without bassoon-puncta. Although these terminals clearly lacked bassoon-stained puncta in the partially denervated regions, the relative proportion of the junction affected was not large (≤15%)(e.g. Figure 5 H,K) so the effect on puncta counts was small. Counts for the 10 partially denervated junctions had a similar mean, median and range as those without any evident loss of presynaptic nerve (mean=689 vs. 720, median=616 vs. 632, range=233-2049 vs. 134-1840). Taken together

these data show that release sites in *Gars*^{P278KY} muscles are retained so long as the presynaptic terminal persists. Therefore, at partially denervated LAL junctions release sites could be reduced in proportion to the extent of partial denervation. However, other factors must also contribute because half of the NMJs in 2-month-old *Gars*^{P278KY}, and ~85% in *Gars*^{C201R} LAL muscles, retain complete innervation (Figure 2).

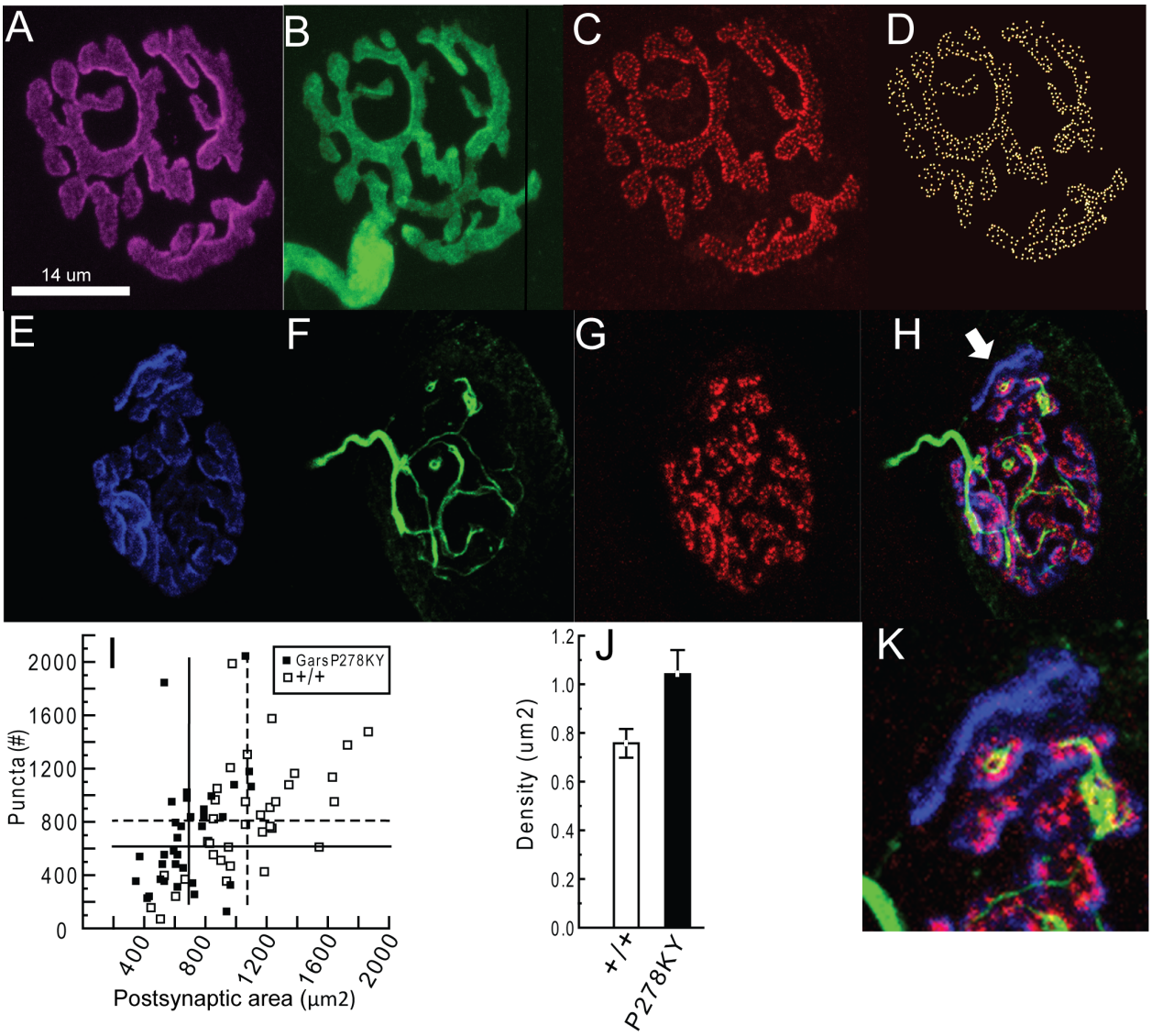

Figure 5. Quantification of bassoon-stained release sites in 2-month-old Gars^{P278KY} LAL muscles. Process of visualization and quantification of bassoon-stained release sites is shown for a wild-type LAL terminal (A-D). Analysis included assessment of: (A) the postsynaptic receptor area, (B) presence of presynaptic nerve and (C) bassoon-stained puncta. Puncta were identified using a three-step process to render a 3-D image (D) for automated counting of release sites (Imaris, see Methods for details). Typical *Gars*^{P278KY} NMJ (E-H) have more diffuse postsynaptic staining (E), apposed by a thinned presynaptic nerve (F), that nonetheless retains bassoon-stained puncta (G) at innervated locations (N.B. the areas where YFP appears to not overlie bassoon labeling due to the faint YFP signal in portions of the axon and the thresholding of the image; at higher gain YFP was detectable in the vicinity of all bassoon-stained puncta). However, as expected, when a portion of the presynaptic nerve vacates, bassoon-stained release sites are no longer evident (arrow in merged image H, expanded in K). *Gars*^{P278KY} sample included a total of 34 synapses that included 10 terminals with small areas of evident partial denervation. (I) Scatterplot shows NMJ area and counts of bassoon-positive puncta at

Figure 5 Continued:
individual synapses of *Gars*^{P278KY} (solid) and wild-type (open) NMJs. Vertical and horizontal lines indicate sample means (*Gars*^{P278KY} and wild-type, solid and dashed respectively). Mean area of LAL NMJs was significantly smaller ($p<0.002$) compared to wild-type (solid vs. dashed vertical line). Individual puncta counts covered a similar range and neither mean counts (dashed and solid horizontal lines) nor density (J) were significantly different between genotypes ($p=0.4$ and 0.17, respectively). Analysis included 5-10 (mean=7) terminals from each of 5 LAL muscles of each genotype (n=34 & 35, *Gars*^{P278KY} and wild-type respectively). Comparisons with nested ANOVA.

Vesicle Number and Localization

Given that a change in the number of release sites was insufficient to account for changes observed in evoked release, we next used electron microscopy to compare vesicle parameters at wild-type (Figure 6 A) and NMJs from the severely affected Gars^{P278KY} mice (Figure 6 B). We analyzed electron micrographs of portions of 5-10 NMJs (median 8) from each of five animals per genotype. Consistent with the lack of difference in MEPC amplitude, vesicle size was similar for mutant and wild-type terminals (50 ± 0.71 vs. 54 ± 1.2, respectively). Average vesicles counts tended to be lower at Gars^{P278KY} NMJs compared to wild-type, but due to large inter-animal variation, for both genotypes, the difference did not quite reach our statistical cutoff for significance ($p=0.08$) (Figure 6 C, inset). However, consistent with light microscopy results above (Figure 6 I) and other work (Sleigh et al. 2014) Gars^{P278KY} mutant synapses are smaller than wild-type and therefore, the areas of captured portions of mutant NMJs in our electron micrographs also tended to be smaller (mean = 14 vs. 28 μm^2, respectively, $p=0.04$). When vesicle number is plotted against area (Figure 6 C) it is evident that mutant muscle had fewer terminals with areas > 20 μm^2 and vesicle counts > 250 (ellipse, Figure 6 C), and a preponderance of small (<20 μm^2) terminals with vesicle counts of less than 150 (inset, Figure 6 C). In general, mutant vesicle numbers still scaled with terminal area, as the density of the vesicles (# per μm^2) was not different than wild-type (Table, Figure 6 D). However, there are several examples of mutant terminals with vesicle counts below any found at wild-type terminals (ellipse inset, Figure 6 C). Thus, despite the fact that the comparison of average wild-type and

mutant vesicle counts did not reach our statistical cutoff, we contend that quantal content is likely limited by vesicle number for at least some terminals among the generally smaller Gars^{P278KY} mutant terminals. Note, however, that the micrograph in 5B is an example from among those terminal portions that were clearly "depleted" in the Gars^{P278KY} muscles. In a preliminary study we also examined 2 mutant muscles (5 NMJs each) from the distal plantaris muscle, which has more severe NMJ dysmorphology than the proximal LAL, and terminals such as shown in Figure 6 B were not found. Thus, such terminals should be considered worst-case, and if present at all, are not widespread in even in the more severely affected distal plantaris of the mild Gars^{C201R} allele.

To complete our electron microscopy analysis of vesicles we evaluated their location relative to the presynaptic membrane. We counted the number of vesicles within 200 nm of the presynaptic membrane and the number of docked vesicles (within 20nm) and found no significant changes at mutant terminals for either absolute counts or counts normalized per micron of presynaptic membrane (Table, Figure 6 D).

Finally, we also counted the number of identifiable mitochondria visible in electron micrographs. Interestingly, on average, there were significantly fewer mitochondria observed at Gars^{P278KY} terminals compared to wild-type (Figure 6 E). However, there was wide variation in counts from terminal to terminal for both genotypes, but the median was also shifted (14 vs. 6, Gars^{P278KY} and wild-type respectively) suggesting the reduction in the mean number of mitochondria observed at NMJs of CMT2D mice was not due to a small number of mutant terminals with very few or no mitochondria.

Taken together electron microscopy analysis of NMJs suggests that smaller terminals with fewer vesicles likely contributes to lower quantal content for at least a portion of NMJs in muscles of the severe Gars^{P278KY} mice. Vesicles at mutant terminals were of normal size and

were localized to the presynaptic membrane similar to wild-type, suggesting vesicle processing/trafficking is operating normally at CMT2D NMJs.

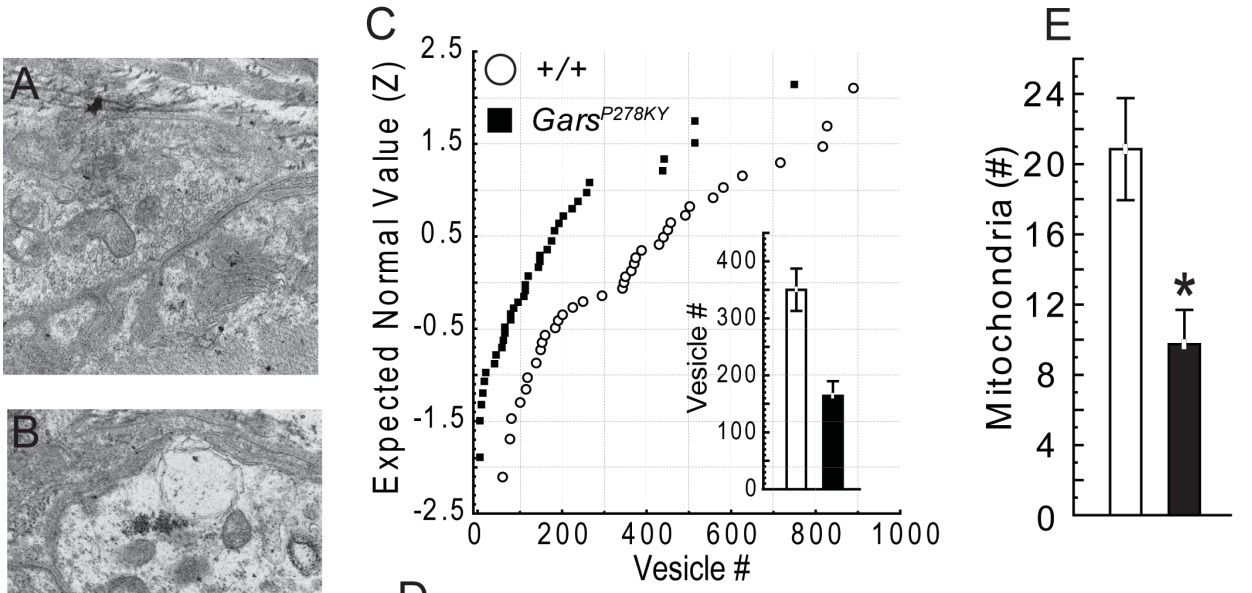

D

	Density(#/um2)	Count (#/200nm)	Count (#/20nm)	Count(#/20nm/um)
+/+	15 ± 1.4	45 ± 3	8 ± 1	1.2 ± 0.1
GarsP278KY	13 ± 1.5	38 ± 4	7 ± 1	7 ± 0.3

Figure 6. Electron microscopic analysis of NMJs. Electron micrographs of NMJs from LAL muscles of 2- month-old (A) wild-type and (B) Gars^{P278KY} mice were captured (5 animals per genotype, 5-10 NMJs (median 8) per muscle). Mutant NMJ shown is representative of a "severely" affected NMJ with a low-vesicle count. Note junctional folds and other synaptic specializations are still evident at mutant synapses. Analysis showed vesicle size was similar for mutant and wild-type terminals (50 vs. 54 nm, respectively) (not shown). (C) Scatterplot shows that the area of terminal portions analyzed scale with vesicle counts for both genotypes. Note the relative absence of large, high vesicle count terminals (ellipse) and the preponderance of small, low vesicle count NMJs in the mutant (lower quadrant in C, expanded in inset). Counts at some mutant NMJs were lower than values recorded at any wild-type NMJ (ellipse, inset). However, due to large inter-animal variability for both genotypes differences in average vesicle counts for wild-type, Gars^{P278KY} NMJs (p=0.08) did not reach our statistical cutoff (see Results). (D) The density of the vesicles present in Gars^{P278KY} terminals was not different than wild-type. Detailed analysis of vesicle location revealed no differences in the number of docked vesicles (within 20nm), or within 200 nm for either absolute or normalized counts (per micron of membrane). (E) Average counts of mitochondria (e.g. arrows in A,B) were significantly lower at Gars^{P278KY} terminals (median14 vs. 6, wild-type and Gars^{P278KY} respectively).

Enhancing Synaptic Function Improves Wire Hang Performance of CMT2D Mice

Prior work has shown that CMT2D mice have significant muscle weakness.(Achilli et al. 2009b; Motley et al. 2011a; Seburn et al. 2006) Our data reveal significant synaptic dysfunction that could contribute to weakness in the CMT2D mice, so we next tested whether enhancing synaptic function could improve in vivo performance of the Gars mutants in a task requiring strength. We first confirmed that mutant synapses were capable of responding to the two test drugs in vitro: 3,4-DAP (amifampridine), which acts pre-synaptically to increase quantal content (Thomsen and Wilson 1983) and physostigmine (eserine) which acts postsynaptically to enhance current duration at postsynaptic receptors (Shaw et al. 1985). In vitro recordings confirmed that both drugs acted as predicted to increase EPC amplitude at 4-month $Gars^{C201R}$ NMJs (n≥18 NMJs) (data not shown). We next evaluated whether the enhanced synaptic currents could translate to better whole animal performance on the wire-hang test. Mice first performed an initial wire-hang and then were injected with 3,4-DAP, physostigmine or saline vehicle and re-tested sixty minutes later. We first tested the more mildly affected $Gars^{C201R}$ mice and found that administration of physostigmine significantly improved wire-hang times, while 3,4-DAP caused a significant decrease (Figure 7 A,1 month) or no change (Figure 7 B, 4 month) in performance. $Gars^{P278KY}$ mice also showed improved wire-hang times after physostigmine administration (Figure 7 B). However, because the more severe disease causes them to perform so poorly in general, (latency to fall ≤ 8 seconds) we did not test 3,4-DAP to see if it decreased performance in the $Gars^{P278KY}$ mice.

The improved performance of CMT2D mice after administration of physostigmine, the lack of improved performance in the presence of 3,4-DAP, and the existence of evident failures in evoked release with 1 second long trains, are consistent with a presynaptic defect that can be counteracted by enhanced activation of postsynaptic receptors, but limited capacity for increasing or maintaining quantal content.

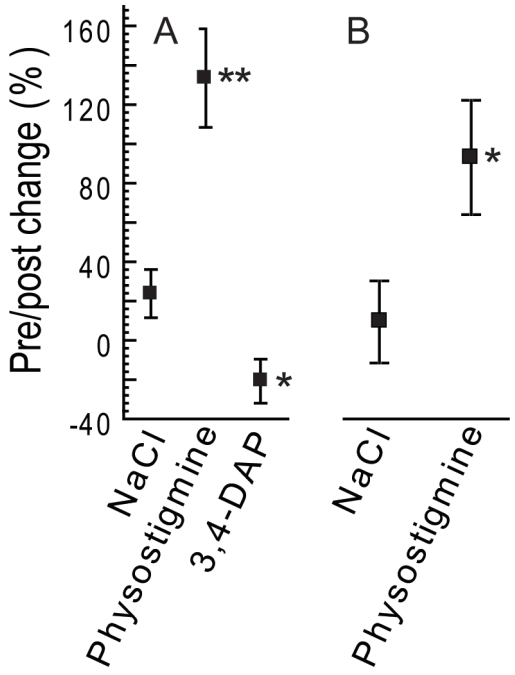

Figure 7. Wire-hang performance of CMT2D mice. Performance is expressed as the percentage change in wire-hang time after treatment ((post-pre)/post)/100) (see Methods for protocol details). (A) $Gars^{C201R}$ mice (1-month-old) were able to perform better with physostigmine (postsynaptic), but showed a decrease in performance after administration of 3,4-DAP (presynaptic) or (B) no change to 3,4 DAP injection at 4 months of age. (C) $Gars^{P278KY}$ mice showed a similar response to physostigmine, but were not tested with 3,4 DAP. Mice were 30-40 days old for testing ($Gars^{C201R}$, n=6 and +/+, n=5) ($Gars^{P278KY}$, n=5 and +/+, n=4). Wild-type (+/+) mice typically perform the task to completion (60 s max.) and showed no drug-related change in performance at the dosages used (physostigmine 0.1 mg/kg; 3,4 DAP 2.5 mg/kg), so data are not shown. Pairwise comparisons drug-treated vs. NaCl with Student's T-test: **($t(9)=4.2, p<0.01$); *($t(8)\geq 2.3$, $p\leq 0.047$).

Quantal Analysis in the Presence of 3,4 DAP

To assess the capacity of mutant NMJs to increase quantal release, we performed an additional set of voltage-clamp experiments using muscles from $Gars^{C201R}$ to assess NMJ function in the presence 20μM 3,4 DAP. The data presented in Figure 8 show that mutant NMJs in 2- and 4-month-old LAL muscles are able to respond to the 3,4 DAP in a manner that is qualitatively similar to wild-type NMJs (N.B. Control values are replotted from Fig. 3). Lengthening the presynaptic depolarization increased EPC amplitude at mutant NMJs to values similar to control (Figure 8 C). However, mean quantal content at mutant 2-month-old NMJs remained significantly lower than the respective wild-type mean (Figure 8 D) and though it was still visibly reduced at 4-month old mutant NMJs, it was not statistically different. Thus, in response to a single stimulus, mutant NMJs have the capacity to respond to 3,4 DAP and normalize EPC amplitude and increase quantal content to values at or near control. So why was wire-hang performance not improved by in vivo administration of 3,4 DAP? By the end of the the 200ms 50 Hz stimulation, the 20 μM 3,4 DAP reduced EPC amplitude to only 20% of initial values for both mutant and wild-type NMJs (Figure 8 E). To improve the wire-hang performance of the mutants would require an improvement in sustained release for up to a minute, so an equivalent in vivo dose would be expected to worsen performance. To examine this further we also calculated the quantal content of the last EPC (10^{th}) in the 50Hz train (Figure 8 F). Under non-drug control conditions quantal content of the 10^{th} EPC is significantly lower at mutant NMJs than wild-type (compare Control mutant vs. wild-type in Figure 8 F). Importantly, introduction of 3,4 DAP reduces quantal content even further at mutant NMJs and even reduces wild-type quantal content to values similar to those seen at mutant NMJs. Thus, despite the capacity of mutant and wild-type NMJs to increase their quantal release in the presence of 3,4

DAP (Figure 8 C), release is not well sustained for even 200ms of 50 Hz stimulation and, at least at the dose tested, would not be effective in the treatment of the presynaptic defect in the Gars mutant mice.

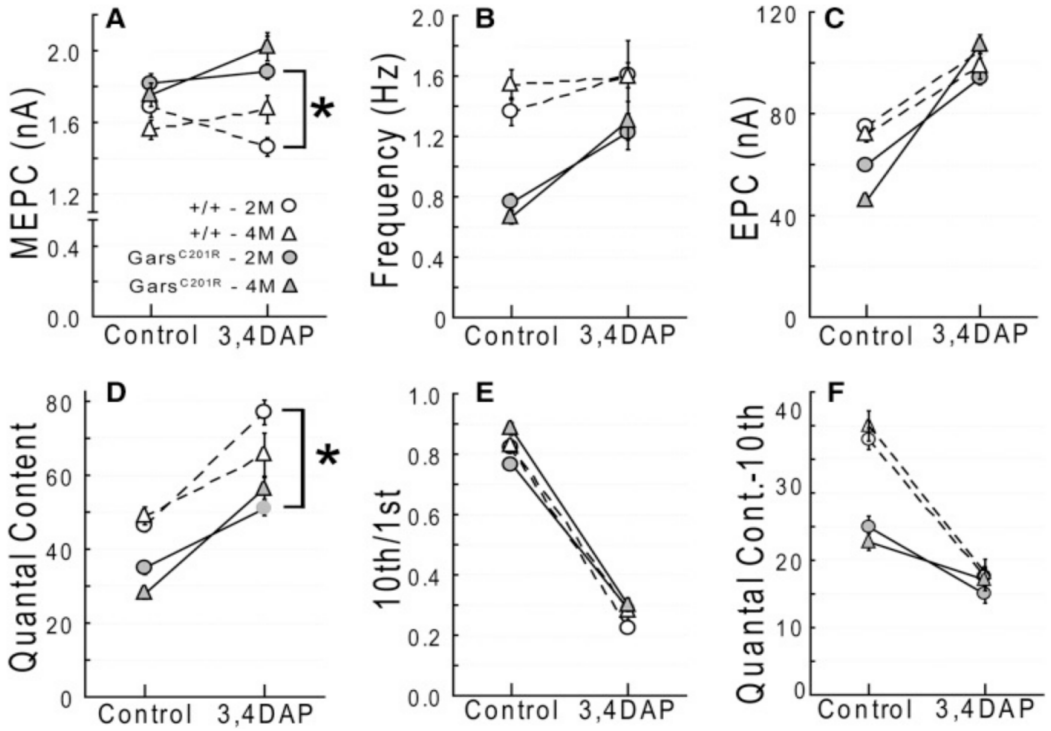

Figure 8. Quantal analysis in the presence of 3,4 DAP. Voltage clamp experiments were conducted on cohorts of 2- and 4-month-old *Gars*^{C201R} and wild-type mice with 3,4 DAP added to the bath (20uM). Dashed lines are wild-type, solid lines are *Gars*^{C201R} and 2 and 4 month data are shown with circles and triangles respectively. Control values without DAP are re-plotted from Figure 2. The addition of 3,4 DAP to prolong presynaptic depolarization caused qualitatively similar changes at mutant and wild-type NMJs. Differences that existed between mutant and wild-type measures without 3,4 DAP (Figure 2) were eliminated at 4-month old mutant NMJs when 3,4 DAP was present, although quantal content was still somewhat lower. At 2-month-old mutant NMJs, quantal content remained significantly lower ($p=0.01$) compared to wild-type.

Discussion

The objective of this study was to determine if NMJ dysfunction is a previously unrecognized aspect of CMT2D and could therefore present a novel treatment avenue using drugs available for treatment of neuromuscular disorders characterized by reduced presynaptic release. Overall our data confirm the presence of a presynaptic defect at the mutant NMJs that likely contributes to muscle weakness and can be overcome by administration of the cholinesterase inhibitor physostigmine. To our knowledge this is the first detailed examination of NMJ function in a type 2 axonal CMT.

We studied the relatively mildly affected proximal LAL muscle from animals carrying two different *Gars* mutations that produce disease phenotypes in mice that vary, as does CMT2D, from mild ($Gars^{C201R}$) to severe ($Gars^{P278KY}$). These new data describing synaptic defects are consistent with other previously described phenotypes (Achilli et al. 2009b; Motley et al. 2011a; Seburn et al. 2006; Sleigh et al. 2014; Stum et al. 2011) insofar as the different mutations did not produce distinct NMJ phenotypes, but rather produced changes that vary along a continuum both within and across genotype/age. As such, we propose these data represent at least a portion of a spectrum of NMJ dysfunction that, if present in patients, could present differently in each patient and to varying degrees at different times. The spectrum is evident within the LAL and would likely be expanded if examined across muscles because morphological data for the NMJ in CMT2D mice has consistently shown that distal muscles (lumbricals, tibialis anterior,plantaris) have more marked degeneration than NMJs in more proximal muscles (transversus abdominis, levator auris longus) (Achilli et al. 2009b; Motley et al. 2011a; Seburn et al. 2006; Sleigh et al. 2014). On the basis of the more prevalent distal partial denervation alone, it is reasonable to assume that NMJ dysfunction in our mice is likely worse in distal muscles, a notion that is also consistent with disease presentation in humans (Saporta and Shy 2013b).

Taken together these data indicate that the mutant GARS has a broad effect that leaves the fundamental release machinery intact but "weakens" NMJ function in the CMT2D mice. Overall, the results point clearly to a presynaptic problem that reduces quantal content, but examination of key determinants of quantal content did not reveal a primary mechanism. Instead, our data suggest that release processes overall are not functioning optimally and that dysfunction includes a spectrum of effects that for a given NMJ could include: i) reduced terminal areas that may contain fewer total vesicles (inset Figure 6 C) and, ii) morphological breakdown of the presynaptic nerve including some loss of associated release sites (Figure 5). For example, despite statistical differences in average vesicle number not reaching the 5% statistical cutoff, it seems clear that reduced vesicle number could contribute at some NMJs, at least in the severe *Gars*^{P278KY} allele (Figure 6 C). However, if reduced vesicle number was the sole disease mechanism for mutant *Gars,* we would also have expected administration of 3,4 DAP to cause greater relative depression at *Gars*^{C201R} NMJs than at wild-type with 50 Hz stimulation. Instead the relative depression induced by the 3,4 DAP was nearly identical (Figure 8 E). Similarly, while NMJ area is significantly smaller in distal *Gars*^{P278KY} muscles, in *Gars*^{C201R} muscles NMJ areas are not different than wild-type and do not change between 1 and 3 months of age (see Fig. 3,(Sleigh et al. 2014)), yet in these experiments quantal content is reduced between 2 and 4 months. Thus, reduced NMJ area likely contributes, but is also insufficient as a primary mechanism. Finally, although we found partially denervated NMJs where a reduction in the number of release sites could contribute to reduced quantal content, this too seems insufficient to account entirely for the observed dysfunction in both alleles. While approximately 50% of NMJs in the LAL of the severe *Gars*^{P278KY} allele are partially denervated, only ~10% partial denervation is present in LAL of the mild *Gars*^{C201R} allele at 4 months of age.

The paucity of mitochondria in mutant nerve terminals in our electron micrographs is also potentially interesting. Reduced mitochondria in terminals may influence synaptic transmission

through a variety of mechanisms, including deficits in ATP production or changes in intracellular calcium dynamics.(Stowers et al. 2002) The mitochondria that were present in *Gars*^{P278KY} terminals were not vacuolated or otherwise obviously degenerating. Their reduced number may reflect a failure in axonal transport, biogenesis or turnover, but the association of *MFN2* with CMT2A makes it clear that defects in neuronal mitochondria can directly lead to axonal neuropathy.(Zuchner et al. 2004) The *Gars* gene in mammals encodes both the mitochondrial and cytosolic forms of the protein through alternative start codon usage.(Mudge et al. 1998; Shiba et al. 1994; Williams et al. 1995) All mutations associated with CMT2D and neuropathy in humans and mice are in the common, downstream domains of the GARS protein that are shared by both isoforms. For most other tRNA synthetases, separate nuclear genes encode the mitochondrial and cytosolic enzymes and overall the genetics of tRNA synthetase-associated CMTs (Scheper et al. 2007; Tolkunova et al. 2000) (Isohanni et al. 2010; McLaughlin et al. 2010; Scheper et al. 2007) does not clearly indicate a mitochondrial basis for the neuropathies. Nonetheless, mitochondrial dysfunction, whether primary or secondary, also cannot be ruled out as a contributing to the synaptic dysfunction we observed.

Our data also indicate ongoing, apparently compensatory changes in synaptic transmission at the NMJ. A variety of mechanisms could compensate for reduced synaptic currents to help maintain muscle function. The finding that the 4-month mutant NMJs again show some initial potentiation in response to 50Hz activation, may be an example of such compensation, but other changes may occur outside the synapse as well. We know that changes in muscle activity can modify passive properties of muscle (Lomo and Rosenthal 1972) and such changes may occur in the CMT2D mice. Voltage-clamp measures are unaffected by changes in specific membrane resistance and capacitance or other changes (e.g. Na^+ channels) that could alter muscle excitability. Thus, while our voltage-clamp data definitively establish the presence of synaptic defects in the CMT2D mice, it is possible that muscle fiber characteristics or other

processes might increase or decrease the likelihood of transmission failures that could lead to weakness.

Based on the combined results presented here, we propose that CMT2D, and perhaps other type 2 axonal CMTs, display synaptic dysfunction that could contribute both variably and intermittently to weakness or fatigue. In wild type mice, NMJs operate in a "failsafe" manner, such that firing the nerve produces sufficient depolarization in the muscle to cause an action potential without fail. This requires a "safety factor" of excess synaptic current to insure reliable muscle contraction (Paton and Waud 1967; Rich 2006) In the CMT2D mice, we show that average quantal content of mutant NMJs is significantly lower than wild-type (Figure 3), and based on examination of distributions of mutant quantal content values, we propose a model of CMT2D synaptic transmission (Figure 9) where disease processes diminish presynaptic release to a variable extent at most, if not all, NMJs. Distributions of quantal content at mutant NMJs each show a distinct leftward shift relative to wild-type, including between 15-30% of NMJs (depending on age and genotype) with a quantal content lower than any recorded at wild-type NMJs (Fig. 8A, left of vertical dashed line). We suggest currents at these severely affected NMJs could regularly fail to initiate muscle action potentials. At the other end of the range, fully 40% of wild-type NMJs have quantal contents ≥50 while only ~20% of values are in this range for NMJs in muscles of 2-month old *Gars*^{C201R} mutants, and for the NMJs in muscles of severe *Gars*^{P278KY} and 4-month *Gars*^{C201R} mice, exactly 2 NMJs fall in this range. The extent to which the population of mutant NMJs with quantal contents within normal range contributes to transmission failures and therefore weakness is unknown. However, based on the failures observed at some 2-month old *Gars*^{C201R} mutant NMJs during sustained 1 second stimulation at 70 Hz (Figure 4) and previously reported EMG decrements during in-situ tetanic muscle contractions with 700 ms 80 Hz stimulation (Fig. 3B in (Seburn et al. 2006)), it seems likely such failure is substantial. The cartoon in Figure 8B demonstrates how NMJs with severely reduced

quantal content (e.g. *Gars*^{P278KY} or 4 month *Gars*^{C201R}) may not reach threshold for initiation of an action potential, even in the absence of failures. Actual raw traces from relatively mildly affected mutant NMJs in Figure 9X (see Fig. 3 also), demonstrate how depression during repetitive activation could reduce release below the safety factor and cause failure of muscle activation.

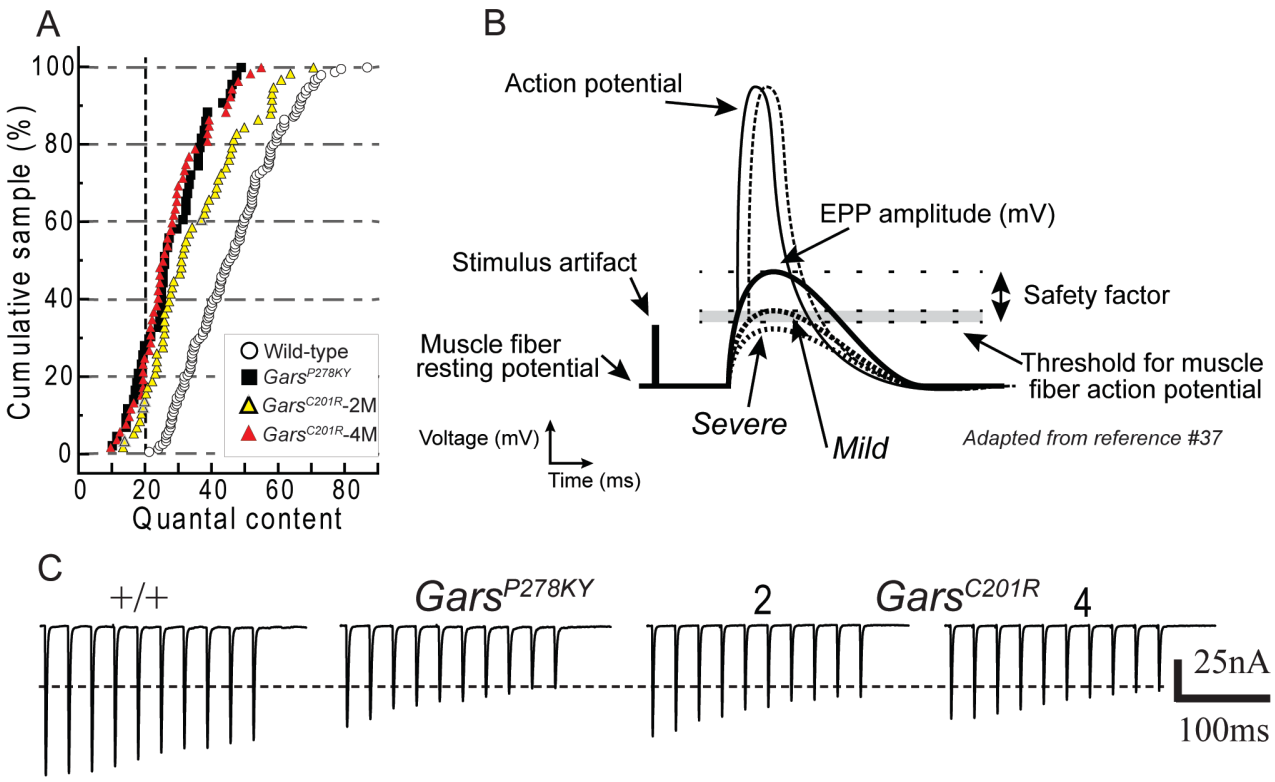

Figure 9. ***NMJ dysfunction in CMT2D mice.*** **(**A) Plot of individual values for quantal content calculated for NMJs of each of the four experimental groups reveal CMT2D distributions are shifted to lower values compared to combined wild-type sample (white). Release at a proportion of terminals is severely reduced (≤20, left of dashed vertical line), while the majority is mildly or moderately affected with quantal content values shifted to the left of the wild-type mean (~50), while the highest wild-type values (60-90) are largely absent for mutant NMJs. Note also, the 2 to 4 month progression at *Gars*^{C201R} NMJs (yellow vs. red) with the latter overlapping the distribution for severe *Gars*^{P278KY}. In (B) we show a hypothetical model of how the widespread NMJ dysfunction could produce variable and intermittent muscle weakness in CMT2D. Normal wild-type NMJs have a significant safety factor such that EPCs reliably depolarize the muscle above the threshold for an action potential (AP). In the CMT2D mice, terminals with a mild/moderate reduction in release (mild) would have a reduced safety factor and EPCs may intermittently fail to initiate an AP, while EPCs at severely affected terminals (severe) consistently do not reach the AP threshold. Note also, that because EPCs at affected terminals would initiate APs closer to their peak, APs would be slightly delayed (dotted action potential) and EMG recordings of an affected muscle would be expected to display significant "jitter", a clinical measure used to identify transmission failure. (C) Repetitive activation increases the extent and variability of transmission failure (Fig. 3). This scenario is depicted by example raw EPC traces of the 50 Hz response of moderately affected mutant terminals and typical wild-type. The horizontal dashed line through these traces indicates the EPC amplitude equivalent to a quantal content of 20 for the wild-type NMJ (equivalent to vertical dashed line in A). This cutoff was selected because all values measured at wild-type NMJs exceeded it, while ~20% of the values for each mutant population were below it. For the 50Hz trains shown wild-type the amplitude of final EPCs persists well above this level, but depression at mutant NMJs is sufficient to approach this value for the 4-5 final EPCs.

CHAPTER 3

THE INTEGRATED STRESS RESPONSE CONTRIBUTES TO TRNA SYNTHETASE-MEDIATED PERIPHERAL NEUROPATHY IN MICE

Abstract

Dominant mutations in glycyl-tRNA synthetase (*GARS*) cause CMT type 2D (CMT2D). How mutations in *GARS* cause neurodegeneration is unclear, but impaired translation has emerged as a potential toxic gain-of-function mechanism based on work with *Drosophila*. To test this mechanism in mice, we have profiled translation in motor neurons of mice with mutations in *Gars* that are validated as CMT2D models. *In vivo*, cell type-specific, fluorescent non-canonical amino acid-tagging (FUNCAT) has revealed reduced translation in motor neuron cell bodies of mutant *Gars* mice. To complement the protein analysis, i*n vivo* ribosome-tagging from mutant *Gars* motor neuron cell bodies was used to identify mRNAs undergoing translation. This revealed an upregulation of transcripts associated with the integrated stress response, including ATF4 and several of its gene targets. Using RNAScope *in situ* hybridization, we show that (1) activation of the stress response occurs in approximately 70% of mutant motor neurons, (2) most gamma motor neurons do not show this response, (3) large-medium fiber mechanosensitive and proprioceptive sensory neurons in dorsal root ganglia also upregulate the stress response, and (4) no other cell types in the spinal cord or dorsal root ganglia activate this response. The stress response is also activated in alpha motor neurons of mutant Yars-E196K mice, a model of dominant intermediate CMT type C. Genetic experiments reveal that removing GCN2, a kinase that activates the stress response, from mutant *Gars* mice prevents expression shuts off expression of the stress response and ATF4 gene targets. Removing GCN2 also significantly alleviates neuropathy, resulting in increased body weight, improved grip strength, less denervation at the neuromuscular junction, increased nerve conduction velocity, and less

motor axon loss. Because chronic stress response activation is detrimental to motor neurons in this disease context, inhibiting GCN2 in human patients with mutations in tRNA synthetase genes may be beneficial.

Introduction

Charcot-Marie-Tooth disease (CMT) is a debilitating inherited peripheral neuropathy resulting in progressive distal muscle weakness, atrophy, and loss of sensation (Saporta and Shy 2013a). CMT is genetically heterogeneous, with thousands of mutations in over 80 different genes leading to demyelinating or axonal forms (Timmerman, Strickland, and Zuchner 2014). There are genetically similar subgroups, including the largest protein family implicated in the disease, the tRNA synthetases (ARSs). ARSs are the enzymes responsible for aminoacylation of tRNAs during translation and are therefore ubiquitously expressed and essential proteins. Dominant mutations in at least five ARSs cause axonal forms of CMT, including glycyl ARS (GARS), tyrosyl ARS (YARS), histidyl ARS (HARS), tryptophanyl ARS (WARS), and alanyl ARS (AARS) (Antonellis and Green 2008). How mutations in ARSs cause CMT is unclear, however, the overall similar clinical presentation of patients suggests shared disease mechanisms (Wei, Zhang, and Yang 2019).

Disruption of the canonical aminoacylation function of ARSs is an obvious candidate. However, while some CMT-associated mutations do impair aminoacylation, some do not (Griffin et al. 2014; Xie et al. 2007; Froelich and First 2011). In humans, only dominant mutations in ARSs cause CMT, whereas recessive or bi-allelic loss-of-function mutations cause multi-system syndromes that may or may not include peripheral neuropathy (Boczonadi, Jennings, and Horvath 2018). Work in mice also argues against loss of aminoacylation function as the cause of CMT. Mice with a heterozygous gene-trap allele in the *Gars* gene, resulting in mRNA expression levels around 50% of wild-type, show no signs of neuropathy, suggesting that one loss-of-function allele is not sufficient to cause CMT (Seburn et al. 2006). In two well-established mouse models of CMT type 2D (CMT2D) , overexpression of wild-type *Gars* at

levels resulting in a greater than 10-fold increase in aminoacylation activity fail to rescue neuropathy (Motley et al. 2011b). Perhaps most convincingly, allele-specific knockdown of mutant *Gars* using RNAi almost completely prevents onset of neuropathy in multiple mouse models (Morelli, et al., submitted). Thus, a toxic gain-of-function mechanism is most consistent with human clinical data and mouse genetic experiments.

Two notable gain-of-function mechanisms have been proposed: (1) He, et al shows that binding of some mutant human and mouse forms of GARS to Neuropilin 1 and corresponding antagonism of VEGF signaling contributes to CMT2D neuropathy (He et al. 2015). (2) Gain-of-function impairments in translation are supported by work in *Drosophila*, in which overexpressing human mutant *GARS* over and above normal expression of wild-type *drosophila-gars* in motor and sensory neurons causes a peripheral neuropathy that correlates with decreased translation rates. Overexpression of human mutant *YARS* also reduces translation in peripheral neurons. In addition, genetic reduction of translation in sensory and motor neurons is sufficient to cause neuropathy (Niehues et al. 2015).

Because all ARSs participate in translation, impairment in this process is an attractive disease mechanism to test in mammalian models of tRNA synthetase-associated CMT. To this end, we have performed *in vivo*, cell type-specific translational and transcriptional profiling in motor neurons of three well-established mouse models of CMT2D (Seburn et al. 2006; Achilli et al. 2009a) (Morelli, et al., submitted). This profiling reveals impaired translation in mutant *Gars* motor neurons and the selective activation of the integrated stress response (ISR) in the largest motor and sensory peripheral neurons. Activation of the ISR occurs through the translational homeostasis-sensing kinase, GCN2, indicating that GCN2 could be responding to impairments in translation. Genetic removal of GCN2 kinase significantly alleviates mutant *Gars* neuropathy, suggesting that chronic activation of the ISR contributes to CMT2D. The ISR is also activated in motor neurons of mice with mutations in *Yars*, a model of dominant intermediate CMT type C.

Together, these data support impairments in translation as a toxic gain-of-function disease mechanism in mice with dominant mutations in *Gars* and *Yars*.

Results

Translation is Impaired in Mutant *Gars* Motor Neurons

We performed our first translational profiling experiments in two well-established CMT2D mouse models, the relatively mild $Gars^{C201R/+}$, and the more severe $Gars^{P278KY/+}$ (Achilli et al. 2009a; Seburn et al. 2006). To evaluate translation in motor neurons *in vivo*, we performed fluorescent non-canonical amino acid-tagging (FUNCAT), a technique which allows for the visualization and quantification of newly synthesized protein. A mouse engineered to express a Cre-inducible form of bacterial methionyl-ARS ($MARS^{L274G}$), which loads the methionine analog, azidonorleucine (ANL), onto cognate tRNA was crossed to the choline acetyltransferase-Cre (*ChAT*-Cre) driver mouse line to induce transgene expression in motor neurons (Alvarez-Castelao et al. 2017). Unlike methionine, ANL contains an azide group which undergoes copper catalyzed azide-alkyne cycloaddition in the presence of an alkyne-conjugated substrate. ANL was delivered as an intraperitoneal injection of 400mg/kg body weight in $MARS^{L274G}$;*ChAT*-Cre mice on a $Gars^{+/+}$, $Gars^{P278KY/+}$, or $Gars^{C201R/+}$ background. Following 8 hours of ANL incorporation into proteins, the copper-catalyzed cycloaddition reaction was performed using an alkyne-conjugated fluorophore directly on spinal cord sections, and intensity of fluorescence quantitatively measures abundance of newly translated protein in motor neurons (Figure 10 A).

ANL incorporation in $Gars^{+/+}$ spinal cord is specific to motor neurons of the ventral horn (Figure 10 B), with the exception of *ChAT*-expressing pre-sympathetic ganglionic neurons in thoracic sections that can be easily distinguished from motor neurons (not shown). Thus, abundance of newly translated protein can be measured reliably in motor neuron populations of cervical, thoracic, lumbar, and sacral spinal cord. At 8 weeks of age, well past disease onset in both CMT2D models, $Gars^{C201R/+}$ and $Gars^{P278KY/+}$ motor neurons show reduced fluorescence compared to $Gars^{+/+}$ in all regions of the spinal cord (Figure 10 C-E). The milder $Gars^{C201R/+}$

mouse model showed a ~55-60% reduction in all motor neuron populations (Figure 10 F). The more severe *Gars*$^{P278KY/+}$ showed a ~60% reduction in cervical, thoracic, and lumbar motor neurons, and a ~70% reduction in sacral motor neurons (Figure 10 G). These results indicate that translation is severely impaired in *Gars*$^{C201R/+}$ and *Gars*$^{P278KY/+}$ motor neurons.

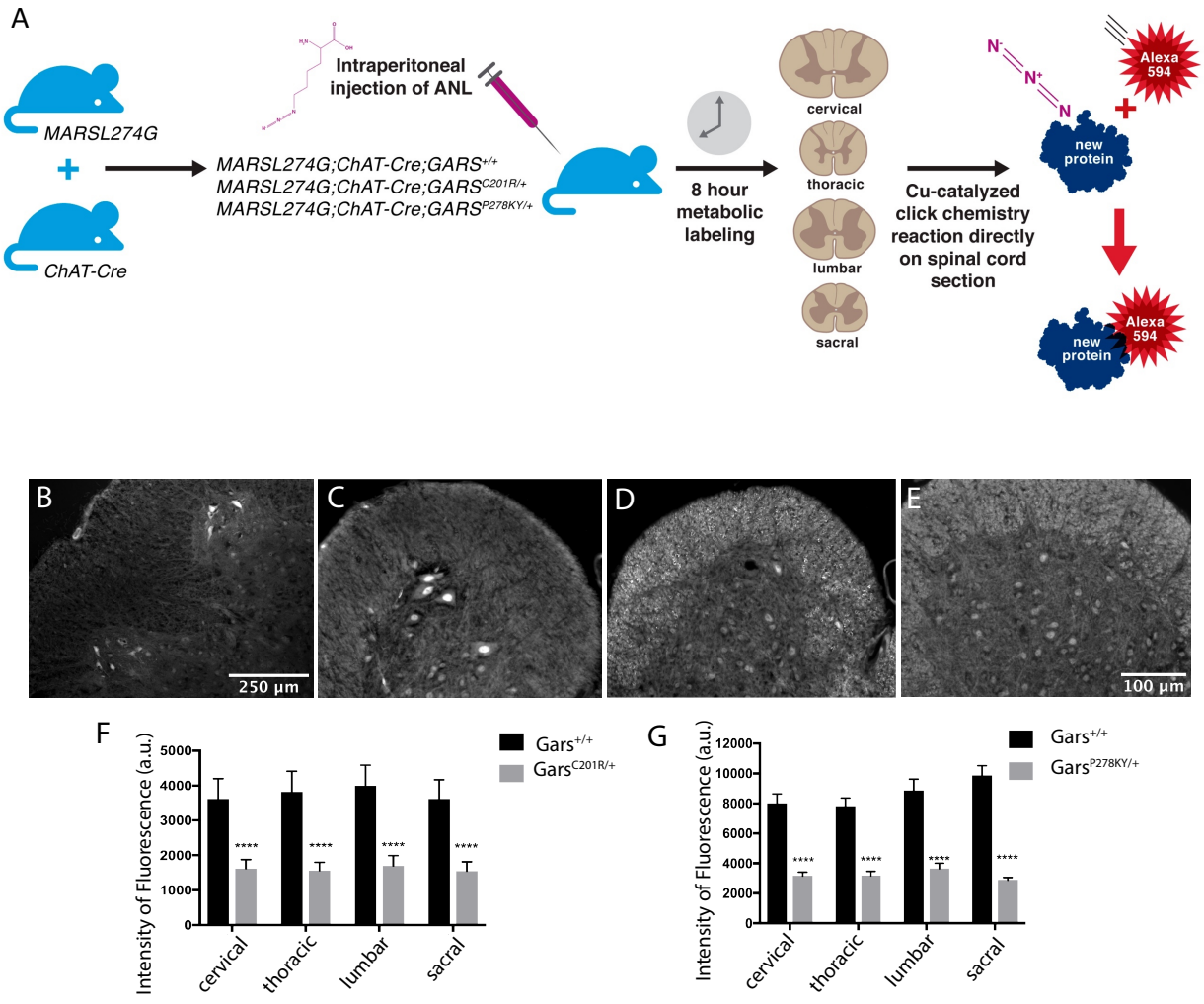

Figure 10. *In vivo* fluorescent non-canonical amino acid-tagging reveals impaired translation in mutant *Gars* motor neurons. (A) Overview of FUNCAT protocol. MARS^{L274G};ChAT-Cre mice are injected with 400mg/kg body weight ANL and metabolic labeling occurs for 8 hours. Cervical, thoracic, lumbar, and sacral regions of the spinal cord are then cryo-sectioned and copper-catalyzed click chemistry is performed directly on the slide. Proteins tagged with ANL react with alkyne-conjugated Alexa594 and are fluorescently labeled. (B) Within the spinal cord FUNCAT labeling is specific to motor neurons of the ventral horn. 10x image. (C) Newly synthesized protein in *Gars*$^{+/+}$, (D) *Gars*$^{C201R/+}$, and (E) *Gars*$^{P278KY/+}$ sacral motor neurons. 20x images. (F) Translation, as represented by intensity of fluorescence, is decreased in *Gars*$^{C201R/+}$ motor neurons by approximately 55-60% compared to *Gars*$^{+/+}$. (G) Translation is decreased by approximately 60% in *Gars*$^{P278KY/+}$ cervical, thoracic, and lumbar motor neurons, and by approximately 70% in sacral motor neurons. Analysis was performed on 3 females and 3 males per genotype at 8 weeks of age. Values in F and G are the sum of fluorescence for all 6 animals per genotype ± SD. *****=p<.0001. Scale bar in E also applies to C and D.

To determine if translation is also impaired pre-disease onset, we performed FUNCAT in 2 week-old *Gars*$^{C201R/+}$ mice, a time just before any overt signs of neuropathy are evident. Although there are trends of reduced fluorescence in all *Gars*$^{C201R/+}$ motor neuron populations, none has a reduction that amounts to a statistical difference from *Gars*$^{+/+}$ (Supplemental Figure 1 A-C). These data indicate that impairments in translation are just starting to manifest at this early timepoint, and could correlate with disease onset.

Because mutant *Gars* is expressed in every cell type of the body, we asked if translation is impaired in other tissue types unaffected by disease. To measure translation in the liver and heart we turned to puromycin labeling. Puromycin is a bacterial metabolite that structurally resembles an aminoacylated tRNA. Incorporation into nascent polypeptide chains causes translation termination, and blotting with a puromycin antibody provides a quantitative measure of translation. We injected mice with 60mg/kg body weight puromycin and allowed it to incorporate into nascent polypeptides for 1 hour. Mice treated with puromycin show a smear of anti-puromycin-labeled protein in tissues, while untreated mice show no smear (Supplemental Figure 2 A). We were unable to find evidence of impaired translation in liver or heart tissue of *Gars*$^{P278KY/+}$ or *Gars*$^{C201R/+}$ mice, or in *Gars*$^{delETAQ/+}$ mice that contain a mutation found in a young CMT2D patient (Supplemental Figure 2 B,C) (Morelli, et al; submitted 2019). These experiments indicate that in mice, impairments in translation are restricted to cell types affected by disease.

Motor Neuron Translational and Transcriptional Gene Expression Signatures are Shared Among Multiple *Gars* Alleles, Including the Human Mutation, *Gars*$^{delETAQ/+}$

To determine which mRNA species are undergoing differential translation in mutant *Gars* motor neurons we performed *in vivo* ribosome-tagging (RiboTagging). RiboTag mice contain a transgene consisting of a loxP-flanked, triple HA-tagged ribosomal protein, RPL22 (Sanz et al. 2009). When used in combination with *ChAT*-Cre, HA-RPL22 can be immunoprecipitated from motor neurons with anti-HA antibody and the mRNA presumably undergoing active translation at

the ribosome is eluted and sequenced. When mRNA immunoprecipitated from *Gars*$^{+/+}$;HA-RPL22;*ChAT*-Cre spinal cords is compared to nonspecific mRNA immunoprecipitated from no-Cre controls, motor neuron-enriched mRNA encompassed 1,907 transcripts, including the well-known markers ChAT (enriched ~15-fold) and chondrolectin (Chodl) (enriched ~33 fold), as well as additional markers of projection neurons including neurofilament heavy, medium, and light chains (Nefh, Nefm, Nefl) (enriched ~6, 8, and 9-fold, respectively). In contrast, the 3,725 transcripts more abundant in nonspecific spinal cord pulldowns are correspondingly de-enriched in motor neurons, and include the astrocytic marker glial fibrillary acid protein (GFAP) (de-enriched ~4-fold) and the oligodendrocytic markers myelin oligodendrocyte protein (mog) (de-enriched ~3-fold) and myelin associated protein (mag) (de-enriched ~4-fold) (Figure 11 A).

As an additional test of the reliability of RiboTagging, as well as to provide a disease-relevant comparison to mutant *Gars* motor neurons, we sequenced ribosome associated mRNA from *Gars*$^{+/+}$ motor neurons of the spinal cord 4 days after unilateral sciatic nerve crush. 144 transcripts were upregulated and 68 downregulated in *Gars*$^{+/+}$ motor neurons after nerve crush compared to those from *Gars*$^{+/+}$ mice that had not undergone the crush surgery (Figure 11 B). Among the top 10 upregulated transcripts after crush were small proline-rich repeat protein 1A (Sprr1a), activating transcription factor 3 (Atf3), and neuropeptide tyrosine (Npy), all known to be markers of regeneration in peripheral neurons after injury (Starkey et al. 2009; Linda, Skold, and Ochsmann 2011; Zhang et al. 1993). These experiments confirm reliability of the RiboTagging technique, as well as create a complete catalog of motor neuron ribosome-associated mRNA following sciatic nerve crush for comparison against mutant *Gars*.

We next compared ribosome-associated mRNA immunoprecipitated from *Gars*$^{+/+}$ motor neurons to that from *Gars*$^{C201R/+}$ or *Gars*$^{P278KY/+}$ motor neurons at 8 weeks of age, the same age at which we performed FUNCAT. Compared to *Gars*$^{+/+}$, *Gars*$^{C201R/+}$ motor neurons showed 1,978 upregulated and 126 downregulated transcripts with an absolute log FC of 1.5 or greater and a FDR and p value of less than .05 (Figure 11 C). *Gars*$^{P278KY/+}$ motor neurons contained 633

upregulated and 237 downregulated transcripts that also met these requirements (Figure 11 D). The top upregulated transcripts in *Gars*$^{C201R/+}$ and *Gars*$^{P278KY/+}$ motor neurons represent a distinct and reproducible disease signature, as none are in common with the top upregulated transcripts following sciatic nerve crush, but over half are shared between the two mutant *Gars* alleles (Figure 11 E). We also performed RiboTagging in 2 week-old, pre-disease onset *Gars*$^{C201R/+}$ motor neurons, and confirmed early upregulation of six of the top upregulated transcripts identified at 8 weeks (Supplemental Figure 2 A). Thus, before neuropathy is detectable, gene expression changes are already taking place.

To determine if the translational changes seen in mutant *Gars* motor neurons are also occurring at the transcriptional level, we performed whole spinal cord RNA sequencing on 8 week old *Gars*$^{C201R/+}$ and *Gars*$^{P278KY/+}$ mice, as well as the additional *Gars*$^{delETAQ/+}$ model. We observed a striking similarity among the top 10 upregulated transcripts from both RiboTagging and RNA sequencing experiments, and among all three mouse models (Figure 11 E). These data suggest that gene expression changes are present at both translational and transcriptional levels, and that the same disease mechanism is likely occurring with all three mutations in *Gars*, including the human mutation, delETAQ.

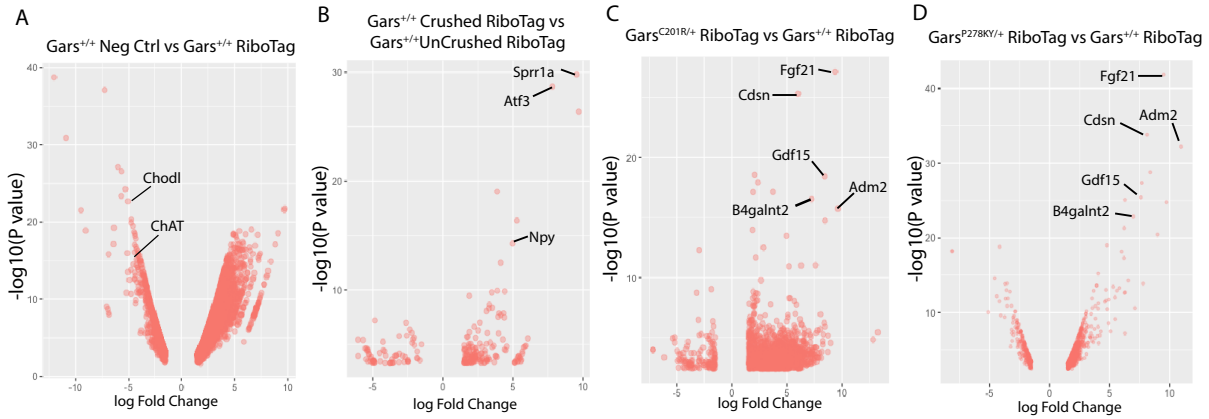

E

GarsC201R/+ motor neurons	P Value	GarsP278KY/+ motor neurons	P Value	GarsC201R/+ spinal cord	P Value	GarsP278KY/+ spinal cord	P Value	GarsdelETAQ/+ spinal cord	P Value
Fgf21	7.3E-28	Fgf21	1.4E-42	Cfd	1.4E-137	Fgf21	6.1E-64	Fgf21	1.2E-160
Cdsn	4.9E-26	Cdsn	1.6E-34	Adipoq	4.0E-130	Cdsn	2.7E-52	Myh4	3.1E-103
Atf4	2.7E-19	Adm2	5.93E-33	Fgf21	1.0E-128	Adm2	8.2E-23	Cdsn	1.8E-90
Gdf15	3.8E-19	Cass4	1.6E-29	Fabp4	1.8E-119	Gdf15	9.7E-15	P2rx3	2.2E-70
Psph	1.2E-18	Fev	4.6E-28	Plin1	1.1E-81	B4galnt2	1.9E-13	B4galnt2	6.8E-47
Phgdh	7.1E-18	Cox6a2	8.2E-26	Cidec	5.5E-78	P2rx3	4.7E-07	Plac9b	1.1E-47
Clic4	7.3E-18	Gdf15	3.8E-26	Ces1d	8.5E-72	Taf71	2.8E-07	Duxbl1	1.6E-41
B4galnt2	3.0E-17	Ostn	1.7E-25	Cdsn	1.5E-49	Fev	2.3E-05	Fev	7.7E-25
Adm2	1.8E-16	B4galnt2	1.4E-23	B4galnt2	2.4E-20	Steap1	1.6E-04	Cass4	3.6E-23
Cox6a2	1.8E-15	Cyb5r2	5.0E-22	Mup10	2.4E-20			Mylk2	3.6E-23

Figure 11: *In vivo* characterization of ribosome-associated mRNA in motor neurons using RiboTagging. (A) Ribosome-associated mRNA enriched in *Gars*$^{+/+}$ motor neurons vs whole spinal cord. Genes plotted have a log FC≥ |1.5|, FDR<.05 and p value <.05. There are 1907 enriched genes in motor neurons (log FC<-1.5; p value<.05) and 3725 genes enriched in non-motor neuron cell types of the spinal cord (log FC>1.5; p value<.05). Analysis was performed on 4-5 animals per genotype at 8 weeks of age. (B) Ribosome-associated mRNA up- or downregulated in *Gars*$^{+/+}$ motor neurons 4 days after unilateral sciatic nerve crush. 144 genes are upregulated (log FC>1.5; p value<.05) and 68 are downregulated (log FC<-1.5; p value<.05). Analysis was performed on 2 animals per condition at 8 weeks of age. (C) Ribosome-associated mRNA up- or downregulated in *Gars*$^{C201R/+}$ motor neurons compared to *Gars*$^{+/+}$. 1978 genes are upregulated (log FC>1.5; p value<.05) and 126 are downregulated (log FC<-1.5; p value<.05). Analysis was performed on 5-6 animals per genotype at 8 weeks of age. (D) Ribosome-associated mRNA up- (log FC>1.5; p value<.05) or downregulated (log FC<-1.5; p value<.05) in *Gars*$^{P278KY/+}$ motor neurons compared to *Gars*$^{+/+}$. 633 genes are upregulated and 237 are downregulated. Analysis was performed on 4-5 animals per genotype at 8 weeks of age. (E) Table of the top 10 upregulated transcripts based on p value significance. All transcripts in red are present in at least 2 datasets. 3 males and 3 females per genotype at 8 weeks of age were used for each RNA sequencing experiment.

Alpha Motor Neurons are the Only Cell Type to Express Disease Signature Within the Spinal Cord

To validate our gene expression data, as well as to address questions of cell type-specificity within the spinal cord, we used RNAscope *in situ* hybridization. All motor neurons were labelled with ChAT and probed for expression of five of the top upregulated transcripts from RiboTagging and RNA sequencing data that were in common among multiple *Gars* models. These transcripts were fibroblast growth factor 21 (Fgf21), growth differentiation factor 15 (Gdf15), adrenomedullin 2 (Adm2), corneodesmosin (Cdsn), and Beta-1,4-N-Acetyl-Galactosaminyltransferase 2 (B4galnt2). No or very little expression of the five transcripts were seen in any cell types within $Gars^{+/+}$ spinal cord (Figure 12 A,B). In contrast, robust upregulation of all five transcripts was confirmed in $Gars^{P278KY/+}$ motor neurons, but in no other cell type of the spinal cord (Figure 12 A,B). Fgf21 is a metabolic regulator most highly expressed by the liver, but also expressed from skeletal muscle and central nervous system neurons upon mitochondrial dysfunction (Fisher and Maratos-Flier 2016). Together with Fgf21, Gdf15 is also known to signal mitochondrial dysfunction, but neither has ever been shown to be expressed from motor neurons. We also show Cdsn expression from motor neurons for the first time. Cdsn is a component of tight junctions in the skin, but is also highly upregulated in $Gars^{P278KY/+}$ motor neurons.

Interestingly, only about 70% of $Gars^{P278KY/+}$ motor neurons express the disease signature (Figure 12 C). Spinal cord motor neurons can be divided into gamma and alpha populations. Gamma motor neurons are smaller, provide sensitivity to muscle stretch, and comprise about 30% of the total population. Alpha motor neurons are larger, provide muscle force, and make up the resulting 70% (Stifani 2014). Because approximately 70% of mutant *Gars* motor neurons express the disease signature and because in $Gars^{P278KY/+}$ mice the largest motor axons are preferentially lost, we hypothesized that alpha motor neurons were the population showing these gene expression changes and that gamma motor neurons were correspondingly resistant (Seburn

et al. 2006). To test this hypothesis we labeled all motor neurons with ChAT, used Fgf21 as our marker of the disease signature, and labeled gamma motor neurons with Err3 (Friese et al. 2009). In every case where a ChAT-positive motor neuron showed no expression of Fgf21 (28.9% $\pm$ 4.6) of the total motor neuron population), it was clearly labeled with Err3, indicating that gamma motor neurons are resistant to expressing the disease signature and that alpha motor neurons are the population most susceptible (Figure 12 D,E).

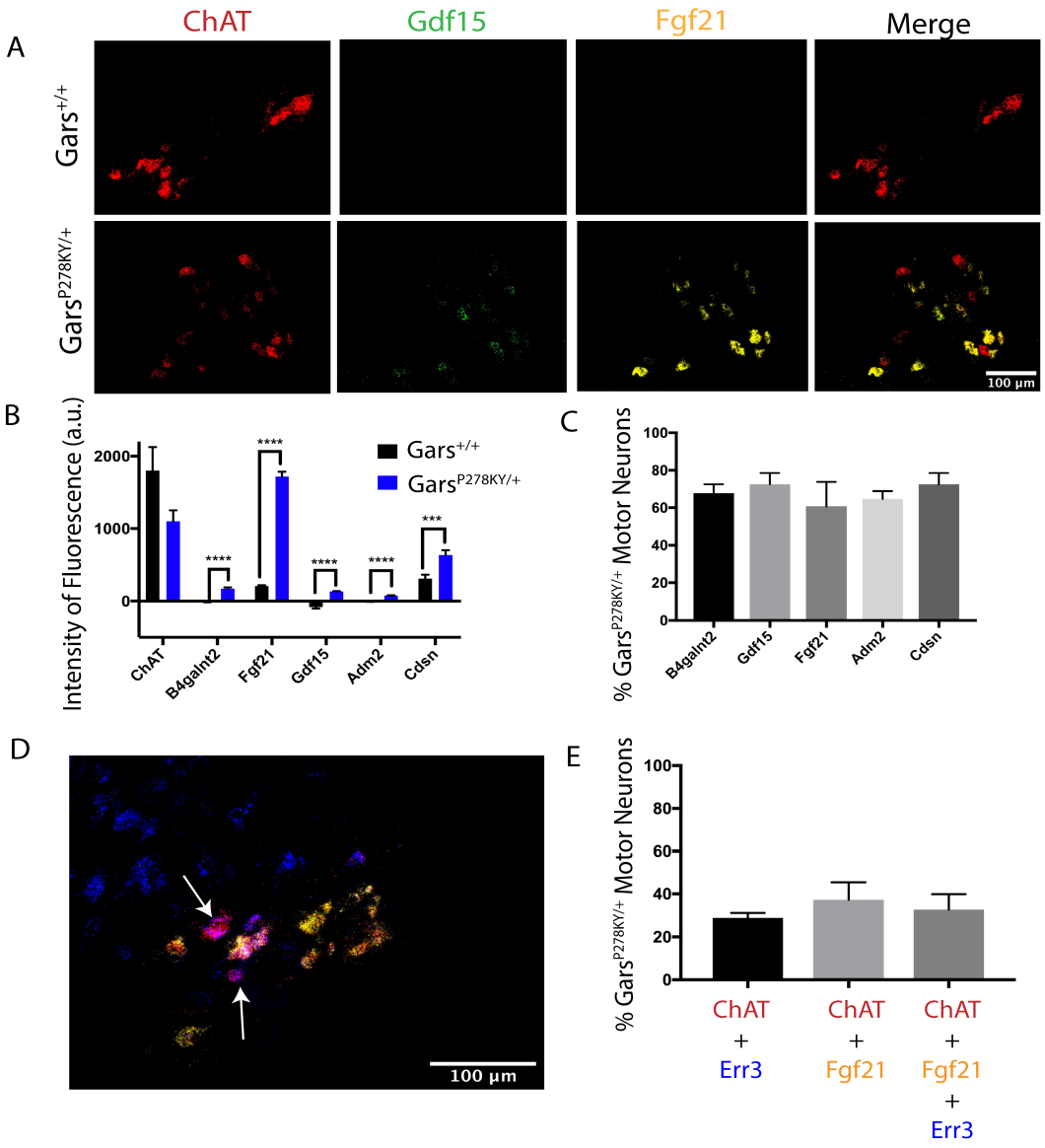

Figure 12: Transcriptional signature is specific to alpha motor neurons within the spinal cord. (A) Representative images of RNAscope *in situ* hybridization using probes for 5 of the upregulated transcripts identified from Ribotagging and RNA sequencing experiments. *Gars*$^{+/+}$ motor neurons are labeled with ChAT (red) but show no expression of disease-related transcripts, Gdf15 (green) or Fgf21 (yellow). *Gars*$^{P278KY/+}$ motor neurons labeled with ChAT (red) show robust upregulation of Gdf15 (green) and Fgf21 (yellow) in a subset of motor neurons. Some ChAT-labelled motor neurons do not show expression of disease-related transcripts (white arrows) (B) Quantification of fluorescence in *Gars*$^{+/+}$ and *Gars*$^{P278KY/+}$ motor neurons. (C) Approximately 70% of *Gars*$^{P278KY/+}$ motor neurons expressed the 5 disease-associated transcripts. (D) All *Gars*$^{P278KY/+}$ motor neurons labeled with ChAT that did not express Fgf21 were labeled with the gamma motor neuron marker, Err3 (white arrows). (E) Quantification of E. Note that some Err3 labeled motor neurons do express Fgf21, probably indicating that Err3 is also expressed in some alpha motor neurons. Analysis was performed using 4 animals per genotype at 8 weeks of age. Values in B are the sum of fluorescence intensity in all 4 animals per genotype ± SD. Values in C and E are mean ± SD. *** = p<.001, **** = p<.0001.

Medium-large Fiber Sensory Neurons Within Dorsal Root Ganglia Express Disease Signature

Because *Gars*$^{P278KY/+}$ mice experience sensory axon degeneration we wondered if the same disease mechanism could be occurring in this neuronal population as in motor neurons. We reasoned that if this was true, sensory neurons would express a similar gene expression signature to motor neurons. To test this we probed for the same five disease-associated transcripts in dorsal root ganglia as in the spinal cord. Again, all five transcripts showed no expression in *Gars*$^{+/+}$ sensory neurons, but a robust upregulation only in a subset of *Gars*$^{P278KY/+}$ sensory neurons (Figure 13 A,B).

In light of our findings in the spinal cord, we tested if expression of the disease signature was associated with neuronal size. Small fiber sensory neurons were labeled with peripherin (Prph) (red), medium-large fiber sensory neurons were labeled with neurofilament heavy chain (Nefh) (green), and Ffg21 was used as the disease marker (Ferri et al. 1990). Only Nefh-positive sensory neurons express Fgf21, indicating that larger sensory neurons are more susceptible to these disease-associated gene expression changes and smaller sensory neurons are resistant (Figure 13 C,D). Because not all Nefh-positive sensory neurons showed expression of Fgf21, we next tested if there was any functional correlation. Mechanosensitive and proprioceptive sensory neurons both express Nefh, but proprioceptive neurons can be distinguished by the additional expression of parvalbumin (Pvalb) (Le Pichon and Chesler 2014). In *Gars*$^{P278KY/+}$ dorsal root ganglia, both mechanosensitive and proprioceptive sensory neurons express Fgf21 (Figure 13 E,F) . Thus, as in the spinal cord, within the dorsal root ganglion, expression of the disease signature is exclusive to sensory neurons and correlates with neuron size.

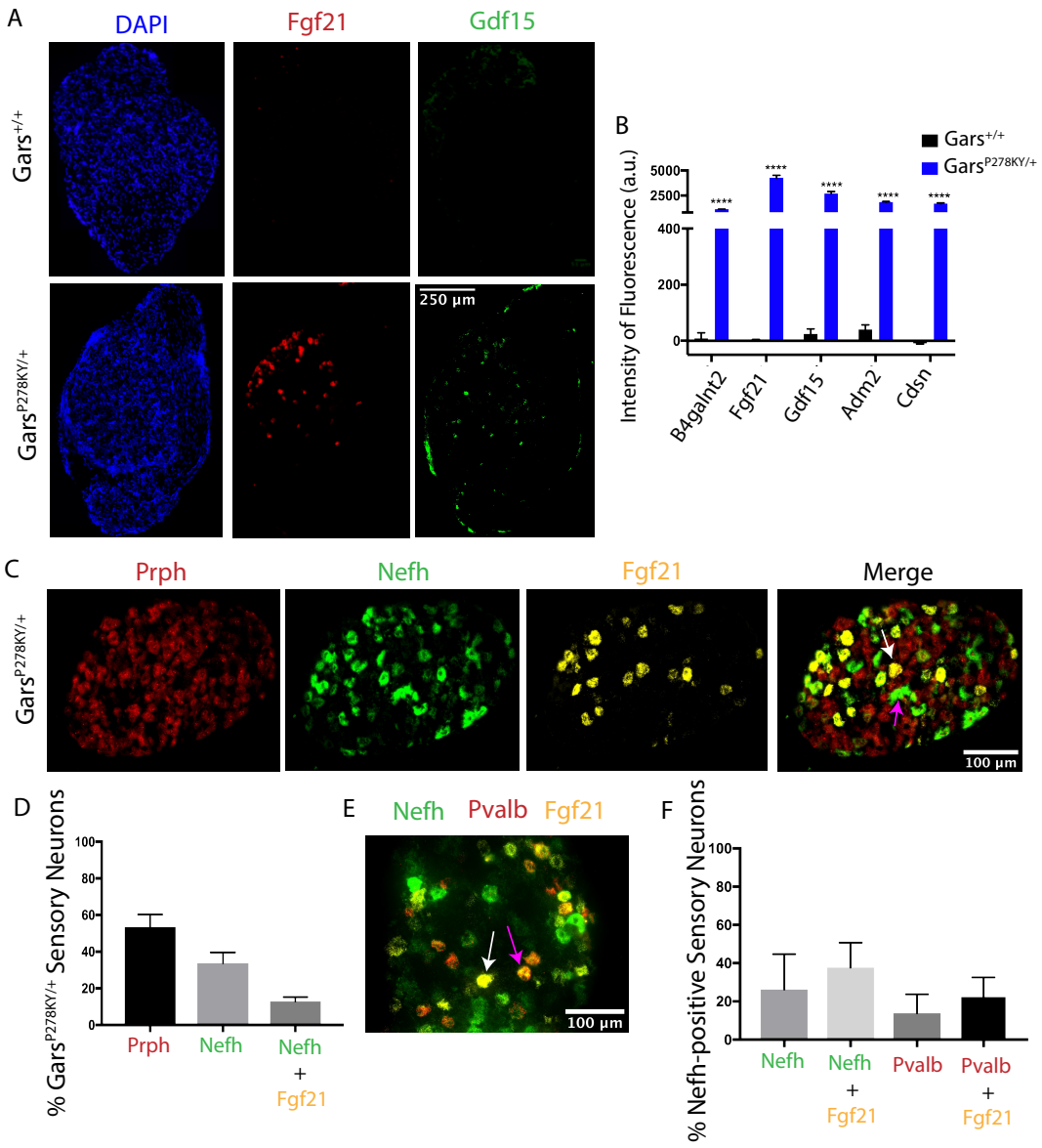

Figure 13: Transcriptional signature is upregulated in medium-large fiber mechanosensitive and proprioceptive sensory neurons in *Gars*$^{P278KY/+}$ lumbar dorsal root ganglia. (A) No expression of disease-associated transcripts in *Gars*$^{+/+}$ dorsal root ganglia. Expression of Fgf21 (red) and Gdf15 (green) in a subset of *Gars*$^{P278KY/+}$ dorsal root ganglia. (B) All five transcripts upregulated in *Gars*$^{P278KY/+}$ motor neurons are also upregulated in sensory neurons. Quantification of A and B. (C) Peripherin (Prph) labels small fiber sensory neurons (red) and Neurofilament-heavy chain (Nefh) labels medium-large fiber neurons (green). Fgf21 expression is only seen in Nefh-expressing neurons (white arrow), although not in all (pink arrow). (D) Quantification of D. (E) Mechanosensitive sensory neurons are labeled solely with Nefh (green), while proprioceptive neurons are labeled with Nefh and parvalbumin (Pvalb) (green and red). Fgf21 expression is seen in mechanosensitive (white arrow) and proprioceptive (pink arrow) sensory neurons. (F) Quantification of F. Analysis used 4 animals per genotype at 8 weeks of age. Values in B are the sum of fluorescence in all 4 animals per genotype ± SD. Values in D and F are mean ± SD. **** = p<.0001.

The Integrated Stress Response is Activated Through GCN2 Kinase in Mutant *Gars* Motor Neurons

To obtain a more global perspective of the mutant *Gars* gene expression signature, we performed Ingenuity Pathway Analysis (IPA) using upregulated genes with a log FC of 1.5 or greater and a p value of .05 or less from the $Gars^{P278KY/+}$ RiboTagging dataset. Among the top predicted upstream pathways was the integrated stress response (ISR) (Figure 14 A). The ISR is a highly conserved cell stress pathway found in all eukaryotic cells that can be triggered by a variety of intrinsic and extrinsic cell stressors, each through a distinct protein kinase. PERK is activated by ER stress, GCN2 by amino acid deprivation, PKR by viral infection, and HRI by heme deprivation (Pakos-Zebrucka et al. 2016). Activation of any one of these four kinases results in phosphorylation of the translation initiation factor, eIF2α, a subsequent reduction in cap-dependent mRNA translation, and upregulation of specific stress response genes through the transcription factor ATF4. We determined that many of the top upregulated transcripts in mutant *Gars* motor and sensory neurons are direct targets of ATF4, including Fgf21, Gdf15, Cdsn, Adm2, and B4galnt2, among others. Thus, the ISR is activated in mutant *Gars* motor and sensory neurons, and we next wanted to test which kinase was responsible for its activation.

Because the IPA also suggested amino acid deprivation as a predicted upstream pathway, we hypothesized that the ISR was being activated by GCN2 kinase. We tested this genetically by crossing GCN2 knockout mice ($Gcn2^{KO/KO}$) with $Gars^{P278KY/+}$ mice. We again probed for expression of the same five ATF4 target genes in the spinal cords of 8 week old mice. $Gars^{+/+}$ mice with GCN2 ($Gcn2^{+/+};Gars^{+/+}$) showed no expression of ATF4 target genes and $Gars^{P278KY/+}$ mice with GCN2 ($Gcn2^{+/+};Gars^{P278KY/+}$) showed robust upregulation in motor neurons (Figure 14 B,C). Genetic removal of GCN2 from $Gars^{P278KY/+}$ mice ($Gcn2^{KO/KO};Gars^{P278KY/+}$) completely shut off expression of all five ATF4 target genes in motor neurons (Figure 14 B,C). This was

confirmed with whole spinal cord RNA sequencing, which revealed that upon removal of GCN2 there are only 9 differentially expressed protein coding genes with established names between *Gars*$^{+/+}$ and *Gars*$^{P278KY/+}$ mice (*Gcn2*$^{KO/KO}$*;Gars*$^{+/+}$ vs *Gcn2*$^{KO/KO}$*;Gars*$^{P278KY/+}$) (Table 1).

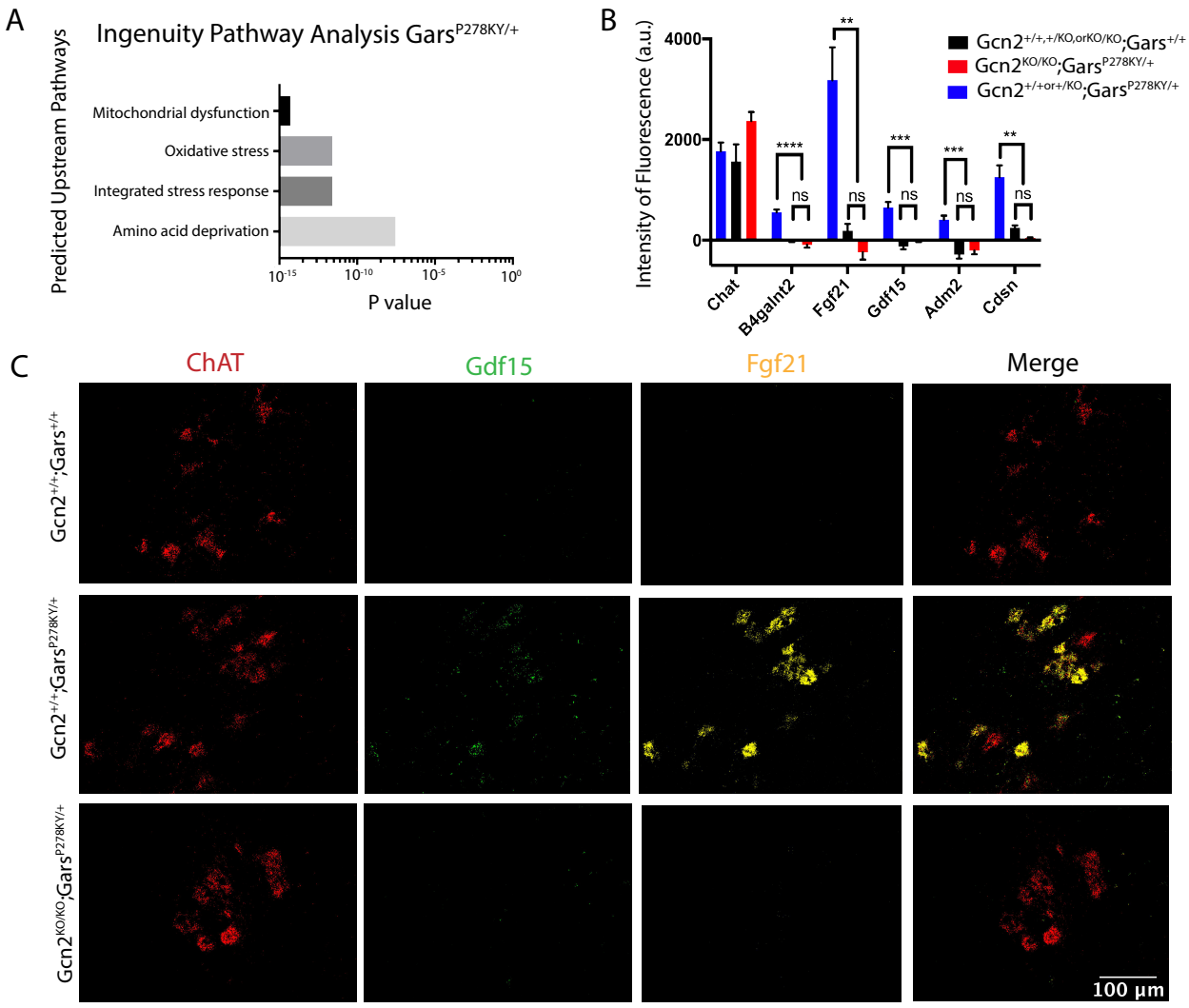

Figure 14: The integrated stress response is activated in *Gars*$^{P278KY/+}$ motor neurons through GCN2 kinase. (A) Ingenuity Pathway Analysis of upregulated ribosome-associated mRNA with log FC≥ 1.5 and FDR<.05 in *Gars*$^{P278KY/+}$ motor neurons. (B) Genetic removal of GCN2 kinase from *Gars*$^{P278KY/+}$ mice shuts off expression of ATF4 target genes in motor neurons. (C) *Gcn2*$^{+/+}$*;Gars*$^{+/+}$motor neurons show no expression of ATF4 target genes, while *Gcn2*$^{+/+}$*;Gars*$^{P278KY/+}$ motor neurons show robust upregulation. *Gcn2*$^{KO/KO}$*;Gars*$^{P278KY/+}$ motor neurons show no expression of ATF4 target genes. Analysis performed with 3 animals per genotype at 8 weeks of age. Values in B are mean ± SD. **= p<.01; ***= p<.001; ****= p<.0001.

Gene Name	logFC	P Value
Hmga1-rs1	11.48	1.8E-74
Lypd3	5.59	1.2E-21
Amd2	3.79	1.1E-40
Lad1	2.93	9.6E-14
Ect2l	2.46	3.4E-11
Myh3	1.67	6.7E-6
Tmsb15b2	1.55	6.9E-9
Calca	-2.0	7.15E-19
Tspan10	-2.4	2.13E-25

Table 1. Differentially Expressed Genes in $Gcn2^{KO/KO}$;$Gars^{P278KY/+}$ spinal cord versus $Gcn2^{KO/KO}$;$Gars^{+/+}$: There are only 7 upregulated and 6 downregulated established protein coding genes in $Gcn2^{KO/KO}$;$Gars^{P278KY/+}$ spinal cord compared to $Gcn2^{KO/KO}$;$Gars^{+/+}$. Analysis performed using 3-5 mice per genotype.

Genetic Removal of GCN2 Kinase Alleviates *Gars* Neuropathy

Whether activation of the ISR is helpful or harmful to cells is highly dependent upon cell type, disease context, and the length of activation of the response. For example, genetic removal of GCN2 kinase and subsequent shutdown of the ISR in a mouse model of rapid cerebellar ataxia exacerbates neurodegeneration (Ishimura et al. 2016). In contrast, genetic removal of GCN2 or PERK from APP/PS1 Alzheimer's disease mice prevents impairments in spatial memory and synaptic plasticity, indicating that long-lasting imbalances in translation contribute to chronic neurodegenerative diseases (Ma et al. 2013).

We found that homozygous genetic removal of GCN2 kinase significantly improves CMT2D neuropathy in mice. Both male (Figure 15 A) and female (not shown) $Gcn2^{KO/KO}$;$Gars^{P278KY/+}$ mice have body weights nearly restored to $Gars^{+/+}$ levels. Motor performance of mice is improved as measured by the wire hang test. $Gars^{+/+}$ mice with or without GCN2 ($Gcn2^{+/+,+/KO,\ or\ KO/KO}$;$Gars^{+/+}$) can hang on to an inverted wire grid for the duration of the test, 60 seconds, while $Gars^{P278KY/+}$ mice with GCN2 ($Gcn2^{+/+or+/KO}$;$Gars^{P278KY/+}$) struggle to hang on for even a few seconds. $Gcn2^{KO/KO}$;$Gars^{P278KY/+}$ mice have an increased latency to fall that approaches that of $Gcn2^{+/+,+/KO,\ or\ KO/KO}$;$Gars^{+/+}$ mice by 16 weeks of age (Figure 15 B).

Gcn2$^{KO/KO}$;*Gars*$^{P278KY/+}$ mice also have improved peripheral nerve function. At 8 weeks of age *Gcn2*$^{+/+,+/KO,\ or\ KO/KO}$;*Gars*$^{+/+}$ mice have an average sciatic nerve conduction velocity of 35.7m/s ± 6.6, *Gcn2*$^{+/+or+/KO}$;*Gars*$^{P278KY/+}$ have an average of 10.7 m/s ± 2.7, and *Gcn2*$^{KO/KO}$;*Gars*$^{P278KY/+}$ mice have an average of 23.9 m/s ± 1.3 (Figure 15 C). Improvements in conduction velocity persist through at least 16 weeks of age. At 16 weeks of age there is no longer a statistical difference between *Gcn2*$^{+/+,+/KO,\ or\ KO/KO}$;*Gars*$^{+/+}$ mice and *Gcn2*$^{KO/KO}$;*Gars*$^{P278KY/+}$ mice, as almost all *Gcn2*$^{KO/KO}$;*Gars*$^{P278KY/+}$ mice have conduction velocities well within the *Gcn2*$^{+/+,+/KO,\ or\ KO/KO}$;*Gars*$^{+/+}$ range (Supplemental Figure 4 A).

A degree of motor axon loss was also prevented by removing GCN2 from *Gars*$^{P278KY/+}$ mice. The motor branch of the femoral nerve contained more axons in *Gcn2*$^{KO/KO}$;*Gars*$^{P278KY/+}$ mice (448 ± 55) than in *Gcn2*$^{+/+or+/KO}$;*Gars*$^{P278KY/+}$ mice (398 ± 23) at 8 weeks of age (Figure 15 D,E), and by 16 weeks of age there was no longer a statistical difference between *Gcn2*$^{KO/KO}$;*Gars*$^{P278KY/+}$ and *Gcn2*$^{+/+,+/KO,\ or\ KO/KO}$;*Gars*$^{+/+}$ (Supplemental Figure 4B). Reduction in motor axon diameter was also partially rescued by removal of GCN2 at 8 weeks of age, and this effect persisted through at least 16 weeks of age (Figure 15 F and Supplemental Fig 4C).

Gars$^{P278KY/+}$ mice typically contain a large percentage of partially innervated or denervated neuromuscular junctions (NMJs) in the gastrocnemius muscle. NMJs were scored as fully innervated if the axon terminal (green) completely overlapped the post-synaptic muscle (red) (Figure 15 G), partially innervated if some of the muscle was without axon coverage (Figure 15 H), and denervated if the axon was entirely absent from the muscle (Figure 15 I). Morphologically, *Gcn2*$^{+/+,+/KO,\ or\ KO/KO}$;*Gars*$^{+/+}$ mice have NMJs with sharp staining in the classic "pretzel" shape. Fully innervated NMJs in *Gcn*$^{+/+\ or\ +/KO}$;*Gars*$^{P278KY/+}$ mice tend to be fragmented and often do not display the pretzel morphology. In contrast, fully innervated NMJs in *Gcn2*$^{KO/KO}$;*Gars*$^{P278KY/+}$ mice largely retained the pretzel morphology (Figure 15 J). Moreover, *Gcn2*$^{KO/KO}$;*Gars*$^{P278KY/+}$ mice had a larger percentage of fully innervated NMJs (66.7% ± 12.3)

and a smaller percentage of partially innervated (23.5% ± 9.7) and denervated (9.8% ± 8.2) NMJs compared to *Gcn*$^{+/+\ or\ +/KO}$;*Gars*$^{P278KY/+}$ (31.3% ± 19.9 fully innervated, 38.8% ± 11.3 partially innervated, and 29.9% ± 17.2 denervated) (Figure 15 K). This return to *Gcn2*$^{+/+,+/KO,\ or\ KO/KO}$;*Gars*$^{+/+}$ innervation status continues at least through 16 weeks of age (Supplemental Figure 4D).

These data demonstrate that chronic activation of the ISR through GCN2 is detrimental to motor neurons. Partial rescue of CMT2D neuropathy is achieved by genetic removal of GCN2 as analyzed at 8 weeks of age. This rescue does not appear to be a delay in the development of neuropathy, as neuropathy is still alleviated at 16 weeks of age. Because removal of GCN2 and deactivation of the ISR provides long-term alleviation of CMT2D neuropathy in mice, GCN2 may be a promising drug target for future therapeutics in humans.

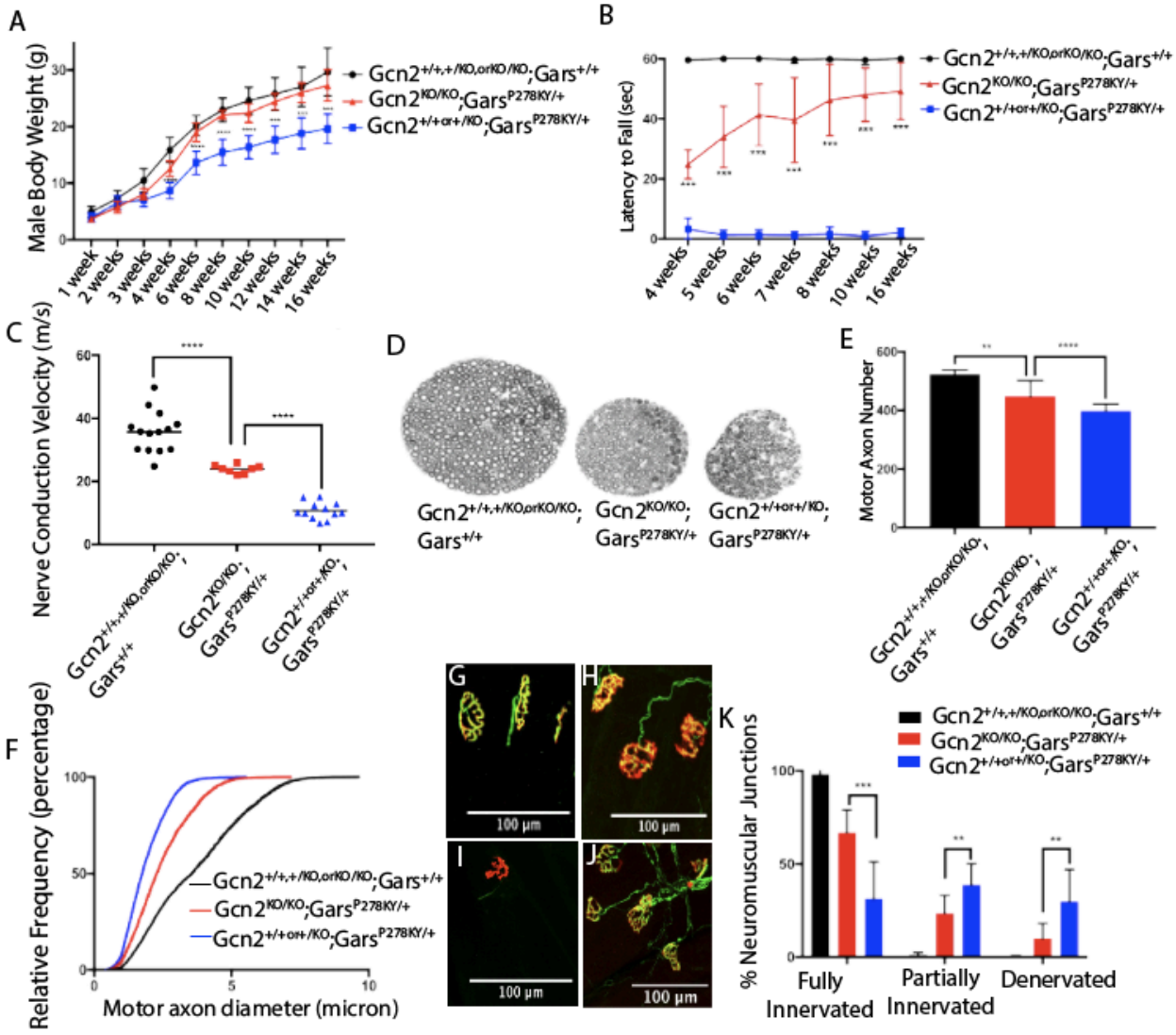

Figure 15: Genetic removal of GCN2 kinase alleviates *Gars*$^{P278KY/+}$ neuropathy. (A) Body weight of male *Gcn2*$^{KO/KO}$;*Gars*$^{P278KY/+}$ mice is significantly increased over *Gcn2*$^{+/+ \text{ or } +/-}$;*Gars*$^{P278KY/+}$. (B) *Gcn2*$^{KO/KO}$;*Gars*$^{P278KY/+}$ mice have improved motor function as measured by the wire hang test. Mice are place on an inverted grid and latency to fall is timed. The test is stopped after 60 seconds and the mean of 3 trials is reported for each day. Analysis performed with 18-22 mice per grouped genotype. (C) *Gcn2*$^{KO/KO}$;*Gars*$^{P278KY/+}$ mice have increased nerve conduction velocity of the sciatic nerve (23.9m/s ± 1.3) compared to *Gcn2*$^{+/+ \text{ or } +/KO}$;*Gars*$^{P278KY/+}$ (10.7m/s ± 2.7), although not completely restored to *Gcn2*$^{+/+,+/KO, \text{ or } KO/KO}$;*Gars*$^{+/+}$ (35.7m/s ± 6.6). Analysis performed with 8-14 mice per grouped genotype. (D) The motor branch of the femoral nerve in *Gcn2*$^{KO/KO}$;*Gars*$^{P278KY/+}$ mice is intermediate in size compared to *Gcn2*$^{+/+,+/KO, \text{ or } KO/KO}$;*Gars*$^{+/+}$ and *Gcn2*$^{+/+ \text{ or } +/-}$;*Gars*$^{P278KY/+}$. (E) Motor axon loss in the femoral nerve is partially rescued in *Gcn2*$^{KO/KO}$;*Gars*$^{P278KY/+}$ mice. *Gcn2*$^{KO/KO}$;*Gars*$^{P278KY/+}$ mice have an average of 448 ± 55 motor axons, compared to 523 ± 15 in *Gcn2*$^{+/+,+/KO, \text{ or } KO/KO}$;*Gars*$^{+/+}$ mice and 398 ± 23 in *Gcn2*$^{+/+ \text{ or } +/KO}$;*Gars*$^{P278KY/+}$ mice. Analysis performed with 13-14 mice per grouped genotype. (F) The diameter of all motor axons in the femoral nerve was measured. There is a higher frequency of smaller diameter axons in *Gcn2*$^{+/+ \text{ or } +/KO}$;*Gars*$^{P278KY/+}$ mice compared to *Gcn2*$^{+/+,+/KO, \text{ or } KO/KO}$;*Gars*$^{+/+}$, which is partially corrected in *Gcn2*$^{KO/KO}$;*Gars*$^{P278KY/+}$ mice. Analysis performed

Figure 15 Continued:
with at least 6 mice per grouped genotype. (G) Examples of fully innervated neuromuscular junctions (NMJs) in the gastrocnemius muscle of *Gcn2*$^{+/+,+/KO,\ or\ KO/KO}$*;Gars*$^{+/+}$ mice. The nerve terminal, labeled in green, fully covers the post-synaptic acetylcholine receptors in red. (H) Example of two partially innervated NMJs (white arrows) in *Gcn2*$^{+/+\ or\ +/KO}$*;Gars*$^{P278KY/+}$ mice. There are several regions of the post-synapse not covered by nerve. The pink arrow shows an example of a fully innervated, but morphologically abnormal, NMJ. Most fully innervated NMJs in *Gcn2*$^{+/+\ or\ +/KO}$*;Gars*$^{P278KY/+}$ mice do not show the classic "pretzel" shape. (I) Example of a completely denervated NMJ in *Gcn2*$^{+/+\ or\ +/KO}$*;Gars*$^{P278KY/+}$ mice, where the post-synapse has no contact with the nerve. (J) Fully innervated NMJs in *Gcn2*$^{KO/KO}$*;Gars*$^{P278KY/+}$ mice. Most fully innervated NMJs look morphologically normal with the classic "pretzel" shape. (K) Quantification of fully innervated, partially innervated, and denervated NMJs by genotype. In *Gcn2*$^{+/+,+/KO,\ or\ KO/KO}$*;Gars*$^{+/+}$ mice the vast majority of NMJS are fully innervated (98.2% $\pm$ 2.1), with a very small minority of partially innervated (1.2% $\pm$ 1.2) or denervated (.2% $\pm$ .6) NMJs identified. *Gcn2*$^{KO/KO}$*;Gars*$^{P278KY/+}$ mice have an increased percentage of fully innervated NMJs (66.8% $\pm$ 12.3) compared to *Gcn2*$^{+/+\ or\ +/KO}$*;Gars*$^{P278KY/+}$ (31.3% $\pm$ 19.9), and a decreased percentage of partially innervated (23.5% $\pm$ 9.7 vs 38.8% $\pm$ 11.3) and denervated (9.9% $\pm$ 8.3 vs 29.9% $\pm$ 17.2) NMJs. Analysis performed with 8-15 mice per grouped genotype. Values in A, B, E, and K are mean $\pm$ SD. Prior to grouping genotypes, all individual genotypes tested negatively for differences with one another. **= p<.01, ***= p<.001; ****= p<.0001.

The Integrated Stress Response is Activated in Alpha Motor Neurons of Mice with Dominant Mutations in Tyrosyl tRNA-Synthetase (*Yars*$^{E196K/E196K}$)

We have recently characterized a mouse model of Dominant Intermediate CMT Type C (CMTDIC) with a human mutation in tryosyl tRNA-synthetase (YARS-E196K). By 7 months of age *Yars*$^{E196K/+}$ mice have no discernable neuropathy, but *Yars*$^{E196K/E196K}$ mice have reduced sciatic nerve conduction velocity and impaired performance on the wire hang test (Supplemental Figure 5) (manuscript in preparation). To test for possible similarities in gene expression signatures between mutant *Yars* and *Gars* motor neurons, we performed RNAscope in *Yars*$^{E196K/+}$ and *Yars*$^{E196K/E196K}$ spinal cords at 7 months of age, probing for the same five ATF4 target genes profiled in mutant *Gars* motor neurons. No expression of ATF4 target genes was seen in 7 month old *Yars*$^{+/+}$ mice (Figure 16 A,B). In contrast, all 5 genes were upregulated in 7 month old *Yars*$^{E196K/+}$ and *Yars*$^{E196K/E196K}$ motor neurons (Figure 16 A,B). Fgf21 and B4galnt2 showed higher expression in *Yars*$^{E196K/E196K}$ motor neurons compared to *Yars*$^{E196K/+}$, whereas Gdf15, Adm2, and Cdsn showed similar expression levels in both genotypes. As in *Gars* spinal cords, only a subset of motor neurons expressed ATF4 target genes (Figure 16 A). A higher subset of motor neurons showed ATF4 target gene expression in *Yars*$^{E196K/E196K}$ spinal cord compared to *Yars*$^{E196K/+}$, ranging from approximately 46-67% and 11-44%, respectively. In *Yars*$^{E196K/E196K}$ spinal cord, all motor neurons that were resistant to ATF4 target gene expression were positive for the gamma motor neuron marker, Err3, indicating that alpha motor neurons are the subtype of motor neuron expressing the disease signature in *Yars*$^{E196K/E196K}$ spinal cord, as in the *Gars*$^{P278KY/+}$ spinal cord (Figure 16 D,E). The presence of gene expression changes in *Yars*$^{E196K/+}$ motor neurons precedes overt neuropathy, which is also the case in the *Gars* mice. In addition, the percentage of motor neurons showing gene expression changes correlates with onset of overt neuropathy, as a greater subset of motor neurons in symptomatic *Yars*$^{E196K/E196K}$ mice express ATF4 target genes compared to asymptomatic *Yars*$^{E196K/+}$ mice at 7 months of age. The percentage of motor neurons showing gene expression changes also correlates with

disease severity, as the very severe *Gars*$^{P278KY/+}$ mice show gene expression changes of all five ATF4 target genes in 70% of motor neurons, but the milder *Yars*$^{E196K/E196K}$ mice only show expression in 46-67% of motor neurons, depending on the gene. In the cases of B4galnt2 and Fgf21, the level of gene expression also correlates with onset of neuropathy, as higher expression is observed in *Yars*$^{E196K/E196K}$ mice compared to *Yars*$^{E196K/+}$. These correlations suggest that ATF4 target gene expression is strongly associated with the central disease mechanism. In addition, the striking similarities in mutant *Gars* and *Yars* gene expression signatures and in the patterns of cell type-specificity provide strong molecular and cellular evidence of a related disease mechanism in mouse models of two different ARS-associated forms of CMT.

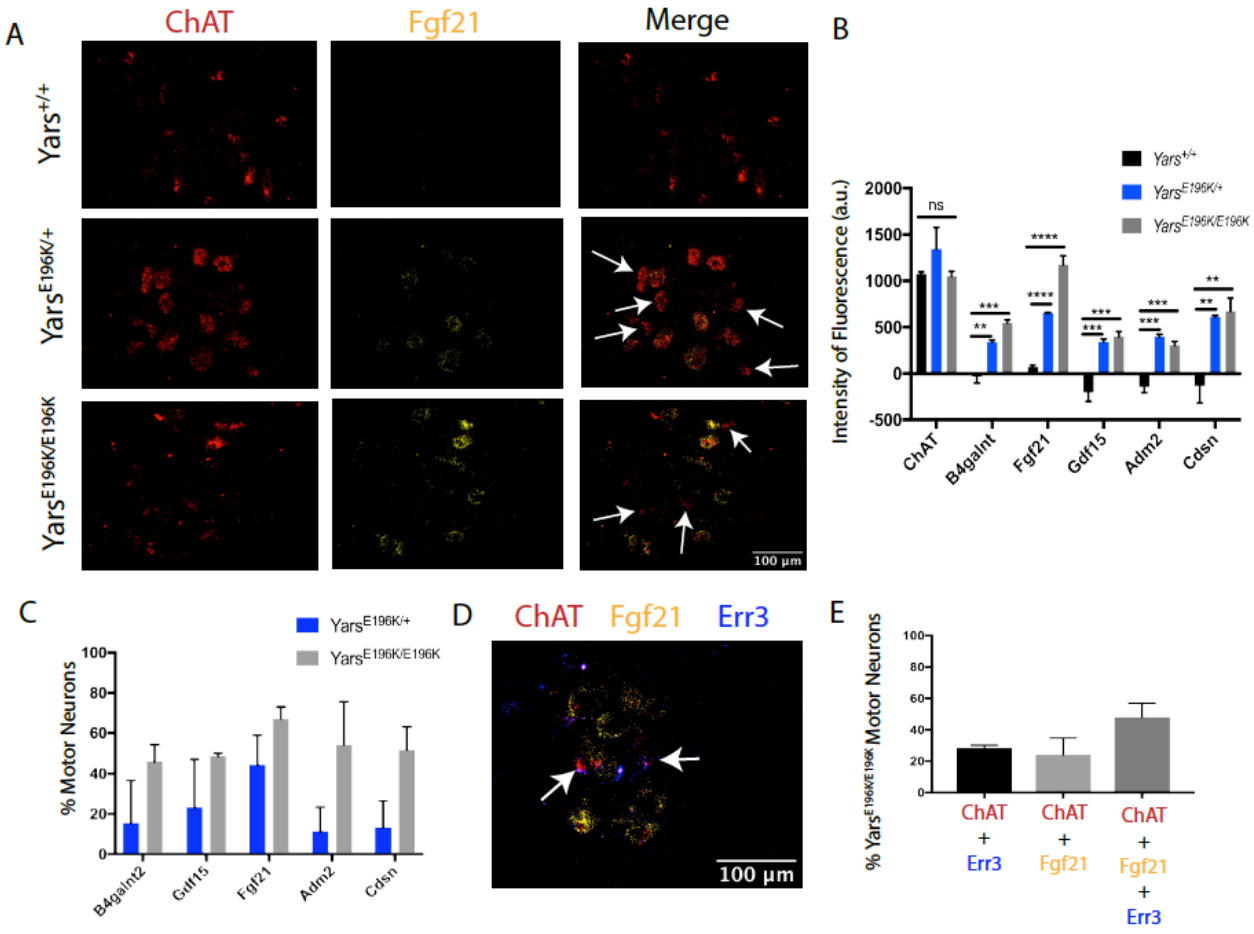

Figure 16: ATF4 target genes expressed in alpha motor neurons of *Yars*$^{E196K/E196K}$ post-disease onset and *Yars*$^{E196K/+}$ pre-disease onset mice. (A) *Yars*$^{+/+}$ motor neurons of the spinal cord labeled with ChAT (red) show now expression of the ATF4 target, Fgf21 (yellow). A subset of *Yars*$^{E196K/+}$ motor neurons labeled with ChAT (red) express Fgf21 (yellow) at the pre-disease onset age of 7 months. A larger subset of *Yars*$^{E196K/E196K}$ motor neurons labeled with ChAT (red) express Fgf21 (yellow) at 7 months of age. Chat-labeled *Yars*$^{E196K/+}$ and *Yars*$^{E196K/E196K}$ motor neurons that do not express Fgf21 are marked with white arrows. (B) Quantification of ATF4 target gene expression. *Yars*$^{E196K/+}$ and *Yars*$^{E196K/E196K}$ motor neurons express all 5 ATF4 target genes probed compared to little or no expression in *Yars*$^{+/+}$ motor neurons. B4galnt2 and Fgf21 show greater expression levels in *Yars*$^{E196K/E196K}$ motor neurons compared to *Yars*$^{E196K/+}$. Gdf15, Adm2, and Cdsn show approximately the same expression levels between *Yars*$^{E196K/E196K}$ and *Yars*$^{E196K/+}$. (C) Between 11-44% of *Yars*$^{E196K/+}$ motor neurons express any one of the 5 ATF4 target genes. Between 46-67% of *Yars*$^{E196K/E196K}$ motor neurons express any one of the 5 ATF4 target genes. (D) *Yars*$^{E196K/E196K}$ motor neurons that do not express Fgf21 are always labeled with the gamma motor neuron marker, Err3 (white arrows). (E) Quantification of experiment shown in E. Analysis was performed using 3 mice per genotype at 7 months of age. Values in B are the sum of average fluorescence per mouse per genotype ± SD. Values in C and E are mean ± SD. **= p<.01, ***= p<.001; ****= p<.0001.

Discussion

We have taken an *in vivo*, cell type-specific approach to profile translation and transcription in multiple mouse models of CMT2D. Our study has revealed that translation is impaired in motor neurons of mice with dominant mutations in *Gars*. Mutant *Gars* motor neurons in three CMT2D mouse models, including a human allele, show upregulation of ATF4 target genes in a pattern that reveals striking cell type-specificity. Only the largest motor neurons of the spinal cord and largest sensory neurons in dorsal root ganglia display these gene expression changes, which point to activation of the ISR. The ISR is activated in mutant *Gars* motor neurons by the translational homeostasis-sensing kinase, GCN2. Genetic removal of GCN2 alleviates CMT2D neuropathy, indicating that chronic activation of the ISR is intrinsically toxic to motor neurons. Finally, we have shown that motor neurons of mice with a human mutation in *Yars*, E196K, also upregulate the ISR with the same cell type-specificity seen in *Gars* spinal cord.

Activation of the ISR through GCN2 implies either excess uncharged $tRNA^{Gly}$ or stalled ribosomes, or both. Although activation of GCN2 has traditionally thought to be primarily through uncharged tRNA, recent work has shown much more potent direct activation by stalled ribosomes, a mechanism that was first suggested based on mouse genetic experiments (Inglis et al. 2019; Ishimura et al. 2016). Although the C201R and P278KY mutations in *Gars* may confer some decrease in aminoacylation efficiency, previous mouse studies make it clear that this is not the cause of neuropathy (Morelli, et al., 2019 submitted) (Seburn et al. 2006; Motley et al. 2011b). Thus, while we cannot rule out that GCN2 is in part activated by uncharged $tRNA^{Gly}$, we hypothesize that dominant mutations in *Gars* lead to primary impairments in translation and stalled ribosomes at glycine codons. These stalled ribosomes directly activate GCN2 and trigger the ISR, resulting in an additional dampening of translation and ATF4 target gene expression (Figure 17 B).

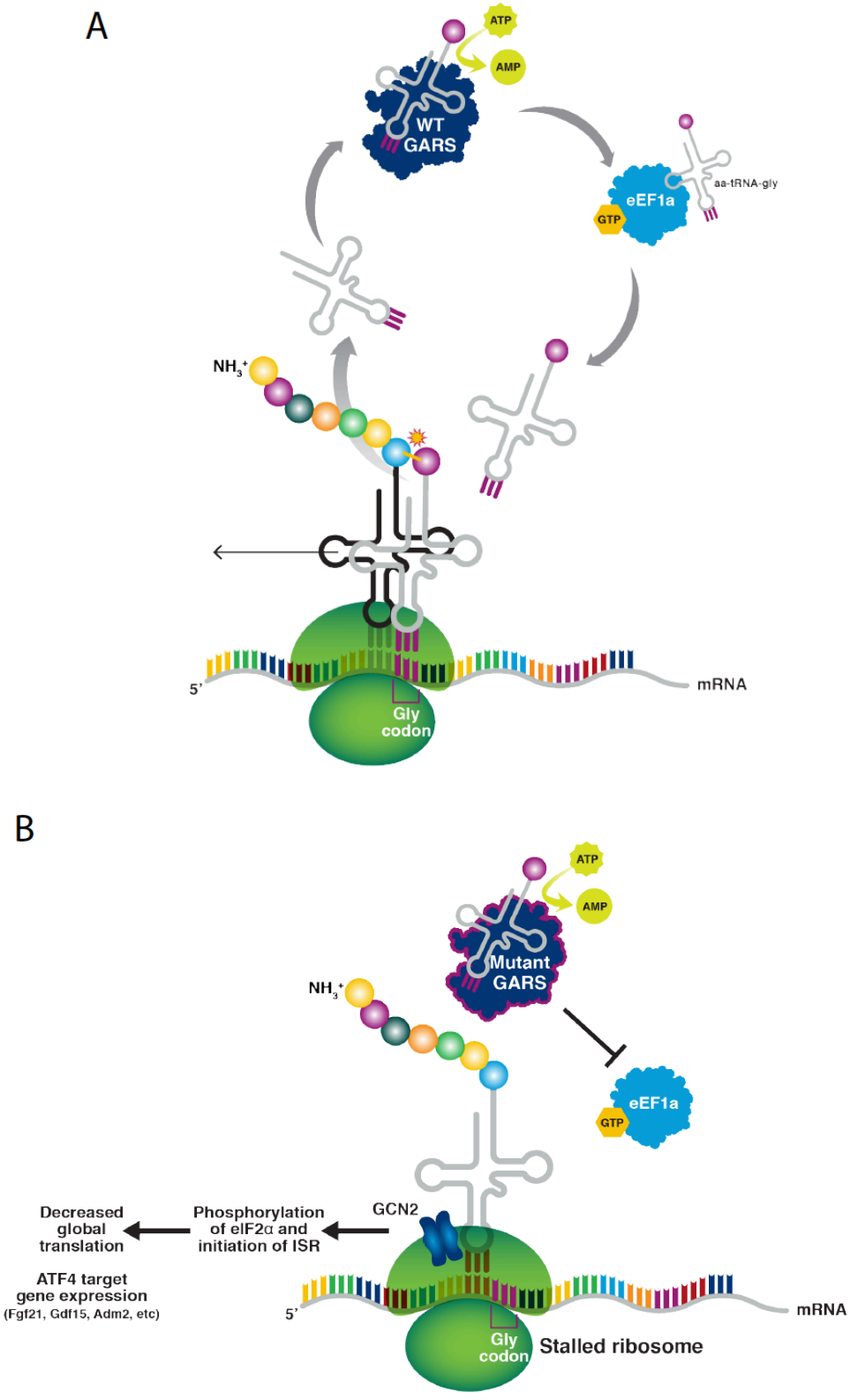
A
ATP
AMP
WT
GARS
aa-tRNA-gly
eEF1a
GTP
NH3+
5'
mRNA
Gly
codon
B
ATP
AMP
Mutant
GARS
NH3+
eEF1a
GTP
GCN2
Phosphorylation
of eIF2α and
initiation of ISR
Decreased
global
translation
ATF4 target
gene expression
(Fgf21, Gdf15, Adm2, etc)
5'
mRNA
Gly
codon
Stalled ribosome

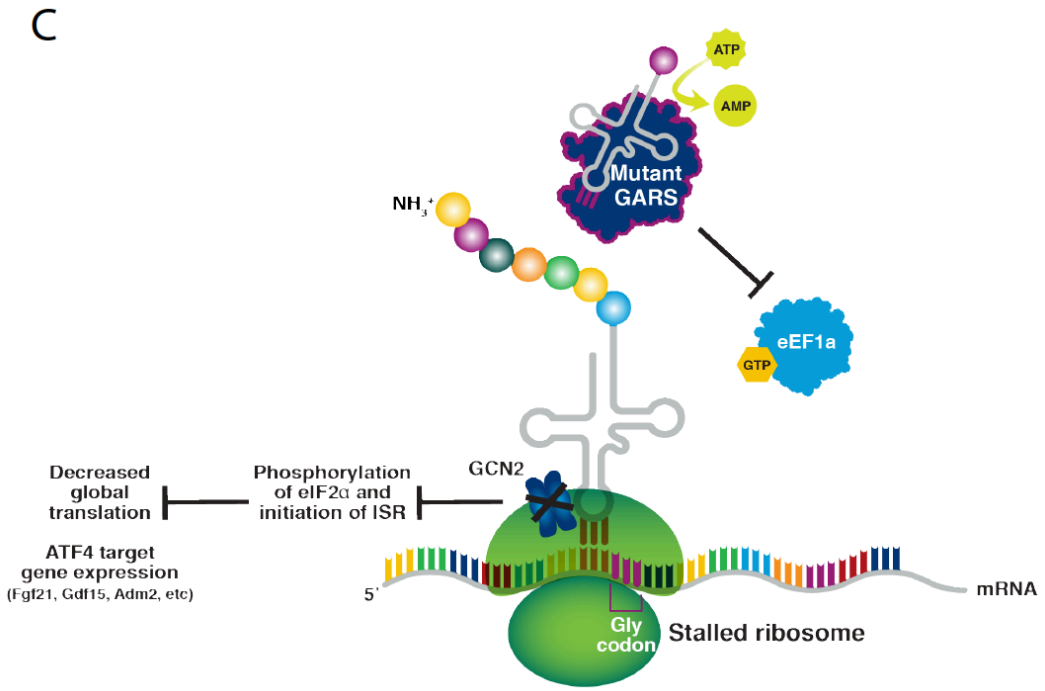

Figure 17: Model of how dominant mutations in *Gars* cause neuropathy through primary impairments in translation and stalled ribosomes. (A) The wild-type GARS enzyme binds glycine and ATP, forms an aminoacyl adenylate, and then transfers this moiety to the 3' acceptor end of $tRNA^{Gly}$. The chaperone protein, eEF1A, binds the aminoacylated $tRNA^{Gly}$ and presents it to the A site of the ribosome where the $tRNA^{Gly}$ anticodon binds a glycine codon on the mRNA. $tRNA^{Gly}$ is shifted to the P site where it glycine is added to the growing polypeptide chain. The uncharged $tRNA^{Gly}$ then moves to the E site, is released by the ribosome and rebound by GARS where it can be aminoacylated again, completing the tRNA cycle. (B) We propose that mutations in GARS result in a higher affinity of mutant GARS for $tRNA^{Gly}$ and a slower release rate of aminoacylated tRNA-gly to eEF1A. The lack of aminoacylated $tRNA^{Gly}$ at the ribosome causes stalling at glycine codons. Stalled ribosomes activate GCN2 kinase, which then results in phosphorylation of eIF2α, a further reduction in translation, and ATF4 target gene upregulation. (C) Genetic removal of GCN2 kinase from $Gars^{P278KY/+}$ prevents ATF4 target gene upregulation and presumably also stops eIF2α phosphorylation and any dampening of translation. We hypothesize that this allows translation to rebound slightly in mutant motor neurons, alleviating a portion of the neuropathy phenotype. However, translation in mutant *Gars* motor neurons is still impaired because of the primary GARS insult, and stalled ribosomes are still present, explaining the remainder of the neuropathy phenotype.

There is currently no way to perform ribosome footprinting *in vivo* in a cell type-specific manner, which would be essential to show stalled ribosomes at glycine codons in only a subset of an already small neuronal population (~70% of the 50,000-100,000 motor neurons in the spinal cord). To genetically test for the involvement of stalled ribosomes in the primary disease mechanism, crosses between *Gars*$^{C201R/+}$ mice and mice with homozygous loss-of-function mutations in the ribosome recycling factor, *Gtpbp2,* were created. Importantly, *Gars*$^{C201R/+}$ mice ordinarily express a central nervous system-specific C57BL/6J-derived mutant tRNA^{Arg}, which in combination with homozygous mutations in *Gtpbp2* result in cerebellar ataxia between 4-6 weeks of age and could confound the study. To remove this variable, mice were bred to the congenic nTr20 strain, which contains a wild-type B6N-derived tRNA^{Arg} (*nTr20*$^{+/-}$) that shows no genetic interaction with mutant Gtpbp2. In support of the involvement of stalled ribosomes in the primary disease mechanism, genetic crosses between *Gars*$^{C201R/+}$ mice and mice with homozygous loss-of-function mutations in the ribosome recycling factor, *Gtpbp2,* have exacerbated peripheral neuropathy. *Gtpbp2*$^{-/-}$*;nTr20*$^{+/-}$*;Gars*$^{C201R/+}$ mice have decreased body weight (Supplemental Figure 6A), nerve conduction velocity (Supplemental Figure 6B), and motor function (Supplemental Figure 6C) compared to *Gtpbp2*$^{+/+}$*;Gars*$^{C201R/+}$. This study is still ongoing, and all control genotypes will be filled in, as well as a more complete analysis of peripheral neuropathy including motor axon counts and diameter and NMJ innervation status.

Activation of the ISR through GCN2 results in ATF4 target upregulation, but will also lead to a global decrease in mRNA translation. Removing GCN2 presumably alleviates this chronic decrease in translation, correspondingly alleviating neuropathy phenotypes. However, although complete shutdown of the ISR does improve *Gars* phenotypes, it does not restore them to normal. We hypothesize the lingering phenotype is due to the primary impairment in translation conferred by mutant GARS (Figure 17 C). It will be important to test in the future if impairments in translation are still present in motor neurons after removal of GCN2.

How is mutant GARS causing these putative stalled ribosomes? The wild-type GARS protein binds glycine and ATP, forms an aminoacyl adenylate, and then transfers this moiety to the 3' acceptor end of the $tRNA^{Gly}$. The chaperone protein, eEF1A, binds the aminoacylated $tRNA^{Gly}$ and presents it to the A site of the ribosome. After the amino acid is added to the growing polypeptide chain, the uncharged $tRNA^{Gly}$ is rebound by GARS, and the tRNA cycle can continue (Figure 17 A). The constant supervision of tRNA molecules by translation factors strongly suggests that the efficient cycling of tRNA is critical to translational homeostasis. In alignment with mouse genetic studies that suggest impaired aminoacylation is not the cause of neuropathy, we have previously shown that dietary supplementation of glycine does nothing to alleviate CMT2D neuropathy. Because the only other substrate of GARS is $tRNA^{Gly}$, we hypothesize that dominant mutations in *Gars* cause disruption of $tRNA^{Gly}$ cycling.

At physiological pH, the association of ARSs with tRNAs is much weaker than most protein-DNA interactions, with dissociation constants several orders of magnitude larger. This feature of the ARS-tRNA physical interaction allows for the rapid turnover of the aminoacylation reaction which feeds the translational burden of a cell (Schimmel and Soll 1979). Therefore, equally important as the accurate creation of the aminoacylated tRNA is its timely release from the ARS. Because the majority of CMT-associated mutations in ARSs confer a net positive charge to the mutant enzyme in regions that might be expected to contact the tRNA, we hypothesize that dominant mutations in *Gars* result in an increased affinity of mutant GARS for $tRNA^{Gly}$ and a corresponding slowdown of tRNA cycling (Figure 17 B). The best way to test this hypothesis is to overexpress $tRNA^{Gly}$ and look for phenotypic rescue. If uncharged $tRNA^{Gly}$ is primarily responsible for activating the ISR, increasing its levels should worsen the phenotype. If instead, mutant GARS is sequestering $tRNA^{Gly}$, increasing its levels should alleviate neuropathy phenotypes. It is also possible that some mutations could slow down the tRNA cycle through sequestration of eEF1A or a combination of $tRNA^{Gly}$ and eEF1A sequestration.

The striking cell type-specificity of ATF4 target upregulation calls into question how a disease mechanism based just on the biochemistry of an increased affinity of mutant GARS for $tRNA^{Gly}$ or eEF1A could create such a specific pattern of phenotypes. We suggest that expression levels of genes directly related to translation elongation, ribosome recycling, or stress response activation could impact cell type phenotypes. The best precedent for such an explanation comes from mouse genetics experiments. Expression levels of a central nervous system-specific $tRNA^{Arg}$ modulate neurodegeneration in *Gtpbp2*$^{-/-}$ mice and tissue-specific expression levels of an AARS editing co-factor influence neurodegeneration in *Aars*$^{sti/sti}$ mice (Ishimura et al. 2014; Vo et al. 2018). Thus, we could envision a precise gene expression state in mature motor and sensory neurons that predisposes them to sensitivity to dominant mutations in certain ARSs. The size of the neuron may also play a role in the level of sensitivity to impairments in translation.

In conclusion, our work demonstrates that activation of the ISR through GCN2 is central to CMT2D pathology in mice. Inhibition of GCN2 represents a new potential therapeutic target for human patients with CMT2D. We propose that toxic gain-of-function disruption of $tRNA^{Gly}$ cycling by mutant GARS causes impairments in translation, stalled ribosomes, and activation of GCN2 and the downstream stress response. We also hypothesize that the same mechanism occurs with dominant mutations in *Yars*, broadening impairments in translation as a potential feature of at least two forms of ARS-associated CMT.

CHAPTER 4

IMPAIRMENTS IN TRANSLATION AS THE CENTRAL DISEASE MECHANISM OF TRNA SYNTHETASE-MEDIATED PERIPHERAL NEUROPATHY

Impaired Translation in Neurological Disease

The translation of mRNA into protein is essential for every cell type of the body, yet neurons show a special sensitivity to even minor disruptions in this process. A striking number of neurological diseases are linked to impairments in almost every major step of translation. A large body of work has highlighted the roles of translation initiation and elongation, expression and post-transcriptional modification of tRNA, and ribosome quality control as important contributors to neuronal homeostasis (Kapur, Monaghan, and Ackerman 2017; Kapur and Ackerman 2018).

Dysregulation of Translation Initiation in Neurodegenerative Disease

The Mammalian Target of Rapamycin (mTOR) Signaling Pathway.

Regulation of translation initiation is a complex process with many players that is highly dependent upon the state of the cell, and ultimately of the entire organism. The mammalian target of rapamycin (mTOR) signaling pathway integrates extrinsic and intrinsic cellular signals to act as a central regulator of cell metabolism, growth, proliferation, and survival. mTORC1, one of the two multi-protein complexes at the center of the pathway, positively regulates translation by (1) phosphorylating the eukaryotic initiation factor 4E (eIF4E)-binding protein 1 (4E-BP1), which prevents binding to eIF4E, freeing eIF4E to stimulate cap-dependent mRNA translation, (2) phosphorylating the initiation factors, eIF4G and eIF4B, which leads to promotion of cap-dependent mRNA translation, (3) phosphorylation of the p70 ribosomal kinase S6 kinase 1 (S6K1), which results in increased mRNA biogenesis, cap-dependent translation, and the translation of ribosomal proteins, and (4) ribosome biogenesis (Leon et al. 2014; Holz et al. 2005; Haghighat et al. 1995; Ma and Blenis 2009; Mayer et al. 2004). Although mTOR

involvement in neurodegenerative disease is complex, an overall upregulation of mTOR signaling has been observed in brains of Alzheimer's disease (AD) patients and in AD mouse models. Included in this aberrant activation is increased levels of phosphorylated 4E-BP1 in the brains of AD patients, which positively correlates with tau levels (Li et al. 2005). Although the correlation between increased translation and neurodegeneration may seem counterintuitive, it has been suggested that upregulation of translation in AD pathology results in the accumulation of proteins that form toxic aggregates, such as tau (Perluigi, Di Domenico, and Butterfield 2015).

The Integrated Stress Response.

Translation initiation is also highly sensitive to cell stress through the conserved pathway, the integrated stress response. Four kinases are responsive to a variety of cell stressors: PKR (protein kinase R) responds to double stranded RNA during viral infection, PERK (PKR-like endoplasmic reticulum kinase) responds either directly or indirectly to unfolded proteins associated with ER stress, HRI (heme-regulated inhibitor) responds to heme deprivation, and GCN2 (general control nonderepressible 2) responds to amino acid deprivation. The activation of any one of these four kinases results in phosphorylation of the alpha subunit of the translation initiation factor, eIF2. Upon phosphorylation at serine 51, eIF2α cannot undergo GDP→GTP exchange by the eIF2 guanine exchange factor, eIF2B, thereby reducing the amount of eIF2 available to form the initiator ternary complex (eIF2-GTP-Met-tRNA$_i$). This limits the global translation of capped mRNA, instead shunting cellular resources towards managing the stress. Shutdown of translation is also beneficial in preventing further buildup of unfolded proteins in the case of ER stress, preventing the translation of viral RNA in the case of infection, and reducing the need for amino acids and heme in the cases of deprivation of either resource (Pakos-Zebrucka et al. 2016).

In contrast to the shutdown of cap-dependent translation, the translation of stress response genes is upregulated, including a central mediator of the ISR, activating transcription factor 4 (ATF4). The expression of ATF4 and other stress genes is normally limited by the presence of

upstream open reading frames (uORFs). uORFs are located in the 5' UTR of many mRNAs. Under normal conditions translation is initiated at the uORF instead of the main ORF, preventing translation of the full protein. Under stress conditions the ternary complex is limited, reducing translation initiation at the uORF and increasing translation from the primary ORF (Barbosa, Peixeiro, and Romao 2013). Some of the stress genes induced by ATF4 promote autophagy, which frees up potentially limited cellular resources for immediate use. Other ATF4 targets specifically inhibit apoptosis, thereby promoting cell survival. The role of many ATF4 targets in the stress response is unknown.

As a transcription factor that mediates the expression of potentially hundreds of stress related genes, ATF4 is central to the overall outcome of the ISR. ATF4 has many protein binding partners, including other transcription factors such as C/EBP homologous protein (CHOP), that influence its regulation of gene expression. ATF4 also undergoes extensive regulation at the transcriptional, translational, and post-translational levels. Thus, the cellular outcome of the ISR is highly dependent upon which binding partners are available to ATF4 and the precise balance of its functional regulation within the cell. This means that the ISR is not a "one size fits all" pathway, instead creating a response that is tailored to both the stress triggering its activation and the cellular context in which it occurs (Pakos-Zebrucka et al. 2016).

It is broadly accepted that appropriate activation of the ISR is beneficial to cells under stress. However, timely ISR termination is necessary in order to ultimately bring the cell back into homeostatic balance and restore normal translational activity. When the stress is resolved, the ISR is terminated when protein phosphatase I (PP1) complex recruits a catalytic unit and regulatory subunit to eIF2. In mammals either growth arrest and DNA-damage inducible protein (GADD34) or constitutive repressor of eIF2α phosphorylation (CReP) targets the phosphatase to eIF2α. While CReP is constitutively expressed in cells, GADD34 is part of a negative

feedback loop, whose cap-independent translation is induced by ATF4 during the later stages of the stress response (Trinh and Klann 2013).

There are several examples of how failure to turn off the ISR and the resulting long-term depression of translation initiation contribute to neurodegenerative diseases such as amyotrophic lateral sclerosis, Parkinson's disease, prion disease, and Huntington's disease (Kapur, Monaghan, and Ackerman 2017). However, the earliest association between global reductions in translation and neurodegeneration was made in the context of AD. Given that *de novo* protein synthesis has long been linked to synaptic plasticity, learning, and memory, it may not be surprising that reduced translation is associated with Alzheimer's disease (AD) (Trinh and Klann 2013). Increased levels of phosphorylated eIF2α have been found in the brains of AD patients and mouse models (Chang, Wong, et al. 2002; Kim et al. 2007). There is evidence for the involvement of PKR, PERK, and GCN2 in causing the increased levels of phosphorylated eIF2α observed in AD. Removal of PKR is protective in neurons exposed to beta-amyloid peptides and reduction of PERK rescues memory deficits and cholinergic neurodegeneration in AD mice (Chang, Suen, et al. 2002; Devi and Ohno 2014). Genetic removal of GCN2 from amyloid precurser protein/presinilin 1 (APP/PS1) AD mice prevented defects in synaptic plasticity and memory, but in the 5x Familial AD (5xFAD) AD model its removal caused increases in activated PERK, phosphorylated eIF2α, and beta-amyloid plaque burden and failed to rescue memory deficits (Ma et al. 2013; Devi and Ohno 2013). These seemingly contrasting results may point to the extreme dependence of ISR outcomes on precise disease context, suggesting that a "one size fits all" therapeutic strategy to mediating the ISR in neurogenerative disease will not be effective.

Dysregulation of Translation Elongation in Neurodegenerative Disease

Accurate and timely translation elongation depends on a robust supply of correctly aminoacylated tRNA, the correct matching of the cognate tRNA anticodon to the mRNA codon,

and the highly coordinated movement of the ribosome to the next codon. The elongation factors eEF1A and eEF2 are essential in this process. eEF1A is the molecular chaperone that brings the aminoacylated tRNA from the ARS to the ribosome A site for matching to the mRNA, and eEF2 stabilizes the ribosome as it undergoes translocation; the structural shift that allows for the tRNA to move stepwise from the A site to the P site. Both of these factors have been implicated in neurodegenerative disease in humans and/or animal models. In vertebrates two distinct eEF1A genes are present: *eEF1A1*, which is expressed ubiquitously during development but downregulated in adult neurons and muscle, and *eEF1A2*, which is expressed only in neurons and muscle (Lee, Wolfraim, and Wang 1993; Lee et al. 1995). In mice, a recessive loss-of-function mutation in *eef1a2* results in motor neuron degeneration and muscle wasting (Chambers, Peters, and Abbott 1998). In humans, missense mutations in *eEF1A2* have been associated with epilepsy, intellectual disability, and progressive microcephaly (Lam et al. 2016; Veeramah et al. 2013). A mutation in *eEF2* that is predicted to interfere with ribosome translocation is linked to dominant spinocerebellar ataxia (Hekman et al. 2012).

tRNA Expression and Processing in Neurodegenerative Disease

The world of tRNA biology shows a vast complexity that is only beginning to be understood. Despite the fact that there are only 20 amino acids, humans have, on average, 500 tRNA genes, although this varies from person to person. Each tRNA family is comprised of isoacceptors (different anticodon, different body) and isodecoders (same anticodon, different body). tRNA molecules can potentially undergo more than 90 different post-transcriptional base modifications. The average human tRNA contains 11-13 of these modifications and has the potential for many protein binding partners. tRNA fragments are also active in many biological processes, including stress responses, tumorigenesis, and hematopoiesis (Schimmel 2018). There are still many unknowns regarding tRNA biology and neuronal homeostasis, but the link between tRNAs and neurodegeneration is clear.

Mutations in proteins that comprise RNA polymerase III, the enzyme complex responsible for tRNA transcription, result in reduced tRNA production and cause a group of disorders called leukodystrophies that are characterized by cerebellar degeneration (Saitsu et al. 2011). The brain-specific phenotype is hypothesized to be related to decreases in expression of tRNA species that are especially important for CNS neurons (Kapur, Monaghan, and Ackerman 2017). These tissue specific sensitivities to tRNA processing defects are supported by the previously mentioned mutation in a CNS-specific mouse $tRNA^{Arg}$ gene that decreases the amount of mature tRNA produced and causes ribosome stalling in the CNS (Ishimura et al. 2014).

Nuleoside modification of tRNA influences the affinity of anticodon-codon interactions, therefore regulating translation efficiency and accuracy while tailoring the specific repertoire of proteins that are synthesized in a given cell. These modifications are also known to influence aminoacylation and the structure and stability of the tRNA itself (Bednarova et al. 2017). Defects in tRNA modification due to mutations in modification machinery have been linked to several neurological conditions including intellectual disability, epilepsy, and ALS (Najmabadi et al. 2011; Alazami et al. 2013; Landers et al. 2009; Reinthaler et al. 2014).

Ribosome-associated Protein Quality Control and Neurodegeneration

The ribosome has emerged as a point of intersection for mRNA and protein quality control. The truncated polypeptides that reside on a paused ribosome due to defective mRNA or other factors that impair translation elongation are immediately targeted for degradation to prevent potentially negative downstream consequences. The mechanisms involved in this type of protein degradation sense the state of the ribosome itself, rather than the specific folding state of individual proteins, making this approach global and unbiased to the actual protein it degrades. By monitoring the ribosome, as opposed to the protein or the mRNA, the cell takes a “heavy handed” approach in degrading any mRNA or protein associated with a stall.

Ribosome stalling can be induced by several different types of defects in mRNA sequence or structure. Stalling reporters that encode fluorescent proteins before and after a potential stall sequence provide a quantitative readout of translation arrest. These tools have been instrumental in determining stalls due to several features present in mRNA species, including lack of a stop codon, stretches of basic residues, truncating mutations within the coding region, rare codons, or strong secondary structure (Brandman and Hegde 2016).

Many of the studies that have identified the factors involved in ribosome-associated quality control and the sequential steps of the process have been done using yeast genetics. These experiments have helped to delineate the complex process into four major steps: (1) recognition of the stalled ribosome (2) splitting of the stalled ribosome, (3) nascent polypeptide chain ubiquitination, and (4) nascent polypeptide chain extraction and degradation. Recognition of the stalled ribosome occurs by the ubiquitin ligase, ZNF598. Collision of two ribosomes opens a 40S-40S interface at which ZNF598 ubiquitination targets reside. The recognition by ZNF598 is independent of the cause of the stall, as the 60S rotation state does not affect ZNF target ubiquitination (Juszkiewicz et al. 2018). Splitting of the stalled ribosome occurs by ribosome recycling factors, including Pelota (Dom34 in yeast), Hbs1, and ABCE1 (Rli1 in yeast). After binding of the GTP-Hbs1-Dom34 complex to a stalled ribosome, Hbs1 dissociates, Dom34 moves into the empty A site, and both Dom34 and Rli1 catalyze subunit separation (Shoemaker, Eyler, and Green 2010). Removal of the small subunit from the nascent chain-80S complex exposes the intersubunit face of the nascent chain-60S complex. The subsequent exposure of the P site tRNA has been hypothesized to be involved in recruitment of the ubiquitin ligase responsible for nascent chain ubiquitination, listerin (LTN1) (Bengtson and Joazeiro 2010). Nuclear export mediator factor (NEMF, or Rqc2 in yeast) is an important cofactor that stabilizes the association between LTN1 and the 60S complex (Shao et al. 2015). The mechanism of nascent chain degradation and recycling of the 60S-ubiquitination complex has

not been fully worked out, but in yeast a protein complex called Cdc48 could potentially use ATP to force the nascent chain away from the ribosome (Stolz et al. 2011).

Several factors involved in ribosome-associated quality control have been linked to neurodegenerative disease. Recessive hypomorphic mutations in the mouse gene, *Ltn1*, cause motor and sensory neuron degeneration (Chu et al. 2009). As previously mentioned, the ribosome rescue factor, GTPBP2, resolves stalls which are due to a loss of function mutation in a mouse CNS-specific $tRNA^{Arg}$ gene. Homozygous loss of GTPB2 results in unresolved ribosome stalls at cognate AGA codons and severe neurodegeneration and ataxia (Ishimura et al. 2014). GTPBP2 is also relevant to human disease, as loss-of-function mutations in the gene have been found in a family with neurodegeneration in the brain and retina (Jaberi et al. 2016). Due to the apparent importance of ribosome-associated quality control in neuronal homeostasis, it would not be surprising if additional factors in this process were soon linked to other human neurological diseases.

How Dominant Mutations in tRNA Synthetase Genes Might Cause Impaired Translation

There are only three substrates of ARSs: ATP, amino acids, and tRNA. Keeping in mind the gain-of-function conclusion from animal model experiments, if dominant mutations in ARSs are impairing translation, it seems most likely that it would be through a gain-of-function sequestration of one of these substrates. Dietary supplementation of amino acids has not been effective at alleviating neuropathy (Bais et al. 2016). Although ATP replacement has not been tested in animal models, some CMT-causing mutations do not impair aminoacylation, so ATP availability and function at the ARS is most likely unaffected. That leaves the tRNA as the only remaining substrate that might be affected by mutations in ARSs. Because of the exquisite complexity of tRNA biology and its tight regulation in translation, it is reasonable to suggest that sequestration of the tRNA substrate and disruption of its cycling to the ribosome could cause neurodegenerative disease.

Almost all CMT-causing mutations in ARSs are predicted to result in a net positive charge on the protein within a region that could come into contact with the tRNA (Wei, Zhang, and Yang 2019). The normal interaction between an ARS and its cognate tRNA is weaker than most protein-nucleic acid interactions, allowing for the rapid turnover of the aminoacylated tRNA to eEF1A. An increased affinity for the tRNA could result in a slowing down of this turnover and a paucity of aminoacylated tRNAs at the ribosome.

GARS represents the only bi-functional ARS linked to CMT. Especially in light of the reduced number of mitochondria available at the motor terminal in mutant *Gars* mice, defects in mitochondrial translation could also be a feature of CMT2D (Spaulding et al. 2016). It is expected that mitochondrial translation would be impaired because of the same mechanism in the cytosol: sequestration of the tRNA by the mitochondrially-localized form of mutant GARS. It should be noted that two of the ATF4 target genes expressed by mutant *Gars* motor neurons, Fgf21 and Gdf15, are well-known markers of mitochondrial translation impairments in skeletal muscle. However, because removal of GCN2 shuts off expression of these genes in mutant *Gars* motor neurons, they are most likely a feature of the ISR in this disease context, as opposed to a direct signal of mitochondrial translation impairment.

Testing for Sequestration of tRNA by Mutant ARSs

One way to test for an increased affinity of mutant ARSs for their cognate tRNA is through surface plasmon resonance (SPR). SPR is a powerful technique used to determine the affinity of two ligands by comparing the dissociation rate to the association rate. A “bait” ligand is attached to the surface of the SPR sensor and a solution containing a known concentration of the “prey” ligand is washed over the surface. As the two ligands bind, an increase in resonance signal is observed which corresponds to the association rate. Next, a solution lacking the “prey” ligand is washed over the surface that disassociates the bound complex. The observed decrease in resonance signal corresponds to the dissociation rate. From the association and dissociation rates, the equilibrium dissociation constant can be calculated (Myszka, Jonsen, and

Graves 1998). Some of the primary advantages of SPR are its measurement of reaction kinetics in real time, its label-free approach, and the small quantity of material needed (Vo et al. 2019). This technique has been used for the study of protein-RNA interactions for almost two decades and has also been used to study binding affinities of tRNAs with ARSs and other proteins (Park et al. 2000; Kushwaha, Bange, and Bhavesh 2019; Crnkovic et al. 2018). By using the ARSs as the bait and the cognate tRNA as the prey, the binding affinities of wild-type and mutant ARSs to the tRNA can be compared.

One advantage of this approach is that it can be used to test for the involvement of post-transcriptional modifications in aberrant binding affinity. tRNA *in vitro* transcribed will not contain these modifications, but tRNA purified from *in vivo* will. The binding affinity of mutant ARSs for individual tRNA isoacceptors and decoders can also be determined to test if aberrant sequestration is global to all cognate tRNA species or specific to certain tRNA sequences.

The idea that an increase in positive charge near the ARS-tRNA interaction site will slow down reaction kinetics would predict that inducing additional positively-charged residues on the mutant ARSs would slow down the reaction even more. These experimental mutations may also predict future neuropathy-causing alleles. Correspondingly, introducing negatively-charged residues directly adjacent to mutation sites may reverse the defect in reaction kinetics. All of these scenarios could be tested using the SPR technique and would strengthen the idea of increased ARSs-tRNA affinity as the cause of translational impairment *in vivo*.

Cellular Consequences of tRNA Sequestration by Mutant tRNA Synthetases

Sequestration of aminoacylated tRNA at mutant tRNA synthetases would result in a lack of GTP-eEF1A-aminoacylated tRNA at the ribosome during translation elongation. This lack would be expected to result in stalled ribosomes at cognate codons, similar to what may happen under conditions of nutrient deprivation and amino acid starvation. These stalled ribosomes would most likely be resolved by the cell, but the chronic lack of aminoacylated tRNA would result in a continuous cycle of stalled and resolved ribosomes. These conditions should mimic

amino acid starvation and would be expected to activate the ISR through GCN2 kinase, resulting in eIF2α phosphorylation, global shutdown of translation, and activation of ATF4 gene targets. We have confirmed activation of the ISR through GCN2, impaired translation, and ATF4 target upregulation in motor neurons of multiple mouse models of CMT2D.

Some of the mutations in *Gars* used in our study may have decreased aminoacylation efficiency, therefore the method of GCN2 kinase activation is still unclear. Traditionally GCN2 kinase is activated by uncharged tRNA, but strong evidence now suggests that it is more potently activated by stalled ribosomes (Ishimura et al. 2016; Inglis et al. 2019). To unequivocally identify stalled ribosomes in mutant motor neurons we would ideally perform ribosome footprinting. However, without an *in vivo*, cell type-specific approach to ribosome footprinting, detecting stalled ribosomes in the small percentage of affected motor neurons within the entire spinal cord seems unlikely.

Our first attempt at associating stalled ribosomes with CMT2D was to cross mutant *Gars* mice with *Gtpbp2*$^{-/-}$ mice. We hypothesized that if stalled ribosomes are a feature of CMT2D, inhibiting the cell's ability to resolve these stalls would exacerbate neuropathy. Indeed, neuropathy is exacerbated in *Gars*$^{C201R/+}$ mice lacking GTPBP2. Neuropathy is evident at an earlier timepoint (based on clasping and body weight), and double mutant mice have decreased nerve conduction velocity and motor function. This study is ongoing, and it will be important to verify that *Gtpbp2*$^{-/-}$;*Gars*$^{+/+}$ do not have peripheral neuropathy at least through early adulthood. It is also important to determine the potential role of the C57BL/6J mutant tRNA^{Arg} to the development of peripheral neuropathy. Preliminary data suggests that the *tRNA*^{Arg} mutation does influence body weight and wire hang performance, as mice experience severe ataxia and have difficulty obtaining food, but does not influence primary measures of neuropathy, such as nerve conduction velocity. Although this *tRNA*^{Arg} gene is expressed in the spinal cord, northern blots suggest lower levels of expression compared to the brain and higher levels of the rest of the isodecoder family (Ishimura et al. 2014). Expression levels specifically in motor neurons are

not known. Because of the preliminary lack of correlation between neuropathy measures and the *tRNA^{Arg}* mutation, expression of this particular *tRNA^{Arg}* gene may not be as critical for motor neurons as it is for neurons in the brain and retina.

There is always a tradeoff between the reduced complexity and increased feasibility of *in vitro* studies and the obvious disease relevance of *in vivo* studies. CMT-causing mutations in *Gars* do not cause a disease-relevant phenotype in cultured motor neurons, probably because they never reach a state of full maturation. However, because our hypothesis of increased affinity of mutant ARS for tRNA is simply based on biochemistry, we expect that expressing a high enough level of mutant ARS in any cell type would result in ribosome stalling. Thus, we can directly test for ribosome stalling *in vitro* by overexpressing mutant ARS in the context of a stalling reporter. As mentioned previously, these reporters code for one fluorescent protein before a stall-inducing sequence, and for another fluorescent protein after the sequence. By placing a series of cognate amino acid codons between the two fluorescent reporters, we could quantitatively measure ribosome stalling in cells that express mutant ARSs. The makeup of cognate codons could be modified to test for differences in ribosome stalling due to the sequestration of specific isoacceptors. Upon verification and characterization of ribosome stalling, individual ARS substrates could be added to the medium to attempt to rescue stalling, including the tRNA, the amino acid, or ATP. We predict that tRNA replacement would reduce stalling with most mutant forms of ARS. However, it is possible that mutations that also reduce aminoacylation efficiency may show rescued stalling with amino acid replacement.

Why Impairments in Translation and Chronic Activation of the Integrated Stress Response are Harmful to Motor and Sensory Neurons

Our data supports a double hit on translation in mutant *Gars* motor and sensory neurons. The first hit comes directly from the mutant GARS protein: sequestering tRNA^{Gly} results in impaired translation elongation, stalled ribosomes, and truncated nascent polypeptides. The fact that the ISR is activated through GCN2 and not PERK in mutant motor neurons suggests

that a build-up of unfolded protein is not the primary insult resulting from elongation impairment. Instead, it may be that a lack of successful translation of proteins critical for cell function underlies the axon dieback. The huge distance between the cell body and the nerve terminal requires a constant transport of proteins, and any slowdown in the supply chain would likely be detrimental to the sites furthest from the source. This is an especially attractive explanation, given that the largest and longest axons tend to be preferentially affected in CMT2D mouse models and CMT patients as a group. However, slowed translation elongation may also increase the error rate of amino acid incorporation into proteins. Perhaps errors in proteins crucial for motor neuron health also contribute to motor neuron sensitivity to impairments in translation.

Activation of the ISR potentially through stalled ribosomes provides the second hit on translation. An additional dampening of translation through inhibited initiation is clearly detrimental to motor neurons in the context of CMT2D, probably because of the same reasons discussed above. Removing the ISR through GCN2 presumably allows global translation initiation to resume and may relieve some of the protein supply deficit in the axon, preventing degeneration.

Determining the extent to which translation recovers, but is still impaired, in mutant *Gars* motor neurons lacking GCN2 will be critical to estimating the contribution of each translational insult to the phenotype and in supporting the presence of primary impairments in translation due to mutant GARS. We are currently attempting to do this using intracerebroventricular (ICV) administration of puromycin. Ideally, we could also perform biorthogonal non-canonical amino acid-tagging (BONCAT), a sister approach to FUNCAT that allows for the identification and quantification of nascent proteins. BONCAT in $Gcn2^{KO/KO};Gars^{P278KY/+}$ motor neurons would identify exactly how the proteome changes due to mutations in *Gars*, without the confounding translational changes due to activation of the ISR. However, the extremely small amount of

material expected to be recovered from such a small affected cell population, and the complicated mouse breeding required, makes this experiment not feasible at this time.

Interestingly, the chronic dampening of translation initiation through the ISR seems at least as toxic to motor neurons as the original GARS insult, as its removal relieves around 50% of the neuropathy phenotype. Although we have not performed global motor neuron-specific gene expression analysis beyond a few ATF4 target genes in mutant *Gars* mice lacking GCN2, whole spinal cord RNA sequencing reveals surprisingly few changes compared to wild-type *Gars* mice lacking GCN2. This again supports the chronic activation of the ISR as a major contributor of the CMT2D phenotype.

This conclusion is in direct contrast to the protective role of ISR activation through GCN2 in mice with a loss-of-function $tRNA^{Arg}$ mutation that lack GTPBP2 ($nmf205^{-/-}$). In these mice, genetic removal of GCN2 accelerates neurodegeneration (Ishimura et al. 2016). Why would the ISR be protective to CNS neurons in one model of ribosome stalling and not in another?

The cerebellar ataxia that develops in $nmf205^{-/-}$ mice is a fast moving form of neurodegeneration. Mice progress from indistinguishable from wild-type at 3 weeks of age to death at 8-9 weeks. The rapid phenotype progression in $nmf205^{-/-}$ mice is likely due to the widespread ribosome stalling at AGA codons. These cells are under such stress due to the widespread stalling that the ISR helps to alleviate some of this stress by reducing translation initiation (which presumably decreases ribosome stalling and the amount of truncated protein produced). The ISR also may induce expression of stress response genes that prevent cell death programs from being turned on earlier. In this model, the inability to resolve stalled ribosomes at AGA codons due to the loss of GTPBP2 is the major insult to the cell.

In comparison to $nmf205^{-/-}$ mice, mutant *Gars* mice have an earlier onset of neurodegeneration between 1-2 weeks of age that “levels off” by 6-8 weeks of age and does not progress further (although synaptic dysfunction does get worse at least through 4 months of age) (Spaulding et al. 2016). Mutant *Gars* mice routinely live to at least 1 year of age. Mutant

Gars motor neurons may be under a much lower amount of stress compared to *nmf205*$^{-/-}$ mice, given that degeneration progresses fairly slowly and does not proceed to cell death or even get worse after early adulthood. This implies a lower amount of ribosome stalling. In these mice, sequestration of tRNA by GARS, and potentially impaired translation elongation, is hypothesized to be the major insult to the cell, not a failure to resolve stalled ribosomes. The lower level of stalled ribosomes induced by mutant GARS is enough to cause axon degeneration, but not enough to kill the cell. The ISR is activated by these stalled ribosomes, which then represents a "double hit" on translation. Because mutant *Gars* motor neurons are under a lower level, but longer-term stress, the ISR remains on throughout the life of the motor neuron. Thus, this chronic "double hit" to translation elongation and initiation is toxic rather than helpful to motor neurons.

The genetic experiments with *Gars* and *Gtpbp2* suggest that a failure to resolve stalled ribosomes does add an additional insult to the cell. This insult may lie in the paucity of recycled translation machinery available and/or in increased accumulation of truncated protein. Future gene expression analysis on *Gtpbp2*$^{-/-}$*;Gars*$^{C201R/+}$ spinal cord will help to illuminate the state of motor neurons with what is potentially a triple insult to translation: elongation slowdown due to mutant GARS, initiation inhibition via the ISR, and failure to resolve stalled ribosomes with the loss of GTPBP2.

Cell Type-Specificity of Translational Impairments

We have attempted to determine the cell type-specificity of translation impairment in unaffected tissues using puromycin labeling. However, because puromycin does not cross the blood-brain barrier, we have thus far been limited to tissues such as the liver and heart muscle. Ideally, we could use puromycin labeling to verify impairments in translation in motor neurons found with FUNCAT as well as compare to other neuronal types in the spinal cord. As mentioned earlier, we are attempting to measure translation in motor neurons and other cell types of the spinal cord using ICV administration of puromycin and immunohistochemical

analysis of puromycin incorporation. We would predict that motor neurons will be the only cell type with a severe translation impairment, both because CMT2D is a purely motor and sensory neuropathy and because of the striking restriction of ATF4 target gene expression to motor neurons in the spinal cord. While it is possible that other cell types of the spinal cord do undergo translation impairment and upregulate a different set of ATF4 target genes than the five we probed for using RNAscope, it seems surprising that these ATF4 target genes were not identified with whole spinal cord sequencing. Every ATF4 target gene identified in whole spinal cord was expressed in motor neurons based on RiboTagging. Levels of phosphorylated eIF2α could also be used to determine ISR activation in other cell types of the spinal cord. It is possible that impairments in translation are present in other cell types of the spinal cord but do not lead to activation of the ISR. However, the ATF4 target gene expression signal in whole spinal cord RNA sequencing is so strong, despite the relatively small population of cells expressing it, that it is hard to reconcile how major changes in other cell types wouldn't be evident in the gene expression signature.

Thus, the question remains, how could impairments in translation due to the sequestration of tRNA by a ubiquitously expressed ARS cause such striking cell type and subtype specificity? Whether because of the sheer scope of metabolic requirement of neurons, or because of the requirement for precisely coordinated translation at the synapse, the large size and highly polarized structure of neurons is often used as an explanation for the low tolerance neurons show towards translation dysregulation. This suggestion may be at least a partial explanation for the restriction of ATF4 target gene expression to mutant *Gars* alpha motor neurons and the largest sensory neurons. A mechanism by which mutant ARSs sequester tRNA is also unlikely to perturb non-canonical functions of ARSs, which may explain why dominant mutations that only impair translation do not cause multi-system syndromes seen in recessive loss-of-function patients.

Recent work has highlighted cell type-specific gene expression patterns of factors related to translation. Thus, cell type-specific differences in gene expression may contribute to motor and sensory neuron sensitivity to gain-of-function impairments in translation related to dominant mutations in ARSs. For example, low expression levels of certain tRNA genes in motor and sensory neurons might cause these tRNAs to become limiting in these neuronal subtypes. It is especially attractive to think that expression levels of specific isodecoders, which could vary from individual to individual, might underlie some of the phenotypic heterogeneity seen in human patients. As an indirect attempt to profile tRNA expression in sorted wild-type motor neurons at 7 weeks of age, a time just when neuropathy develops in the severe *Gars*$^{P278KY/+}$ model, we have performed Assay for Transposable Accessible Chromatin-sequencing (ATACseq). In these preliminary experiments we see open chromatin surrounding approximately 50% of all tRNA genes in motor neurons. Mice have 29 *tRNA*^{Gly} genes and in hematopoietic stem/progenitor cell types 26 out of those 29 were in areas of open chromatin. In contrast, in 1 week old motor neurons, only 13 out of 29 were in areas of open chromatin. Although these results are extremely preliminary, and were limited by the difficulty in sorting heavily myelinated motor neurons, this does support the idea that motor neurons could have a unique tRNA gene expression pattern. To ultimately determine if tRNA expression is a factor in determining the cell type-specificity of phenotypes in humans, laser capture of human spinal cord motor neurons and tRNA sequencing or qPCR would be necessary. With this approach tRNA expression could be precisely correlated with the innervation pattern of the motor neuron and mapped to different muscles of the body. This is especially intriguing in GARS patients, as they tend to show a curious tendency towards hand involvement.

In addition to expression levels of the tRNA, expression of the ARS itself could be higher in motor and sensory neurons, causing a greater sequestration of the tRNA. It is also possible that some mutant forms of ARS aberrantly sequester eEF1A during the handoff of aminoacylated tRNA. Higher levels of eEF1A expression in some cell types might counteract

this potential aberrant interaction. This mechanism could be specific for the isoform of eEF1A expressed in motor neurons and muscle, eEF1A2. However, past experiments suggest that muscle is not a primary affected tissue in *Gars* mice, and a translation impairment related to eEF1A2 would be expected to involve both tissue types.

Differences in ribosome recycling efficiency may also contribute to the sensitivity of motor and sensory neurons to dominant mutations in ARSs. Other cell types may be better at resolving stalled ribosomes due to impaired translation, preventing ISR activation. These differences might be due to gene expression of ribosome recycling factors, like GTPBP2. In future studies regarding the cell type-specificity of sensitivity to mutant GARS, it could be interesting to examine other cell types in *Gtpbp2*$^{-/-}$;*Gars*$^{C201R/+}$ mice. Perhaps removing a cell's ability to resolve stalled ribosomes not only worsens the state of motor neurons, but also causes dysfunction in other previously unaffected cell types. This is the case in mice with mutations in *Aars* that cause deficient editing (*Aars*$^{sti/sti}$). Removing a co-editing factor, ANKRD16, from Purkinje cells results in more widespread neurodegeneration. Completely removing ANKRD16 causes dysfunction in other cell types that results in embryonic lethality (Vo et al. 2018). In the case of *Gars*$^{C201R/+}$ mice, if unaffected cells have impaired translation, but simply do a better job at resolving stalled ribosomes, removal of GTPBP2 might bring that to light.

It is also possible that cell type-specificity arises because the motor and sensory neuron translatome is enriched for proteins abundant in the codons cognate to CMT-associated ARSs, making stalled ribosomes more abundant in these cell types. To test this we queried transcripts enriched in 1 week old and 8 week old *Gars*$^{+/+}$ motor neurons compared to whole spinal cord as identified in our RiboTagging data to determine if a potential enrichment for glycine codons exists. Abundance of transcripts enriched in motor neurons is weighted to transcript abundance taken from RNA sequencing data from C57BL/6J liver, a relatively homogenous tissue. We found no evidence for glycine codon enrichment in motor neurons of 1 week or 8 week old mice, indicating that codon bias is not a factor in determining cell type-specificity. Interestingly, a bias

for tryptophan codons was identified. Perhaps codon bias could be involved in the development of CMT associated with dominant mutations in *WARS* (analysis performed by Cedric Gobet).

Expression levels of ISR-activation genes may also differ between affected and unaffected cell types. For example, eIF2B may show higher expression in unaffected cell types, thereby reducing the effect of eIF2α phosphorylation on translation inhibition. Expression levels of eIF2α phosphatases could also be higher in other cell types, shutting of the ISR early and preventing chronic dampening of translation initiation.

Options for Treating Impairments in Translation

Identifying ISR activation through GCN2 as a major contributor to the CMT2D phenotype implies that inhibiting this activation could be therapeutically beneficial for patients. Directly inhibiting GCN2 would be the cleanest way of controlling aberrant activation of the ISR in motor neurons, and would have the least potential of unwanted effects on other tissues. Because *Gcn2*$^{KO/KO}$ mice are completely healthy, negative side effects are unlikely, as long as dietary nutrients and amino acids are in good supply. We are currently having GCN2 inhibitors synthesized for testing in mutant *Gars* mice. In the meantime, we are also treating mice with Integrated Stress Response Inhibitor (ISRIB), which enhances eIF2B's activity and renders the cell insensitive to eIF2α phosphorylation (Sidrauski et al. 2015).

In addition to targeting the ISR, directly targeting the tRNA sequestration mechanism is a possibility. Overexpression of cognate tRNA genes using AAV9 delivery should rescue phenotypes if the tRNA sequestration hypothesis is correct. Extensive studies in mammalian models regarding how much overexpression is required to rescue phenotypes without triggering more activation of the ISR through uncharged tRNA will be crucial. It is also possible that with some ARS mutations the sequestration is anticodon specific, although replacing all codons for a given tRNA family could be a safe approach. Morelli et al., (submitted) has shown good efficacy of selective mutant *Gars* knockdown, which is also a possibility in humans but would need to be

mutation-specific. With viral administration of gene therapy vectors, not all motor and sensory neurons are guaranteed to be infected. Thus, while gene therapy approaches hold great promise, a pharmacological, "one-size-fits-all" treatment approach to dominant mutations in ARSs, such as GCN2 inhibition, is also attractive. Ultimately, a combination of the two treatments may be the most effective at treating neuropathy.

Conclusion

Our first study, Spaulding et al., 2016, extensively characterized progressive synaptic dysfunction in two CMT2D mouse models and identified mitochondrial abnormalities at the synapse. The goal of our second study was to determine how dominant mutations in *GARS* cause CMT2D peripheral neuropathy. To this end, we profiled translation and transcription in motor neurons of three CMT2D mouse models to test for impairments in translation. This study has identified impaired translation in mutant *Gars* motor neurons and has identified the activation of the ISR through GCN2 in alpha motor neurons and the largest sensory neurons. We have also shown activation of the ISR in motor neurons of mice with dominant human mutations in *Yars*. We have yet to determine the exact mechanism by which mutant ARSs trigger GCN2 activation, but it is clear that ISR activation is a large contributor to peripheral neuropathy. We hypothesize that impaired translation, whether through ISR activation, primary mechanisms of mutant ARS, or both, represents a common contributor to disease in mice with mutations in *Gars* and *Yars*. Not all CMT-associated ARSs or all mutations in a given ARSs necessarily cause translational impairment through the same biochemical means. It will be important in the future to determine how translation is impaired on a mutation by mutation basis. It will also be crucial to look for signs of activation of the ISR through GCN2 in motor neurons of human patients, either through blood biomarker analysis or analysis of post-mortem spinal cord. If this mechanism can be extended to humans, our study will provide multiple new avenues for treatment, including regulation of the ISR and genetic replacement of translation factors, such as tRNAs.

CHAPTER 5

ADDITIONAL CONTRIBUTIONS TO THE FIELD

Severity of Demyelinating and Axonal Neuropathy Mouse Models is Modified by Genes Affecting Structure and Function of Peripheral Nodes. (2016), *Cell Reports*. Morelli, KH, Seburn KL, Schroeder DG, Spaulding EL, Dionne LA, Cox GA, Burgess RW.

Charcot-Marie-Tooth (CMT) disease is a clinically and genetically heterogeneous group of inherited polyneuropathies. Mutations in 80 genetic loci can cause forms of CMT, resulting in demyelination and axonal dysfunction. The clinical presentation, including sensory deficits, distal muscle weakness, and atrophy, can vary greatly in severity and progression. Here, we used mouse models of CMT to demonstrate genetic interactions that result in a more severe neuropathy phenotype. The cell adhesion molecule NRCAM and the Na^+ channel SCN8A (NaV1.6) are important components of nodes. Homozygous *Nrcam* and heterozygous *Scn8a* mutations synergized with both an *Sh3tc2* mutation, modeling recessive demyelinating Charcot-Marie-Tooth type 4C, and mutations in *Gars*, modeling dominant axonal Charcot-Marie-Tooth type 2D. We conclude that genetic variants perturbing the structure and function of nodes interact with mutations affecting the cable properties of axons by thinning myelin or reducing axon diameter. Therefore, genes integral to peripheral nodes are candidate modifiers of peripheral neuropathy. My role in this project was to image the femoral motor branches using electron microscopy and measure myelin packing around individual axons.

Trk Receptor Signaling and Sensory Neuron Fate are Perturbed in Human Neuropathy Caused by Gars mutations. (2017), *PNAS*. Sleigh JN, Dawes JM, West SJ, Wei N, Spaulding EL, Gomez-Martin A, Zhang Q, Burgess RW, Cader MZ, Talbot K, Yang XL, Bennett DL, Schiavo G.

Charcot-Marie-Tooth disease type 2D (CMT2D) is a peripheral nerve disorder caused by dominant, toxic, gain-of-function mutations in the widely expressed, housekeeping gene, *GARS* The mechanisms underlying selective nerve pathology in CMT2D remain unresolved, as does the cause of the mild-to-moderate sensory involvement that distinguishes CMT2D from the allelic disorder distal spinal muscular atrophy type V. To elucidate the mechanism responsible

for the underlying afferent nerve pathology, we examined the sensory nervous system of CMT2D mice. We show that the equilibrium between functional subtypes of sensory neuron in dorsal root ganglia is distorted by *Gars* mutations, leading to sensory defects in peripheral tissues and correlating with overall disease severity. CMT2D mice display changes in sensory behavior concordant with the afferent imbalance, which is present at birth and nonprogressive, indicating that sensory neuron identity is prenatally perturbed and that a critical developmental insult is key to the afferent pathology. Through in vitro experiments, mutant, but not wild-type, GlyRS was shown to aberrantly interact with the Trk receptors and cause misactivation of Trk signaling, which is essential for sensory neuron differentiation and development. Together, this work suggests that both neurodevelopmental and neurodegenerative mechanisms contribute to CMT2D pathogenesis, and thus has profound implications for the timing of future therapeutic treatments. My role in this project was to remove lumbar dorsal root ganglia from $Gars^{P278KY/+}$ mice for immunohistochemical analysis.

Paclitaxel-induced Epithelial Damage and Ectopic MMP-13 Expression Promotes Neurotoxicity in Zebrafish. (2016), PNAS. Lisse TS, Middleton LJ, Pellegrini AD, Martin PB, Spaulding EL, Lopes O, Brochu EA, Carter EV, Waldron A, Rieger S.

Paclitaxel is a microtubule-stabilizing chemotherapeutic agent that is widely used in cancer treatment and in a number of curative and palliative regimens. Despite its beneficial effects on cancer, paclitaxel also damages healthy tissues, most prominently the peripheral sensory nervous system. The mechanisms leading to paclitaxel-induced peripheral neuropathy remain elusive, and therapies that prevent or alleviate this condition are not available. We established a zebrafish in vivo model to study the underlying mechanisms and to identify pharmacological agents that may be developed into therapeutics. Both adult and larval zebrafish displayed signs of paclitaxel neurotoxicity, including sensory axon degeneration and the loss of touch response in the distal caudal fin. Intriguingly, studies in zebrafish larvae showed that paclitaxel rapidly promotes epithelial damage and decreased mechanical stress resistance of the skin before induction of axon degeneration. Moreover, injured paclitaxel-treated zebrafish skin and scratch-

wounded human keratinocytes (HEK001) display reduced healing capacity. Epithelial damage correlated with rapid accumulation of fluorescein-conjugated paclitaxel in epidermal basal keratinocytes, but not axons, and up-regulation of matrix-metalloproteinase 13 (MMP-13, collagenase 3) in the skin. Pharmacological inhibition of MMP-13, in contrast, largely rescued paclitaxel-induced epithelial damage and neurotoxicity, whereas MMP-13 overexpression in zebrafish embryos rendered the skin vulnerable to injury under mechanical stress conditions. Thus, our studies provide evidence that the epidermis plays a critical role in this condition, and we provide a previously unidentified candidate for therapeutic interventions. My role in this project was to help establish the initial *in vivo* larval and adult zebrafish models of paclitaxel-induced peripheral neuropathy by piloting delivery method of paclitaxel, motor function outcome measures, live imaging parameters, and quantification of axon degeneration.

REFERENCES

Achilli, F., V. Bros-Facer, H. P. Williams, G. T. Banks, M. AlQatari, R. Chia, V. Tucci, M. Groves, C. D. Nickols, K. L. Seburn, R. Kendall, M. Z. Cader, K. Talbot, J. van Minnen, R. W. Burgess, S. Brandner, J. E. Martin, M. Koltzenburg, L. Greensmith, P. M. Nolan, and E. M. Fisher. 2009a. 'An ENU-induced mutation in mouse glycyl-tRNA synthetase (GARS) causes peripheral sensory and motor phenotypes creating a model of Charcot-Marie-Tooth type 2D peripheral neuropathy', *Dis Model Mech*, 2: 359-73.

Alazami, A. M., H. Hijazi, M. S. Al-Dosari, R. Shaheen, A. Hashem, M. A. Aldahmesh, J. Y. Mohamed, A. Kentab, M. A. Salih, A. Awaji, T. A. Masoodi, and F. S. Alkuraya. 2013. 'Mutation in ADAT3, encoding adenosine deaminase acting on transfer RNA, causes intellectual disability and strabismus', *J Med Genet*, 50: 425-30.

Alvarez-Castelao, B., C. T. Schanzenbacher, C. Hanus, C. Glock, S. Tom Dieck, A. R. Dorrbaum, I. Bartnik, B. Nassim-Assir, E. Ciirdaeva, A. Mueller, D. C. Dieterich, D. A. Tirrell, J. D. Langer, and E. M. Schuman. 2017. 'Cell-type-specific metabolic labeling of nascent proteomes in vivo', *Nat Biotechnol*, 35: 1196-201.

Angaut-Petit, D., J. Molgo, A. L. Connold, and L. Faille. 1987. 'The levator auris longus muscle of the mouse: a convenient preparation for studies of short- and long-term presynaptic effects of drugs or toxins', *Neuroscience letters*, 82: 83-8.

Antonellis, A., R. E. Ellsworth, N. Sambuughin, I. Puls, A. Abel, S. Q. Lee-Lin, A. Jordanova, I. Kremensky, K. Christodoulou, L. T. Middleton, K. Sivakumar, V. Ionasescu, B. Funalot, J. M. Vance, L. G. Goldfarb, K. H. Fischbeck, and E. D. Green. 2003a. 'Glycyl tRNA synthetase mutations in Charcot-Marie-Tooth disease type 2D and distal spinal muscular atrophy type V', *American journal of human genetics*, 72: 1293-9.

———. 2003b. 'Glycyl tRNA synthetase mutations in Charcot-Marie-Tooth disease type 2D and distal spinal muscular atrophy type V', *Am J Hum Genet*, 72: 1293-9.

Antonellis, A., and E. D. Green. 2008. 'The role of aminoacyl-tRNA synthetases in genetic diseases', *Annu Rev Genomics Hum Genet*, 9: 87-107.

Aschrafi, A., A. D. Schwechter, M. G. Mameza, O. Natera-Naranjo, A. E. Gioio, and B. B. Kaplan. 2008. 'MicroRNA-338 regulates local cytochrome c oxidase IV mRNA levels and oxidative phosphorylation in the axons of sympathetic neurons', *J Neurosci*, 28: 12581-90.

Bais, P., K. Beebe, K. H. Morelli, M. E. Currie, S. N. Norberg, A. V. Evsikov, K. E. Miers, K. L. Seburn, V. Guergueltcheva, I. Kremensky, A. Jordanova, C. J. Bult, and R. W. Burgess. 2016. 'Metabolite profile of a mouse model of Charcot-Marie-Tooth type 2D neuropathy: implications for disease mechanisms and interventions', *Biol Open*, 5: 908-20.

Barbosa, C., I. Peixeiro, and L. Romao. 2013. 'Gene expression regulation by upstream open reading frames and human disease', *PLoS Genet*, 9: e1003529.

Bassell, G. J., H. Zhang, A. L. Byrd, A. M. Femino, R. H. Singer, K. L. Taneja, L. M. Lifshitz, I. M. Herman, and K. S. Kosik. 1998. 'Sorting of beta-actin mRNA and protein to neurites and growth cones in culture', *J Neurosci*, 18: 251-65.

Beattie, D. S. 1969. 'The biosynthesis of the protein and lipid components of the inner and outer membranes of rat liver mitochondria', *Biochem Biophys Res Commun*, 35: 67-74.

Bednarova, A., M. Hanna, I. Durham, T. VanCleave, A. England, A. Chaudhuri, and N. Krishnan. 2017. 'Lost in Translation: Defects in Transfer RNA Modifications and Neurological Disorders', *Front Mol Neurosci*, 10: 135.

Bengtson, M. H., and C. A. Joazeiro. 2010. 'Role of a ribosome-associated E3 ubiquitin ligase in protein quality control', *Nature*, 467: 470-3.

Blocquel, D., S. Li, N. Wei, H. Daub, M. Sajish, M. L. Erfurth, G. Kooi, J. Zhou, G. Bai, P. Schimmel, A. Jordanova, and X. L. Yang. 2017. 'Alternative stable conformation capable of protein misinteraction links tRNA synthetase to peripheral neuropathy', *Nucleic Acids Res*, 45: 8091-104.

Boczonadi, V., M. J. Jennings, and R. Horvath. 2018. 'The role of tRNA synthetases in neurological and neuromuscular disorders', *FEBS Lett*, 592: 703-17.

Bolam, J. P., and E. K. Pissadaki. 2012. 'Living on the edge with too many mouths to feed: why dopamine neurons die', *Mov Disord*, 27: 1478-83.

Brandman, O., and R. S. Hegde. 2016. 'Ribosome-associated protein quality control', *Nat Struct Mol Biol*, 23: 7-15.

Bunge, M. B. 1973. 'Fine structure of nerve fibers and growth cones of isolated sympathetic neurons in culture', *J Cell Biol*, 56: 713-35.

Burgess, R. W., G. A. Cox, and K. L. Seburn. 2010. 'Neuromuscular disease models and analysis', *Methods Mol Biol*, 602: 347-93.

Caceres, A., J. Busciglio, A. Ferreira, and O. Steward. 1988. 'An immunocytochemical and biochemical study of the microtubule-associated protein MAP-2 during post-lesion dendritic remodeling in the central nervous system of adult rats', *Brain Res*, 427: 233-46.

Chambers, D. M., J. Peters, and C. M. Abbott. 1998. 'The lethal mutation of the mouse wasted (wst) is a deletion that abolishes expression of a tissue-specific isoform of translation elongation factor 1alpha, encoded by the Eef1a2 gene', *Proc Natl Acad Sci U S A*, 95: 4463-8.

Chang, R. C., K. C. Suen, C. H. Ma, W. Elyaman, H. K. Ng, and J. Hugon. 2002. 'Involvement of double-stranded RNA-dependent protein kinase and phosphorylation of eukaryotic initiation factor-2alpha in neuronal degeneration', *J Neurochem*, 83: 1215-25.

Chang, R. C., A. K. Wong, H. K. Ng, and J. Hugon. 2002. 'Phosphorylation of eukaryotic initiation factor-2alpha (eIF2alpha) is associated with neuronal degeneration in Alzheimer's disease', *Neuroreport*, 13: 2429-32.

Charcot, J.-M., and P. Marie. 1886. ' Sur une forme particulière d'atrophie musculaire progressive, souvent familiale, debutant par les pieds et les jambes et atteignant plus tard les mains', *Rev. Med.*, 6: 97-138.

Chu, J., N. A. Hong, C. A. Masuda, B. V. Jenkins, K. A. Nelms, C. C. Goodnow, R. J. Glynne, H. Wu, E. Masliah, C. A. Joazeiro, and S. A. Kay. 2009. 'A mouse forward genetics screen identifies LISTERIN as an E3 ubiquitin ligase involved in neurodegeneration', *Proc Natl Acad Sci U S A*, 106: 2097-103.

Cosker, K. E., M. F. Pazyra-Murphy, S. J. Fenstermacher, and R. A. Segal. 2013. 'Target-derived neurotrophins coordinate transcription and transport of bclw to prevent axonal degeneration', *J Neurosci*, 33: 5195-207.

Court, F. A., and M. P. Coleman. 2012. 'Mitochondria as a central sensor for axonal degenerative stimuli', *Trends Neurosci*, 35: 364-72.

Court, F. A., W. T. Hendriks, H. D. MacGillavry, J. Alvarez, and J. van Minnen. 2008. 'Schwann cell to axon transfer of ribosomes: toward a novel understanding of the role of glia in the nervous system', *J Neurosci*, 28: 11024-9.

Court, F. A., R. Midha, B. A. Cisterna, J. Grochmal, A. Shakhbazau, W. T. Hendriks, and J. Van Minnen. 2011. 'Morphological evidence for a transport of ribosomes from Schwann cells to regenerating axons', *Glia*, 59: 1529-39.

Crnkovic, A., M. Cavuzic, V. Godinic-Mikulcic, G. Anderluh, I. Weygand-Durasevic, and I. Gruic-Sovulj. 2018. 'An archaeal aminoacyl-tRNA synthetase complex for improved substrate quality control', *Biochimie*, 147: 36-45.

Cruz, L. J., W. R. Gray, B. M. Olivera, R. D. Zeikus, L. Kerr, D. Yoshikami, and E. Moczydlowski. 1985. 'Conus geographus toxins that discriminate between neuronal and muscle sodium channels', *The Journal of biological chemistry*, 260: 9280-8.

Del Bo, R., F. Locatelli, S. Corti, M. Scarlato, S. Ghezzi, A. Prelle, G. Fagiolari, M. Moggio, M. Carpo, N. Bresolin, and G. P. Comi. 2006. 'Coexistence of CMT-2D and distal SMA-V phenotypes in an Italian family with a GARS gene mutation', *Neurology*, 66: 752-4.

Devi, L., and M. Ohno. 2013. 'Deletion of the eIF2alpha Kinase GCN2 fails to rescue the memory decline associated with Alzheimer's disease', *PLoS One*, 8: e77335.

———. 2014. 'PERK mediates eIF2alpha phosphorylation responsible for BACE1 elevation, CREB dysfunction and neurodegeneration in a mouse model of Alzheimer's disease', *Neurobiol Aging*, 35: 2272-81.

Droz, B., and C. P. Leblond. 1963. 'Axonal Migration of Proteins in the Central Nervous System and Peripheral Nerves as Shown by Radioautography', *J Comp Neurol*, 121: 325-46.

Dubourg, O., H. Azzedine, R. B. Yaou, J. Pouget, A. Barois, V. Meininger, D. Bouteiller, M. Ruberg, A. Brice, and E. LeGuern. 2006. 'The G526R glycyl-tRNA synthetase gene mutation in distal hereditary motor neuropathy type V', *Neurology*, 66: 1721-6.

Dyck, P.J. . 1975. 'Definition and basis of classification of hereditary neuropathy with neuronal atrophy and degeneration.' in P.J. Dyck, P.K. Thomas and E.H. Lambert (eds.), *Peripheral Neuropathy* (W.B. Saunders Company: Philadelphia, PA, USA).

Edstrom, A., and J. Sjostrand. 1969. 'Protein synthesis in the isolated Mauthner nerve fibre of goldfish', *J Neurochem*, 16: 67-81.

Eng, H., K. Lund, and R. B. Campenot. 1999. 'Synthesis of beta-tubulin, actin, and other proteins in axons of sympathetic neurons in compartmented cultures', *J Neurosci*, 19: 1-9.

Engel, A. G., X. M. Shen, D. Selcen, and S. M. Sine. 2015. 'Congenital myasthenic syndromes: pathogenesis, diagnosis, and treatment', *The Lancet. Neurology*, 14: 420-34.

Eriani, G., M. Delarue, O. Poch, J. Gangloff, and D. Moras. 1990. 'Partition of tRNA synthetases into two classes based on mutually exclusive sets of sequence motifs', *Nature*, 347: 203-6.

Ermanoska, B., W. W. Motley, R. Leitao-Goncalves, B. Asselbergh, L. H. Lee, P. De Rijk, K. Sleegers, T. Ooms, T. A. Godenschwege, V. Timmerman, K. H. Fischbeck, and A. Jordanova. 2014. 'CMT-associated mutations in glycyl- and tyrosyl-tRNA synthetases exhibit similar pattern of toxicity and share common genetic modifiers in Drosophila', *Neurobiol Dis*, 68: 180-9.

Eyman, M., C. Cefaliello, E. Ferrara, R. De Stefano, Z. S. Lavina, M. Crispino, A. Squillace, J. van Minnen, B. B. Kaplan, and A. Giuditta. 2007. 'Local synthesis of axonal and presynaptic RNA in squid model systems', *Eur J Neurosci*, 25: 341-50.

Fantin, A., B. Herzog, M. Mahmoud, M. Yamaji, A. Plein, L. Denti, C. Ruhrberg, and I. Zachary. 2014. 'Neuropilin 1 (NRP1) hypomorphism combined with defective VEGF-A binding reveals novel roles for NRP1 in developmental and pathological angiogenesis', *Development*, 141: 556-62.

Feng, G., R. H. Mellor, M. Bernstein, C. Keller-Peck, Q. T. Nguyen, M. Wallace, J. M. Nerbonne, J. W. Lichtman, and J. R. Sanes. 2000. 'Imaging neuronal subsets in transgenic mice expressing multiple spectral variants of GFP', *Neuron*, 28: 41-51.

Ferri, G. L., A. Sabani, L. Abelli, J. M. Polak, D. Dahl, and M. M. Portier. 1990. 'Neuronal intermediate filaments in rat dorsal root ganglia: differential distribution of peripherin and neurofilament protein immunoreactivity and effect of capsaicin', *Brain Res*, 515: 331-5.

Fisher, F. M., and E. Maratos-Flier. 2016. 'Understanding the Physiology of FGF21', *Annu Rev Physiol*, 78: 223-41.

Friese, A., J. A. Kaltschmidt, D. R. Ladle, M. Sigrist, T. M. Jessell, and S. Arber. 2009. 'Gamma and alpha motor neurons distinguished by expression of transcription factor Err3', *Proc Natl Acad Sci U S A*, 106: 13588-93.

Froelich, C. A., and E. A. First. 2011. 'Dominant Intermediate Charcot-Marie-Tooth disorder is not due to a catalytic defect in tyrosyl-tRNA synthetase', *Biochemistry*, 50: 7132-45.

Gilley, J., and M. P. Coleman. 2010. 'Endogenous Nmnat2 is an essential survival factor for maintenance of healthy axons', *PLoS Biol*, 8: e1000300.

Giuditta, A., A. Cupello, and G. Lazzarini. 1980. 'Ribosomal RNA in the axoplasm of the squid giant axon', *J Neurochem*, 34: 1757-60.

Giuditta, A., W. D. Dettbarn, and M. Brzin. 1968. 'Protein synthesis in the isolated giant axon of the squid', *Proc Natl Acad Sci U S A*, 59: 1284-7.

Giuditta, A., T. Hunt, and L. Santella. 1986. 'Rapid important paper Messenger RNA in squid axoplasm', *Neurochem Int*, 8: 435-42.

Giuditta, A., E. Menichini, C. Perrone Capano, M. Langella, R. Martin, E. Castigli, and B. B. Kaplan. 1991. 'Active polysomes in the axoplasm of the squid giant axon', *J Neurosci Res*, 28: 18-28.

Glavinovic, M. I. 1979. 'Voltage clamping of unparalysed cut rat diaphragm for study of transmitter release', *J Physiol*, 290: 467-80.

Gomez, C. M., R. Maselli, J. E. Gundeck, M. Chao, J. W. Day, S. Tamamizu, J. A. Lasalde, M. McNamee, and R. L. Wollmann. 1997. 'Slow-channel transgenic mice: a model of postsynaptic organellar degeneration at the neuromuscular junction', *The Journal of neuroscience : the official journal of the Society for Neuroscience*, 17: 4170-9.

Griffin, L. B., R. Sakaguchi, D. McGuigan, M. A. Gonzalez, C. Searby, S. Zuchner, Y. M. Hou, and A. Antonellis. 2014. 'Impaired function is a common feature of neuropathy-associated glycyl-tRNA synthetase mutations', *Hum Mutat*, 35: 1363-71.

Gumy, L. F., G. S. Yeo, Y. C. Tung, K. H. Zivraj, D. Willis, G. Coppola, B. Y. Lam, J. L. Twiss, C. E. Holt, and J. W. Fawcett. 2011. 'Transcriptome analysis of embryonic and adult sensory axons reveals changes in mRNA repertoire localization', *RNA*, 17: 85-98.

Guo, M., and P. Schimmel. 2013. 'Essential nontranslational functions of tRNA synthetases', *Nat Chem Biol*, 9: 145-53.

Guyton, D. L., and F. T. Hambrecht. 1974. 'Theory and design of capacitor electrodes for chronic stimulation', *Medical & biological engineering*, 12: 613-20.

Haghighat, A., S. Mader, A. Pause, and N. Sonenberg. 1995. 'Repression of cap-dependent translation by 4E-binding protein 1: competition with p220 for binding to eukaryotic initiation factor-4E', *EMBO J*, 14: 5701-9.

He, W., G. Bai, H. Zhou, N. Wei, N. M. White, J. Lauer, H. Liu, Y. Shi, C. D. Dumitru, K. Lettieri, V. Shubayev, A. Jordanova, V. Guergueltcheva, P. R. Griffin, R. W. Burgess, S. L. Pfaff, and X. L. Yang. 2015. 'CMT2D neuropathy is linked to the neomorphic binding activity of glycyl-tRNA synthetase', *Nature*, 526: 710-4.

He, W., H. M. Zhang, Y. E. Chong, M. Guo, A. G. Marshall, and X. L. Yang. 2011. 'Dispersed disease-causing neomorphic mutations on a single protein promote the same localized conformational opening', *Proc Natl Acad Sci U S A*, 108: 12307-12.

Hekman, K. E., G. Y. Yu, C. D. Brown, H. Zhu, X. Du, K. Gervin, D. E. Undlien, A. Peterson, G. Stevanin, H. B. Clark, S. M. Pulst, T. D. Bird, K. P. White, and C. M. Gomez. 2012. 'A conserved eEF2 coding variant in SCA26 leads to loss of translational fidelity and increased susceptibility to proteostatic insult', *Hum Mol Genet*, 21: 5472-83.

Hillefors, M., A. E. Gioio, M. G. Mameza, and B. B. Kaplan. 2007. 'Axon viability and mitochondrial function are dependent on local protein synthesis in sympathetic neurons', *Cell Mol Neurobiol*, 27: 701-16.

Hirokawa, N., S. Niwa, and Y. Tanaka. 2010. 'Molecular motors in neurons: transport mechanisms and roles in brain function, development, and disease', *Neuron*, 68: 610-38.

Holz, M. K., B. A. Ballif, S. P. Gygi, and J. Blenis. 2005. 'mTOR and S6K1 mediate assembly of the translation preinitiation complex through dynamic protein interchange and ordered phosphorylation events', *Cell*, 123: 569-80.

Inglis, A. J., G. R. Masson, S. Shao, O. Perisic, S. H. McLaughlin, R. S. Hegde, and R. L. Williams. 2019. 'Activation of GCN2 by the ribosomal P-stalk', *Proc Natl Acad Sci U S A*, 116: 4946-54.

Ishimura, R., G. Nagy, I. Dotu, J. H. Chuang, and S. L. Ackerman. 2016. 'Activation of GCN2 kinase by ribosome stalling links translation elongation with translation initiation', *Elife*, 5.

Ishimura, R., G. Nagy, I. Dotu, H. Zhou, X. L. Yang, P. Schimmel, S. Senju, Y. Nishimura, J. H. Chuang, and S. L. Ackerman. 2014. 'RNA function. Ribosome stalling induced by mutation of a CNS-specific tRNA causes neurodegeneration', *Science*, 345: 455-9.

Isohanni, P., T. Linnankivi, J. Buzkova, T. Lonnqvist, H. Pihko, L. Valanne, P. J. Tienari, I. Elovaara, T. Pirttila, M. Reunanen, K. Koivisto, S. Marjavaara, and A. Suomalainen. 2010. 'DARS2 mutations in mitochondrial leucoencephalopathy and multiple sclerosis', *Journal of medical genetics*, 47: 66-70.

Jaberi, E., M. Rohani, G. A. Shahidi, S. Nafissi, E. Arefian, M. Soleimani, P. Rasooli, H. Ahmadieh, N. Daftarian, M. KaramiNejadRanjbar, B. Klotzle, J. B. Fan, C. Turk, F. Steemers, and E. Elahi. 2016. 'Identification of mutation in GTPBP2 in patients of a family with neurodegeneration accompanied by iron deposition in the brain', *Neurobiol Aging*, 38: 216 e11-16 e18.

James, P. A., M. Z. Cader, F. Muntoni, A. M. Childs, Y. J. Crow, and K. Talbot. 2006. 'Severe childhood SMA and axonal CMT due to anticodon binding domain mutations in the GARS gene', *Neurology*, 67: 1710-2.

Jung, H., B. C. Yoon, and C. E. Holt. 2012. 'Axonal mRNA localization and local protein synthesis in nervous system assembly, maintenance and repair', *Nat Rev Neurosci*, 13: 308-24.

Juszkiewicz, S., V. Chandrasekaran, Z. Lin, S. Kraatz, V. Ramakrishnan, and R. S. Hegde. 2018. 'ZNF598 Is a Quality Control Sensor of Collided Ribosomes', *Mol Cell*, 72: 469-81 e7.

Kang, H., and E. M. Schuman. 1996. 'A requirement for local protein synthesis in neurotrophin-induced hippocampal synaptic plasticity', *Science*, 273: 1402-6.

Kapur, M., and S. L. Ackerman. 2018. 'mRNA Translation Gone Awry: Translation Fidelity and Neurological Disease', *Trends Genet*, 34: 218-31.

Kapur, M., C. E. Monaghan, and S. L. Ackerman. 2017. 'Regulation of mRNA Translation in Neurons-A Matter of Life and Death', *Neuron*, 96: 616-37.

Kellermann, O., H. Tonetti, A. Brevet, M. Mirande, J. P. Pailliez, and J. P. Waller. 1982. 'Macromolecular complexes from sheep and rabbit containing seven aminoacyl-tRNA synthetases. I. Species specificity of the polypeptide composition', *J Biol Chem*, 257: 11041-8.

Kim, H. S., Y. Choi, K. Y. Shin, Y. Joo, Y. K. Lee, S. Y. Jung, Y. H. Suh, and J. H. Kim. 2007. 'Swedish amyloid precursor protein mutation increases phosphorylation of eIF2alpha in vitro and in vivo', *J Neurosci Res*, 85: 1528-37.

Knowles, R. B., J. H. Sabry, M. E. Martone, T. J. Deerinck, M. H. Ellisman, G. J. Bassell, and K. S. Kosik. 1996. 'Translocation of RNA granules in living neurons', *J Neurosci*, 16: 7812-20.

Koenig, E. 1967. 'Synthetic mechanisms in the axon. IV. In vitro incorporation of [3H]precursors into axonal protein and RNA', *J Neurochem*, 14: 437-46.

Koenig, E., R. Martin, M. Titmus, and J. R. Sotelo-Silveira. 2000. 'Cryptic peripheral ribosomal domains distributed intermittently along mammalian myelinated axons', *J Neurosci*, 20: 8390-400.

Kong, L., X. Wang, D. W. Choe, M. Polley, B. G. Burnett, M. Bosch-Marce, J. W. Griffin, M. M. Rich, and C. J. Sumner. 2009. 'Impaired synaptic vesicle release and immaturity of neuromuscular junctions in spinal muscular atrophy mice', *The Journal of neuroscience : the official journal of the Society for Neuroscience*, 29: 842-51.

Kushwaha, G. S., G. Bange, and N. S. Bhavesh. 2019. 'Interaction studies on bacterial stringent response protein RelA with uncharged tRNA provide evidence for its prerequisite complex for ribosome binding', *Curr Genet*.

Lam, W. W., J. J. Millichap, D. C. Soares, R. Chin, A. McLellan, D. R. FitzPatrick, F. Elmslie, M. M. Lees, G. B. Schaefer, D. D. D. study, and C. M. Abbott. 2016. 'Novel de novo EEF1A2 missense mutations causing epilepsy and intellectual disability', *Mol Genet Genomic Med*, 4: 465-74.

Landers, J. E., J. Melki, V. Meininger, J. D. Glass, L. H. van den Berg, M. A. van Es, P. C. Sapp, P. W. van Vught, D. M. McKenna-Yasek, H. M. Blauw, T. J. Cho, M. Polak, L. Shi, A. M. Wills, W. J. Broom, N. Ticozzi, V. Silani, A. Ozoguz, I. Rodriguez-Leyva, J. H. Veldink, A. J. Ivinson, C. G. Saris, B. A. Hosler, A. Barnes-Nessa, N. Couture, J. H. Wokke, T. J. Kwiatkowski, Jr., R. A. Ophoff, S. Cronin, O. Hardiman, F. P. Diekstra, P. N. Leigh, C. E. Shaw, C. L. Simpson, V. K. Hansen, J. F. Powell, P. Corcia, F. Salachas, S. Heath, P. Galan, F. Georges, H. R. Horvitz, M. Lathrop, S. Purcell, A. Al-Chalabi, and R. H. Brown, Jr. 2009. 'Reduced expression of the Kinesin-Associated Protein 3 (KIFAP3) gene increases survival in sporadic amyotrophic lateral sclerosis', *Proc Natl Acad Sci U S A*, 106: 9004-9.

Lasek, R. J., C. Dabrowski, and R. Nordlander. 1973. 'Analysis of axoplasmic RNA from invertebrate giant axons', *Nat New Biol*, 244: 162-5.

Lasek, R. J., H. Gainer, and J. L. Barker. 1977. 'Cell-to-cell transfer of glial proteins to the squid giant axon. The glia-neuron protein trnasfer hypothesis', *J Cell Biol*, 74: 501-23.

Le Pichon, C. E., and A. T. Chesler. 2014. 'The functional and anatomical dissection of somatosensory subpopulations using mouse genetics', *Front Neuroanat*, 8: 21.

Lee, J. W., K. Beebe, L. A. Nangle, J. Jang, C. M. Longo-Guess, S. A. Cook, M. T. Davisson, J. P. Sundberg, P. Schimmel, and S. L. Ackerman. 2006. 'Editing-defective tRNA synthetase causes protein misfolding and neurodegeneration', *Nature*, 443: 50-5.

Lee, S., A. LeBlanc, A. Duttaroy, and E. Wang. 1995. 'Terminal differentiation-dependent alteration in the expression of translation elongation factor-1 alpha and its sister gene, S1, in neurons', *Exp Cell Res*, 219: 589-97.

Lee, S., L. A. Wolfraim, and E. Wang. 1993. 'Differential expression of S1 and elongation factor-1 alpha during rat development', *J Biol Chem*, 268: 24453-9.

Leon, K., T. Boulo, A. Musnier, J. Morales, C. Gauthier, L. Dupuy, S. Heyne, R. Backofen, A. Poupon, P. Cormier, E. Reiter, and P. Crepieux. 2014. 'Activation of a GPCR leads to eIF4G phosphorylation at the 5' cap and to IRES-dependent translation', *J Mol Endocrinol*, 52: 373-82.

Leung, K. M., F. P. van Horck, A. C. Lin, R. Allison, N. Standart, and C. E. Holt. 2006. 'Asymmetrical beta-actin mRNA translation in growth cones mediates attractive turning to netrin-1', *Nat Neurosci*, 9: 1247-56.

Li, X., I. Alafuzoff, H. Soininen, B. Winblad, and J. J. Pei. 2005. 'Levels of mTOR and its downstream targets 4E-BP1, eEF2, and eEF2 kinase in relationships with tau in Alzheimer's disease brain', *FEBS J*, 272: 4211-20.

Linda, H., M. K. Skold, and T. Ochsmann. 2011. 'Activating transcription factor 3, a useful marker for regenerative response after nerve root injury', *Front Neurol*, 2: 30.

Lomo, T., and J. Rosenthal. 1972. 'Control of ACh sensitivity by muscle activity in the rat', *The Journal of physiology*, 221: 493-513.

Ma, T., M. A. Trinh, A. J. Wexler, C. Bourbon, E. Gatti, P. Pierre, D. R. Cavener, and E. Klann. 2013. 'Suppression of eIF2alpha kinases alleviates Alzheimer's disease-related plasticity and memory deficits', *Nat Neurosci*, 16: 1299-305.

Ma, X. M., and J. Blenis. 2009. 'Molecular mechanisms of mTOR-mediated translational control', *Nat Rev Mol Cell Biol*, 10: 307-18.

Magrassi, L., D. Purves, and J. W. Lichtman. 1987. 'Fluorescent probes that stain living nerve terminals', *The Journal of neuroscience : the official journal of the Society for Neuroscience*, 7: 1207-14.

Matsuda, W., T. Furuta, K. C. Nakamura, H. Hioki, F. Fujiyama, R. Arai, and T. Kaneko. 2009. 'Single nigrostriatal dopaminergic neurons form widely spread and highly dense axonal arborizations in the neostriatum', *J Neurosci*, 29: 444-53.

Mayer, C., J. Zhao, X. Yuan, and I. Grummt. 2004. 'mTOR-dependent activation of the transcription factor TIF-IA links rRNA synthesis to nutrient availability', *Genes Dev*, 18: 423-34.

McLaughlin, H. M., R. Sakaguchi, C. Liu, T. Igarashi, D. Pehlivan, K. Chu, R. Iyer, P. Cruz, P. F. Cherukuri, N. F. Hansen, J. C. Mullikin, L. G. Biesecker, T. E. Wilson, V. Ionasescu, G. Nicholson, C. Searby, K. Talbot, J. M. Vance, S. Zuchner, K. Szigeti, J. R. Lupski, Y. M. Hou, E. D. Green, and A. Antonellis. 2010. 'Compound heterozygosity for loss-of-function lysyl-tRNA synthetase mutations in a patient with peripheral neuropathy', *American journal of human genetics*, 87: 560-6.

Merianda, T. T., A. C. Lin, J. S. Lam, D. Vuppalanchi, D. E. Willis, N. Karin, C. E. Holt, and J. L. Twiss. 2009. 'A functional equivalent of endoplasmic reticulum and Golgi in axons for secretion of locally synthesized proteins', *Mol Cell Neurosci*, 40: 128-42.

Meyer-Schuman, R., and A. Antonellis. 2017. 'Emerging mechanisms of aminoacyl-tRNA synthetase mutations in recessive and dominant human disease', *Hum Mol Genet*, 26: R114-R27.

Ming, Gl, A. M. Lohof, and J. Q. Zheng. 1997. 'Acute morphogenic and chemotropic effects of neurotrophins on cultured embryonic Xenopus spinal neurons', *J Neurosci*, 17: 7860-71.

Mirande, M. 2010. 'Processivity of translation in the eukaryote cell: role of aminoacyl-tRNA synthetases', *FEBS Lett*, 584: 443-7.

Mirande, M., Y. Gache, D. Le Corre, and J. P. Waller. 1982. 'Seven mammalian aminoacyl-tRNA synthetases co-purified as high molecular weight entities are associated within the same complex', *EMBO J*, 1: 733-6.

Mo, Z., X. Zhao, H. Liu, Q. Hu, X. Q. Chen, J. Pham, N. Wei, Z. Liu, J. Zhou, R. W. Burgess, S. L. Pfaff, C. T. Caskey, C. Wu, G. Bai, and X. L. Yang. 2018. 'Aberrant GlyRS-HDAC6 interaction linked to axonal transport deficits in Charcot-Marie-Tooth neuropathy', *Nat Commun*, 9: 1007.

Motley, W. W., K. L. Seburn, M. H. Nawaz, K. E. Miers, J. Cheng, A. Antonellis, E. D. Green, K. Talbot, X. L. Yang, K. H. Fischbeck, and R. W. Burgess. 2011a. 'Charcot-Marie-Tooth-Linked Mutant GARS Is Toxic to Peripheral Neurons Independent of Wild-Type GARS Levels', *PLoS genetics*, 7: e1002399.

———. 2011b. 'Charcot-Marie-Tooth-linked mutant GARS is toxic to peripheral neurons independent of wild-type GARS levels', *PLoS Genet*, 7: e1002399.

Mudge, S. J., J. H. Williams, H. J. Eyre, G. R. Sutherland, P. J. Cowan, and D. A. Power. 1998. 'Complex organisation of the 5'-end of the human glycine tRNA synthetase gene', *Gene*, 209: 45-50.

Myszka, D. G., M. D. Jonsen, and B. J. Graves. 1998. 'Equilibrium analysis of high affinity interactions using BIACORE', *Anal Biochem*, 265: 326-30.

Najmabadi, H., H. Hu, M. Garshasbi, T. Zemojtel, S. S. Abedini, W. Chen, M. Hosseini, F. Behjati, S. Haas, P. Jamali, A. Zecha, M. Mohseni, L. Puttmann, L. N. Vahid, C. Jensen, L. A. Moheb, M. Bienek, F. Larti, I. Mueller, R. Weissmann, H. Darvish, K. Wrogemann, V. Hadavi, B. Lipkowitz, S. Esmaeeli-Nieh, D. Wieczorek, R. Kariminejad, S. G. Firouzabadi, M. Cohen, Z. Fattahi, I. Rost, F. Mojahedi, C. Hertzberg, A. Dehghan, A. Rajab, M. J. Banavandi, J. Hoffer, M. Falah, L. Musante, V. Kalscheuer, R. Ullmann, A. W. Kuss, A. Tzschach, K. Kahrizi, and H. H. Ropers. 2011. 'Deep sequencing reveals 50 novel genes for recessive cognitive disorders', *Nature*, 478: 57-63.

Negrutskii, B. S., and M. P. Deutscher. 1992. 'A sequestered pool of aminoacyl-tRNA in mammalian cells', *Proc Natl Acad Sci U S A*, 89: 3601-4.

Niehues, S., J. Bussmann, G. Steffes, I. Erdmann, C. Kohrer, L. Sun, M. Wagner, K. Schafer, G. Wang, S. N. Koerdt, M. Stum, S. Jaiswal, U. L. RajBhandary, U. Thomas, H. Aberle, R. W. Burgess, X. L. Yang, D. Dieterich, and E. Storkebaum. 2015. 'Impaired protein translation in Drosophila models for Charcot-Marie-Tooth neuropathy caused by mutant tRNA synthetases', *Nat Commun*, 6: 7520.

Nishimune, H. 2012. 'Active zones of mammalian neuromuscular junctions: formation, density, and aging', *Annals of the New York Academy of Sciences*, 1274: 24-32.

Nishimune, H., J. R. Sanes, and S. S. Carlson. 2004. 'A synaptic laminin-calcium channel interaction organizes active zones in motor nerve terminals', *Nature*, 432: 580-7.

Olink-Coux, M., and P. J. Hollenbeck. 1996. 'Localization and active transport of mRNA in axons of sympathetic neurons in culture', *J Neurosci*, 16: 1346-58.

Pakos-Zebrucka, K., I. Koryga, K. Mnich, M. Ljujic, A. Samali, and A. M. Gorman. 2016. 'The integrated stress response', *EMBO Rep*, 17: 1374-95.

Park, S., D. G. Myszka, M. Yu, S. J. Littler, and I. A. Laird-Offringa. 2000. 'HuD RNA recognition motifs play distinct roles in the formation of a stable complex with AU-rich RNA', *Mol Cell Biol*, 20: 4765-72.

Paton, W. D., and D. R. Waud. 1967. 'The margin of safety of neuromuscular transmission', *The Journal of physiology*, 191: 59-90.

Pazyra-Murphy, M. F., A. Hans, S. L. Courchesne, C. Karch, K. E. Cosker, H. M. Heerssen, F. L. Watson, T. Kim, M. E. Greenberg, and R. A. Segal. 2009. 'A retrograde neuronal survival response: target-derived neurotrophins regulate MEF2D and bcl-w', *J Neurosci*,29: 6700-9.

Pease, S. E., and R. A. Segal. 2014. 'Preserve and protect: maintaining axons within functional circuits', *Trends Neurosci*, 37: 572-82.

Perluigi, M., F. Di Domenico, and D. A. Butterfield. 2015. 'mTOR signaling in aging and neurodegeneration: At the crossroad between metabolism dysfunction and impairment of autophagy', *Neurobiol Dis*, 84: 39-49.

Perona, J. J., and I. Gruic-Sovulj. 2014. 'Synthetic and editing mechanisms of aminoacyl-tRNA synthetases', *Top Curr Chem*, 344: 1-41.

Perry, R. B., and M. Fainzilber. 2014. 'Local translation in neuronal processes--in vivo tests of a "heretical hypothesis"', *Dev Neurobiol*, 74: 210-7.

Perry, R. B., I. Rishal, E. Doron-Mandel, A. L. Kalinski, K. F. Medzihradszky, M. Terenzio, S. Alber, S. Koley, A. Lin, M. Rozenbaum, D. Yudin, P. K. Sahoo, C. Gomes, V. Shinder, W. Geraisy, E. A. Huebner, C. J. Woolf, A. Yaron, A. L. Burlingame, J. L. Twiss, and M. Fainzilber. 2016. 'Nucleolin-Mediated RNA Localization Regulates Neuron Growth and Cycling Cell Size', *Cell Rep*, 16: 1664-76.

Plomp, J. J., M. N. Vergouwe, A. M. Van den Maagdenberg, M. D. Ferrari, R. R. Frants, and P. C. Molenaar. 2000. 'Abnormal transmitter release at neuromuscular junctions of mice carrying the tottering alpha(1A) Ca(2+) channel mutation', *Brain : a journal of neurology*, 123 Pt 3: 463-71.

Puffenberger, E. G., R. N. Jinks, C. Sougnez, K. Cibulskis, R. A. Willert, N. P. Achilly, R. P. Cassidy, C. J. Fiorentini, K. F. Heiken, J. J. Lawrence, M. H. Mahoney, C. J. Miller, D. T. Nair, K. A. Politi, K. N. Worcester, R. A. Setton, R. Dipiazza, E. A. Sherman, J. T. Eastman, C. Francklyn, S. Robey-Bond, N. L. Rider, S. Gabriel, D. H. Morton, and K. A. Strauss. 2012. 'Genetic mapping and exome sequencing identify variants associated with five novel diseases', *PLoS One*, 7: e28936.

Putney, S. D., and P. Schimmel. 1981. 'An aminoacyl tRNA synthetase binds to a specific DNA sequence and regulates its gene transcription', *Nature*, 291: 632-5.

Rafael, J. A., Y. Nitta, J. Peters, and K. E. Davies. 2000. 'Testing of SHIRPA, a mouse phenotypic assessment protocol, on Dmd(mdx) and Dmd(mdx3cv) dystrophin-deficient mice', *Mammalian genome : official journal of the International Mammalian Genome Society*, 11: 725-8.

Reinthaler, E. M., D. Lal, W. Jurkowski, M. Feucht, H. Steinbock, U. Gruber-Sedlmayr, G. M. Ronen, J. Geldner, E. Haberlandt, B. Neophytou, A. Hahn, J. Altmuller, H. Thiele, M. R. Toliat, Epinomics Consortium Euro, H. Lerche, P. Nurnberg, T. Sander, B. A. Neubauer, and F. Zimprich. 2014. 'Analysis of ELP4, SRPX2, and interacting genes in typical and atypical rolandic epilepsy', *Epilepsia*, 55: e89-93.

Ribas de Pouplana, L., and P. Schimmel. 2001. 'Two classes of tRNA synthetases suggested by sterically compatible dockings on tRNA acceptor stem', *Cell*, 104: 191-3.

Rich, M. M. 2006. 'The control of neuromuscular transmission in health and disease', *The Neuroscientist : a review journal bringing neurobiology, neurology and psychiatry*, 12: 134-42.

Rich, M. M., R. F. Waldeck, L. C. Cork, R. J. Balice-Gordon, R. E. Fyffe, X. Wang, T. C. Cope, and M. J. Pinter. 2002. 'Reduced endplate currents underlie motor unit dysfunction in canine motor neuron disease', *J Neurophysiol*, 88: 3293-304.

Robitaille, R., and M. P. Charlton. 1992. 'Presynaptic calcium signals and transmitter release are modulated by calcium-activated potassium channels', *J Neurosci*, 12: 297-305.

Rohkamm, B., M. M. Reilly, H. Lochmuller, B. Schlotter-Weigel, N. Barisic, L. Schols, G. Nicholson, D. Pareyson, M. Laura, A. R. Janecke, G. Miltenberger-Miltenyi, E. John, C. Fischer, F. Grill, W. Wakeling, M. Davis, T. R. Pieber, and M. Auer-Grumbach. 2007. 'Further evidence for genetic heterogeneity of distal HMN type V, CMT2 with predominant hand involvement and Silver syndrome', *Journal of the neurological sciences*, 263: 100-6.

Ryckelynck, M., R. Giege, and M. Frugier. 2005. 'tRNAs and tRNA mimics as cornerstones of aminoacyl-tRNA synthetase regulations', *Biochimie*, 87: 835-45.

Saitsu, H., H. Osaka, M. Sasaki, J. Takanashi, K. Hamada, A. Yamashita, H. Shibayama, M. Shiina, Y. Kondo, K. Nishiyama, Y. Tsurusaki, N. Miyake, H. Doi, K. Ogata, K. Inoue, and N. Matsumoto. 2011. 'Mutations in POLR3A and POLR3B encoding RNA Polymerase III subunits cause an autosomal-recessive hypomyelinating leukoencephalopathy', *Am J Hum Genet*, 89: 644-51.

Sanz, E., L. Yang, T. Su, D. R. Morris, G. S. McKnight, and P. S. Amieux. 2009. 'Cell-type-specific isolation of ribosome-associated mRNA from complex tissues', *Proc Natl Acad Sci U S A*, 106: 13939-44.

Saporta, M. A., and M. E. Shy. 2013a. 'Inherited peripheral neuropathies', *Neurol Clin*, 31: 597-619.

———. 2013b. 'Inherited peripheral neuropathies', *Neurologic clinics*, 31: 597-619.

Scheper, G. C., T. van der Klok, R. J. van Andel, C. G. van Berkel, M. Sissler, J. Smet, T. I. Muravina, S. V. Serkov, G. Uziel, M. Bugiani, R. Schiffmann, I. Krageloh-Mann, J. A. Smeitink, C. Florentz, R. Van Coster, J. C. Pronk, and M. S. van der Knaap. 2007. 'Mitochondrial aspartyl-tRNA synthetase deficiency causes leukoencephalopathy with brain stem and spinal cord involvement and lactate elevation', *Nature genetics*, 39: 534-9.

Schimmel, P. 1987. 'Aminoacyl tRNA synthetases: general scheme of structure-function relationships in the polypeptides and recognition of transfer RNAs', *Annu Rev Biochem*, 56: 125-58.

———. 2018. 'The emerging complexity of the tRNA world: mammalian tRNAs beyond protein synthesis', *Nat Rev Mol Cell Biol*, 19: 45-58.

Schimmel, P. R., and D. Soll. 1979. 'Aminoacyl-tRNA synthetases: general features and recognition of transfer RNAs', *Annu Rev Biochem*, 48: 601-48.

Schwarz, T. L. 2013. 'Mitochondrial trafficking in neurons', *Cold Spring Harb Perspect Biol*, 5.

Scripture, C. D., W. D. Figg, and A. Sparreboom. 2006. 'Peripheral neuropathy induced by paclitaxel: recent insights and future perspectives', *Curr Neuropharmacol*, 4: 165-72.

Seburn, K. L., L. A. Nangle, G. A. Cox, P. Schimmel, and R. W. Burgess. 2006. 'An active dominant mutation of glycyl-tRNA synthetase causes neuropathy in a Charcot-Marie-Tooth 2D mouse model', *Neuron*, 51: 715-26.

Shao, S., A. Brown, B. Santhanam, and R. S. Hegde. 2015. 'Structure and assembly pathway of the ribosome quality control complex', *Mol Cell*, 57: 433-44.

Shaw, K. P., Y. Aracava, A. Akaike, J. W. Daly, D. L. Rickett, and E. X. Albuquerque. 1985. 'The reversible cholinesterase inhibitor physostigmine has channel-blocking and agonist effects on the acetylcholine receptor-ion channel complex', *Molecular pharmacology*, 28: 527-38.

Shen, H., D. M. Barry, J. M. Dale, V. B. Garcia, N. A. Calcutt, and M. L. Garcia. 2011. 'Muscle pathology without severe nerve pathology in a new mouse model of Charcot-Marie-Tooth disease type 2E', *Human molecular genetics*, 20: 2535-48.

Shiba, K., P. Schimmel, H. Motegi, and T. Noda. 1994. 'Human glycyl-tRNA synthetase. Wide divergence of primary structure from bacterial counterpart and species-specific aminoacylation', *The Journal of biological chemistry*, 269: 30049-55.

Shigeoka, T., H. Jung, J. Jung, B. Turner-Bridger, J. Ohk, J. Q. Lin, P. S. Amieux, and C. E. Holt. 2016. 'Dynamic Axonal Translation in Developing and Mature Visual Circuits', *Cell*, 166: 181-92.

Shoemaker, C. J., D. E. Eyler, and R. Green. 2010. 'Dom34:Hbs1 promotes subunit dissociation and peptidyl-tRNA drop-off to initiate no-go decay', *Science*, 330: 369-72.

Sidrauski, C., J. C. Tsai, M. Kampmann, B. R. Hearn, P. Vedantham, P. Jaishankar, M. Sokabe, A. S. Mendez, B. W. Newton, E. L. Tang, E. Verschueren, J. R. Johnson, N. J. Krogan, C. S. Fraser, J. S. Weissman, A. R. Renslo, and P. Walter. 2015. 'Pharmacological dimerization and activation of the exchange factor eIF2B antagonizes the integrated stress response', *Elife*, 4: e07314.

Sivakumar, K., T. Kyriakides, I. Puls, G. A. Nicholson, B. Funalot, A. Antonellis, N. Sambuughin, K. Christodoulou, J. L. Beggs, E. Zamba-Papanicolaou, V. Ionasescu, M. C. Dalakas, E. D. Green, K. H. Fischbeck, and L. G. Goldfarb. 2005. 'Phenotypic spectrum of disorders associated with glycyl-tRNA synthetase mutations', *Brain : a journal of neurology*, 128: 2304-14.

Skre, H. 1974a. 'Genetic and clinical aspects of Charcot-Marie-Tooth's disease', *Clin Genet*, 6: 98-118.

———. 1974b. 'Genetic and clinical aspects of Charcot-Marie-Tooth's disease', *Clinical genetics*, 6: 98-118.

Sleigh, J. N., J. M. Dawes, S. J. West, N. Wei, E. L. Spaulding, A. Gomez-Martin, Q. Zhang, R. W. Burgess, M. Z. Cader, K. Talbot, X. L. Yang, D. L. Bennett, and G. Schiavo. 2017. 'Trk receptor signaling and sensory neuron fate are perturbed in human neuropathy caused by Gars mutations', *Proc Natl Acad Sci U S A*, 114: E3324-E33.

Sleigh, J. N., A. Gomez-Martin, N. Wei, G. Bai, X. L. Yang, and G. Schiavo. 2017. 'Neuropilin 1 sequestration by neuropathogenic mutant glycyl-tRNA synthetase is permissive to vascular homeostasis', *Sci Rep*, 7: 9216.

Sleigh, J. N., S. J. Grice, R. W. Burgess, K. Talbot, and M. Z. Cader. 2014. 'Neuromuscular junction maturation defects precede impaired lower motor neuron connectivity in Charcot-Marie-Tooth type 2D mice', *Human molecular genetics*, 23: 2639-50.

Spaulding, E. L., J. N. Sleigh, K. H. Morelli, M. J. Pinter, R. W. Burgess, and K. L. Seburn. 2016. 'Synaptic Deficits at Neuromuscular Junctions in Two Mouse Models of Charcot-Marie-Tooth Type 2d', *J Neurosci*, 36: 3254-67.

Stapulionis, R., and M. P. Deutscher. 1995. 'A channeled tRNA cycle during mammalian protein synthesis', *Proc Natl Acad Sci U S A*, 92: 7158-61.

Starkey, M. L., M. Davies, P. K. Yip, L. M. Carter, D. J. Wong, S. B. McMahon, and E. J. Bradbury. 2009. 'Expression of the regeneration-associated protein SPRR1A in primary sensory neurons and spinal cord of the adult mouse following peripheral and central injury', *J Comp Neurol*, 513: 51-68.

Steward, O. 1983. 'Polyribosomes at the base of dendritic spines of central nervous system neurons--their possible role in synapse construction and modification', *Cold Spring Harb Symp Quant Biol*, 48 Pt 2: 745-59.

Steward, O., and W. B. Levy. 1982. 'Preferential localization of polyribosomes under the base of dendritic spines in granule cells of the dentate gyrus', *J Neurosci*, 2: 284-91.

Steward, O., and C. E. Ribak. 1986. 'Polyribosomes associated with synaptic specializations on axon initial segments: localization of protein-synthetic machinery at inhibitory synapses', *J Neurosci*, 6: 3079-85.

Stifani, N. 2014. 'Motor neurons and the generation of spinal motor neuron diversity', *Front Cell Neurosci*, 8: 293.

Stolz, A., W. Hilt, A. Buchberger, and D. H. Wolf. 2011. 'Cdc48: a power machine in protein degradation', *Trends Biochem Sci*, 36: 515-23.

Stowers, R. S., L. J. Megeath, J. Gorska-Andrzejak, I. A. Meinertzhagen, and T. L. Schwarz. 2002. 'Axonal transport of mitochondria to synapses depends on milton, a novel Drosophila protein', *Neuron*, 36: 1063-77.

Stum, M., H. M. McLaughlin, E. L. Kleinbrink, K. E. Miers, S. L. Ackerman, K. L. Seburn, A. Antonellis, and R. W. Burgess. 'An assessment of mechanisms underlying peripheral axonal degeneration caused by aminoacyl-tRNA synthetase mutations', *Mol Cell Neurosci*.

———. 2011. 'An assessment of mechanisms underlying peripheral axonal degeneration caused by aminoacyl-tRNA synthetase mutations', *Molecular and cellular neurosciences*, 46: 432-43.

Tcherkezian, J., P. A. Brittis, F. Thomas, P. P. Roux, and J. G. Flanagan. 2010. 'Transmembrane receptor DCC associates with protein synthesis machinery and regulates translation', *Cell*, 141: 632-44.

Tennyson, V. M. 1970. 'The fine structure of the axon and growth cone of the dorsal root neuroblast of the rabbit embryo', *J Cell Biol*, 44: 62-79.

Thomsen, R. H., and D. F. Wilson. 1983. 'Effects of 4-aminopyridine and 3,4-diaminopyridine on transmitter release at the neuromuscular junction', *The Journal of pharmacology and experimental therapeutics*, 227: 260-5.

Timmerman, V., A. V. Strickland, and S. Zuchner. 2014. 'Genetics of Charcot-Marie-Tooth (CMT) Disease within the Frame of the Human Genome Project Success', *Genes (Basel)*, 5: 13-32.

Tolkunova, E., H. Park, J. Xia, M. P. King, and E. Davidson. 2000. 'The human lysyl-tRNA synthetase gene encodes both the cytoplasmic and mitochondrial enzymes by means of an unusual alternative splicing of the primary transcript', *The Journal of biological chemistry*, 275: 35063-9.

Tom Dieck, S., A. Muller, A. Nehring, F. I. Hinz, I. Bartnik, E. M. Schuman, and D. C. Dieterich. 2012. 'Metabolic labeling with noncanonical amino acids and visualization by chemoselective fluorescent tagging', *Curr Protoc Cell Biol*, Chapter 7: Unit7 11.

tom Dieck, S., L. Sanmarti-Vila, K. Langnaese, K. Richter, S. Kindler, A. Soyke, H. Wex, K. H. Smalla, U. Kampf, J. T. Franzer, M. Stumm, C. C. Garner, and E. D. Gundelfinger. 1998. 'Bassoon, a novel zinc-finger CAG/glutamine-repeat protein selectively localized at the active zone of presynaptic nerve terminals', *The Journal of cell biology*, 142: 499-509.

Tooth, H.H. 1886. *The Peroneal Type of Progressive Muscular Atrophy* (H.K. Lewis and Co : London).

Trinh, M. A., and E. Klann. 2013. 'Translational control by eIF2alpha kinases in long-lasting synaptic plasticity and long-term memory', *Neurobiol Learn Mem*, 105: 93-9.

Twiss, J. L., D. S. Smith, B. Chang, and E. M. Shooter. 2000. 'Translational control of ribosomal protein L4 mRNA is required for rapid neurite regeneration', *Neurobiol Dis*, 7: 416-28.

Veeramah, K. R., L. Johnstone, T. M. Karafet, D. Wolf, R. Sprissler, J. Salogiannis, A. Barth-Maron, M. E. Greenberg, T. Stuhlmann, S. Weinert, T. J. Jentsch, M. Pazzi, L. L. Restifo, D. Talwar, R. P. Erickson, and M. F. Hammer. 2013. 'Exome sequencing reveals new causal mutations in children with epileptic encephalopathies', *Epilepsia*, 54: 1270-81.

Vester, A., G. Velez-Ruiz, H. M. McLaughlin, Nisc Comparative Sequencing Program, J. R. Lupski, K. Talbot, J. M. Vance, S. Zuchner, R. H. Roda, K. H. Fischbeck, L. G. Biesecker, G. Nicholson, A. A. Beg, and A. Antonellis. 2013. 'A loss-of-function variant in the human histidyl-tRNA synthetase (HARS) gene is neurotoxic in vivo', *Hum Mutat*, 34: 191-9.

Vo, M. N., M. Terrey, J. W. Lee, B. Roy, J. J. Moresco, L. Sun, H. Fu, Q. Liu, T. G. Weber, J. R. Yates, 3rd, K. Fredrick, P. Schimmel, and S. L. Ackerman. 2018. 'ANKRD16 prevents neuron loss caused by an editing-defective tRNA synthetase', *Nature*, 557: 510-15.

Vo, T., A. Paul, A. Kumar, D. W. Boykin, and W. D. Wilson. 2019. 'Biosensor-surface plasmon resonance: A strategy to help establish a new generation RNA-specific small molecules', *Methods*.

Wang, E. T., J. M. Taliaferro, J. A. Lee, I. P. Sudhakaran, W. Rossoll, C. Gross, K. R. Moss, and G. J. Bassell. 2016. 'Dysregulation of mRNA Localization and Translation in Genetic Disease', *J Neurosci*, 36: 11418-26.

Wang, X., K. L. Engisch, Y. Li, M. J. Pinter, T. C. Cope, and M. M. Rich. 2004. 'Decreased synaptic activity shifts the calcium dependence of release at the mammalian neuromuscular junction in vivo', *J Neurosci*, 24: 10687-92.

Wang, X., Y. Li, K. L. Engisch, S. T. Nakanishi, S. E. Dodson, G. W. Miller, T. C. Cope, M. J. Pinter, and M. M. Rich. 2005. 'Activity-dependent presynaptic regulation of quantal size at the mammalian neuromuscular junction in vivo', *J Neurosci*, 25: 343-51.

Wang, X., Q. Wang, K. L. Engisch, and M. M. Rich. 2010. 'Activity-dependent regulation of the binomial parameters p and n at the mouse neuromuscular junction in vivo', *Journal of neurophysiology*, 104: 2352-8.

Wei, N., Q. Zhang, and X. L. Yang. 2019. 'Neurodegenerative Charcot-Marie-Tooth disease as a case study to decipher novel functions of aminoacyl-tRNA synthetases', *J Biol Chem*, 294: 5321-39.

Weiss, P., and H. B. Hiscoe. 1948. 'Experiments on the mechanism of nerve growth', *J Exp Zool*, 107: 315-95.

Weterman, M. A. J., M. Kuo, S. B. Kenter, S. Gordillo, D. W. Karjosukarso, R. Takase, M. Bronk, S. Oprescu, F. van Ruissen, R. J. W. Witteveen, H. M. E. Bienfait, M. Breuning, C. Verhamme, Y. M. Hou, M. de Visser, A. Antonellis, and F. Baas. 2018. 'Hypermorphic and hypomorphic AARS alleles in patients with CMT2N expand clinical and molecular heterogeneities', *Hum Mol Genet*, 27: 4036-50.

Williams, J., S. Osvath, T. F. Khong, M. Pearse, and D. Power. 1995. 'Cloning, sequencing and bacterial expression of human glycine tRNA synthetase', *Nucleic acids research*, 23: 1307-10.

Willis, D., K. W. Li, J. Q. Zheng, J. H. Chang, A. B. Smit, T. Kelly, T. T. Merianda, J. Sylvester, J. van Minnen, and J. L. Twiss. 2005. 'Differential transport and local translation of cytoskeletal, injury-response, and neurodegeneration protein mRNAs in axons', *J Neurosci*, 25: 778-91.

Wu, K. Y., U. Hengst, L. J. Cox, E. Z. Macosko, A. Jeromin, E. R. Urquhart, and S. R. Jaffrey. 2005. 'Local translation of RhoA regulates growth cone collapse', *Nature*, 436: 1020-24.

Xie, W., L. A. Nangle, W. Zhang, P. Schimmel, and X. L. Yang. 2007. 'Long-range structural effects of a Charcot-Marie-Tooth disease-causing mutation in human glycyl-tRNA synthetase', *Proc Natl Acad Sci U S A*, 104: 9976-81.

Xing, L., and G. J. Bassell. 2013. 'mRNA localization: an orchestration of assembly, traffic and synthesis', *Traffic*, 14: 2-14.

Zhang, H. L., T. Eom, Y. Oleynikov, S. M. Shenoy, D. A. Liebelt, J. B. Dictenberg, R. H. Singer, and G. J. Bassell. 2001. 'Neurotrophin-induced transport of a beta-actin mRNP complex increases beta-actin levels and stimulates growth cone motility', *Neuron*, 31: 261-75.

Zhang, H. L., R. H. Singer, and G. J. Bassell. 1999. 'Neurotrophin regulation of beta-actin mRNA and protein localization within growth cones', *J Cell Biol*, 147: 59-70.

Zhang, X., B. Meister, R. Elde, V. M. Verge, and T. Hokfelt. 1993. 'Large calibre primary afferent neurons projecting to the gracile nucleus express neuropeptide Y after sciatic nerve lesions: an immunohistochemical and in situ hybridization study in rats', *Eur J Neurosci*, 5: 1510-9.

Zhang, Xh, and M. M. Poo. 2002. 'Localized synaptic potentiation by BDNF requires local protein synthesis in the developing axon', *Neuron*, 36: 675-88.

Zheng, J. Q., T. K. Kelly, B. Chang, S. Ryazantsev, A. K. Rajasekaran, K. C. Martin, and J. L. Twiss. 2001. 'A functional role for intra-axonal protein synthesis during axonal regeneration from adult sensory neurons', *J Neurosci*, 21: 9291-303.

Zheng, J. Q., J. J. Wan, and M. M. Poo. 1996. 'Essential role of filopodia in chemotropic turning of nerve growth cone induced by a glutamate gradient', *J Neurosci*, 16: 1140-9.

Zuchner, S., I. V. Mersiyanova, M. Muglia, N. Bissar-Tadmouri, J. Rochelle, E. L. Dadali, M. Zappia, E. Nelis, A. Patitucci, J. Senderek, Y. Parman, O. Evgrafov, P. D. Jonghe, Y. Takahashi, S. Tsuji, M. A. Pericak-Vance, A. Quattrone, E. Battaloglu, A. V. Polyakov, V. Timmerman, J. M. Schroder, and J. M. Vance. 2004. 'Mutations in the mitochondrial GTPase mitofusin 2 cause Charcot-Marie-Tooth neuropathy type 2A', *Nature genetics*, 36: 449-51.

Zucker, R. S., and W. G. Regehr. 2002. 'Short-term synaptic plasticity', *Annu Rev Physiol*, 64: 355-405.

APPENDIX A: CHAPTER 2: MATERIALS & METHODS

Mice: The mice used in these experiments were obtained from research colonies maintained at The Jackson Laboratory (Bar Harbor, ME). The two strains of *Gars* mutant mice are established models of CMT2D and are described in several previous publications (Achilli et al. 2009b; Motley et al. 2011a; Seburn et al. 2006; Stum et al.). Briefly, one strain of mice (CAST;B6-*Gars*^{Nmf249}/JRwb; Stock# 17540 (Seburn et al. 2006) carry a spontaneous dominant mutation (insertion) that results in a P to KY substitutions at amino acid 278 of the GlyRS protein. These mice hereafter referred to as *Gars*^{P278KY}; develop overt disease symptoms by 2-3 weeks of age. A second strain of mice (C3H.C-*Gars*^{C201R}/H) (Achilli et al. 2009b) carry an ENU-induced dominant point mutation that causes a cysteine to arginine substitution at residue 201 of the GlyRS protein. These mice (hereafter *Gars*^{C201R}) have a qualitatively similar, but generally milder CMT2D phenotype. Both *Gars*^{P278KY} and *Gars*^{C201R} mutant strains are routinely maintained by mating heterozygous male mutant mice to female wild-type mice. For these experiments additional matings were set up using female mice homozygous for a transgene expressing yellow fluorescent protein (B6.Cg-Tg(Thy1-YFP)16Jrs/J; Stock# 3709, hereafter YFP16) (Feng et al. 2000). Litters from these matings produced the necessary controls (YFP16;*Gars*$^{+/+}$) as well as either YFP16;*Gars*^{P278KY} or YFP16;*Gars*^{C201R}. Colonies of *Gars* mice also carrying the YFP transgene have been maintained for several years and neither the onset nor lifespan of either strain has changed. In addition, results of analyses performed on these mice are in good agreement with our previous results on mutants that did not carry the YFP transgene. All mice were maintained in the same vivarium on a 12:12 light/dark cycle and were provided food and water *ad libitum*. Care and procedures were reviewed for compliance and approved by the Animal Care and Use Committee of The Jackson Laboratory.

NMJ immunohistochemistry and analysis of innervation status: CMT2D mice had been crossed to mice carrying the transgene for yellow fluorescent protein that allowed visualization

of the presynaptic nerve (see Mice above for details). Thus, for analysis, the LAL muscle was removed and placed in 2% paraformaldehyde for 15 minutes and then rinsed three times in PBS. Finally, to visualize postsynaptic acetylcholine receptors (AChRs) on the muscle cell surface, muscles were incubated with α-bungarotoxin conjugated with Alexa Fluor 594 (NMJ only) or 647 (NMJ costaining with Bassoon, see below) (1/2000)(Molecular Probes) in cold PBS containing 2% BSA, 2% normal goat serum, and 0.1% Triton for 20 minutes. Muscles were then examined by fluorescent microscopy (Nikon E6000) at a magnification of 63X. In each muscle 100 NMJs were randomly viewed and classified as described previously (e.g (Seburn et al. 2006)). Junctions where the nerve completely overlapped the AChRs on the muscle were defined as fully occupied, those with a portion of receptors clearly vacated by the presynaptic nerve were defined as partially occupied, and those with AChR plaques that had no associated nerve were defined as denervated.

Bassoon staining and quantification of release sites: Muscles were prepared, and pre- and postsynaptic components of the NMJ were visualized, as described above. Immunohistochemistry followed a published protocol (Nishimune 2012). In addition, muscles were incubated overnight with a mouse primary antibody against the active zone protein Bassoon (1/1000) (SAP7F407; Enzo Life Sciences) and fluorescently conjugated secondary (Zenon® Alexa Fluor® 568 Mouse IgG2a, Life Technol. Cat#Z2506). Images were collected as Z-series using a Leica SP5 confocal microscope. Bassoon-stained active zones were quantified using 3D reconstructions (Imaris v. 7.4.2, Bitplane) of NMJs. Using this software each NMJ was reconstructed and then evaluated empirically by rotating and examining the 3-D image from pre- and postsynaptic perspectives to determine that the reconstruction matched the actual staining. Briefly, for each image, the postsynaptic receptor area was rendered by smoothing and thresholding using background subtraction based on local contrast. The result was then filtered based on a minimal voxel size to eliminate any artifactual staining not associated with the

terminal area. The volume and surface area of the rendered volume were determined by the software. Puncta stained with bassoon were identified and counted in a three step process. First, it was determined on wild-type NMJs that a background subtraction that eliminated "spots" with a diameter greater than 0.250μm eliminated the majority of extra-junctional "puncta". For each image this result was then filtered to include only spots above a fixed intensity at the center of the spot. Finally, the spots needed to associate with the pre-synaptic side, within the perimeter defined by postsynaptic staining. The intensities used for filtering were determined empirically for each image by thresholding the appropriate channel and noting the value giving the best representation of visible staining.

Muscle preparation and voltage-clamp: Mice were anesthetized with isoflurane (2%, 300 ml/min) to remove intact the LAL muscle. This flat muscle controls the movement of the ear and is a well-characterized mixed fiber type muscle (Angaut-Petit et al. 1987). Muscles were placed immediately in a specially designed recording chamber and pinned onto the silastic such that solution could flow freely across the tissue on both sides. The recording chamber was perfused continuously with Ringer's solution comprised of (in mmol/l): 118 NaCl, 3.5 KCl, 2 CaCl2, 0.7 MgSO4, 26.2 NaHCO3, 1.7 NaH2PO4, and 5.5 glucose, and equilibrated with 95%O2/5%CO2 to maintain a pH of 7.3–7.4. The solution was at room temperature (20–22°C) for all experiments. Voltage clamp experiments followed previously described methods (Rich et al. 2002; Wang et al. 2004; Wang et al. 2005). Once the muscle was pinned the tissue was stained by the addition of 4-(4-diethylaminostyryl)-*N*-methylpyridinium iodide (4-Di-2ASP) (Magrassi, Purves, and Lichtman 1987) at a concentration of ~2μM for 2.5 minutes. This method provides staining sufficient for visualization of the superficial nerve terminals and the surface of the muscle fibers. A concentric bipolar electrode (FHC, Bowdoin, ME, USA) was placed in contact with the nerve and connected to the stimulator (WPI A360, Sarasota, Fla., USA). Stimulator output was capacitively coupled to the electrode to avoid potential damage

from DC polarizing currents (Guyton and Hambrecht 1974). The preparation was then placed under an upright epifluorescence microscope (Leica DMLFSA). Electrodes (5-10 MΩ) were filled with 3M KCL and 10 ng/ml of sulforhodamine so that the electrode tip could be seen under the microscope. Synapses were located and fibers were impaled within 100 µm of the terminal and voltage clamped to -50 mV. In initial experiments muscle fibers were crushed away from the endplate band to avoid movement induced by nerve stimulation (Glavinovic 1979; Wang et al. 2004; Wang et al. 2005), but in most experiments the muscle-specific sodium-channel blocker (µ-Conotoxin GIIIB, Alomone, Israel)(Cruz et al. 1985; Robitaille and Charlton 1992) was introduced (~1 µM) to eliminate muscle action potentials and contraction.

Wire-hang test: A variation on the wire-hang test (Gomez et al. 1997; Rafael et al. 2000) was used to assess the response to drugs that enhance synaptic function via either pre- or post-synaptic mechanisms. Briefly, mice were placed on a 6”x 9” piece of wire mesh and then the mesh was inverted and held ~6” above the countertop. The latency (seconds) to a fall was timed and recorded, up to a maximum of 1 minute. Tests were performed at approximately the same time each day. Each mouse performed 3 trials in a given session and a rest period of at least 30 s was given between individual trials. To allow the mice time to adjust to the wire hang test and learn how to perform, animals were given at least three consecutive daily practice sessions before drug administration and testing trials.

In drug/vehicle trials, drugs were prepared fresh from frozen stock on each day (in sterile PBS, 0.1mg/kg - physostigmine; 2.5 mg/kg - 3,4 diamino pyridine (DAP) (Sigma, MO, USA). Each mouse performed a pre-injection trial, then was injected intraperitoneally and re-tested 60 minutes later. Mice were dosed three independent times in five days with intervening practice days. The best wire hang score in three trials is reported for that day (three trials/day on three test days). Performance was calculated as pre-injection/post-injection latency-to-fall, expressed

as a percentage. The average percentage difference is calculated from the three independent days of injections.

Data collection and analysis: Custom software was used for collection and analysis of synaptic currents. At each NMJ, spontaneous miniature endplate currents (MEPC) were collected for 1 min. The nerve was then stimulated (0.5 Hz) and 15-20 individual evoked endplate currents (EPC) were recorded. Quantal content was directly calculated by dividing the EPC amplitude by the average MEPC amplitude recorded for each synapse. We used the extent of EPC facilitation/depression during evoked trains(Zucker and Regehr 2002) to indirectly evaluate probability of release following a protocol previously used at the mouse NMJ.(Wang et al. 2010; Kong et al. 2009) We recorded 15-20 responses to a 10-pulse, 50 Hz train delivered to the nerve and 20 responses were recorded. The extent of depression/potentiation was calculated by dividing the averaged amplitude of the 10^{th} pulse by the 1^{st} pulse.

Electron microscopy: For electron microscopy, muscles were processed as described.(Burgess, Cox, and Seburn 2010) In brief, muscles were fixed in 2% paraformaldehyde, 2% glutaraldehyde in 0.1M cacodylate buffer. The endplate-containing region was isolated and embedded and sectioned for transmission electromicroscopy. Seventy-five nm plastic sections were mounted on grids and viewed using a Jeol 1230 electron microscope equipped with a Hamamatsu digital camera system for image collection.

Statistics: Unless otherwise noted averaged numbers are reported as mean ± standard error (s.e.). We used a nested ANOVA (using animal as a random factor) for genotype/age comparisons of electrophysiology, active zones and vesicle data. This statistic controls for animal-to-animal variation and the effect of taking small samples to represent a larger population. We also evaluated interactions for 2 and 4 month electrophysiology data using a standard 2-way ANOVA (genotype by age), but the results did not modify any conclusions so results derived from the more appropriate nested design are reported. A Students *t*-test was

used for comparison of wire-hang and quantal content comparison of 70 Hz voltage clamp data. In all cases the statistical cutoff for declaring a significant difference was $p<0.05$.

APPENDIX B: Chapter 3: Supplemental Data

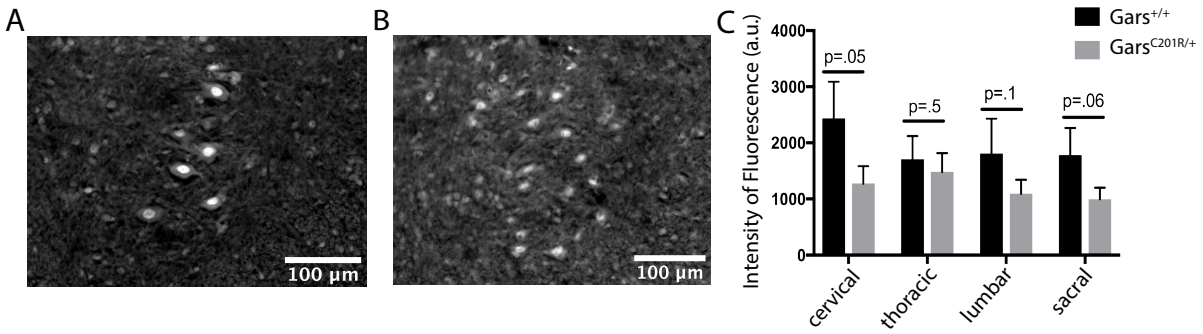

Figure 18: Translation in pre-disease onset *Gars*$^{C201R/+}$ motor neurons. (A) *Gars*$^{+/+}$ and (B) *Gars*$^{C201R/+}$ motor neurons of the cervical spinal cord labeled with ANL. (C) Translation is slightly reduced in all *Gars*$^{C201R/+}$ motor neuron populations compared to *Gars*$^{+/+}$, but does not reach statistical significance. Analysis was performed on 3 males per genotype at 2 weeks of age. Values in C are a sum of fluorescence intensity from all 3 animals per genotype ± SD.

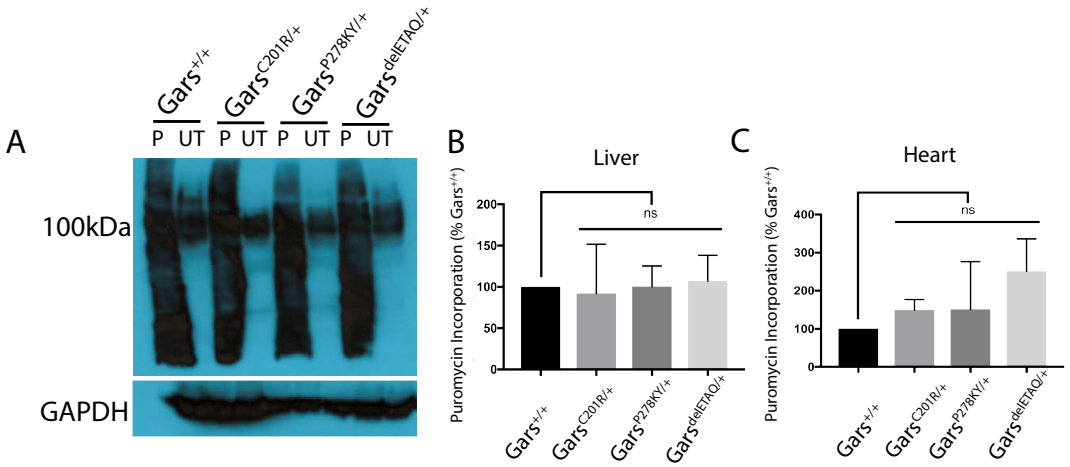

Figure 19. Puromycin labeling in unaffected tissues does not show impaired translation. (A) Representative anti-puromycin blot from liver tissue of *Gars*$^{+/+}$, *Gars*$^{C201R/+}$, *Gars*$^{P278KY/+}$, and *Gars*$^{delETAQ/+}$ mice. (B-C) Intensity of puromycin-labeled protein smear is scaled to GAPDH loading control and compared to *Gars*$^{+/+}$. Puromycin incorporation is not decreased in the liver (B) or heart (C) of any mutant *Gars* models. Analysis was performed on 3 animals per genotype at 8 weeks of age. Values in B and C are mean ± SD.

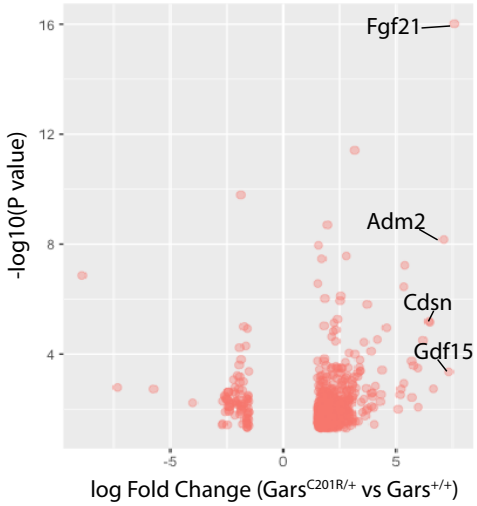

Figure 20: Disease signature is present in *Gars*$^{C201R/+}$ motor neurons pre-disease onset. Ribosome-associated mRNA in *Gars*$^{C201R/+}$ motor neurons compared to *Gars*$^{+/+}$. 643 genes were upregulated (log FC>1.5; p value<.05) and 107 were downregulated (log FC<-1.5; p value<.05). Analysis was performed on 5-6 animals per genotype at 2 weeks of age.

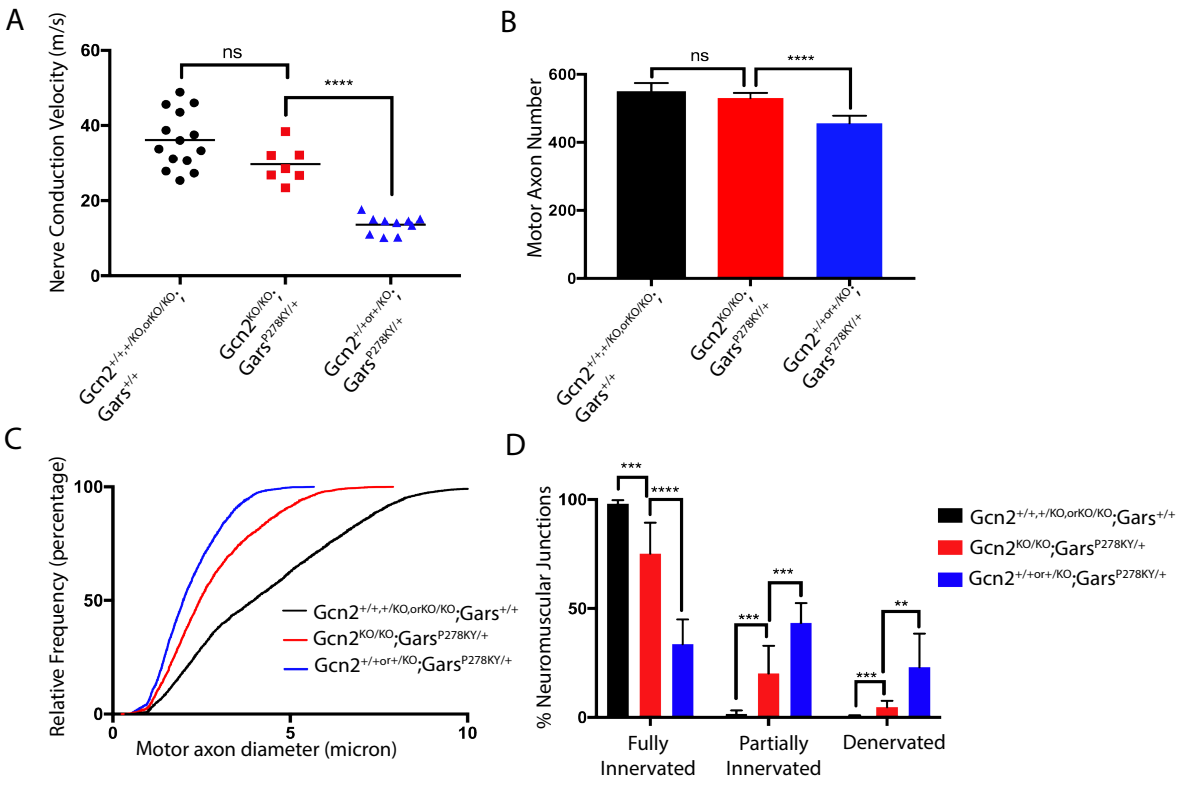

Figure 21: Genetic removal of GCN2 kinase continues to alleviate CMT2D neuropathy through 16 weeks of age. (A) Conduction velocity of the sciatic nerve is increased in *Gcn2*$^{KO/KO}$;*Gars*$^{P278KY/+}$ mice (29.7m/s ± 4.9) compared to *Gcn2*$^{+/+\ or\ +/KO}$;*Gars*$^{P278KY/+}$ (13.6m/s ± 2.4), and no longer statistically different from *Gcn2*$^{+/+,+/KO,\ or\ KO/KO}$;*Gars*$^{+/+}$ (36m/s ± 7.6). (B) The average number of motor axons in the femoral nerve of 16 week old *Gcn2*$^{KO/KO}$;*Gars*$^{P278KY/+}$ mice is greater (530 ± 15 axons) compared to *Gcn2*$^{+/+\ or\ +/KO}$;*Gars*$^{P278KY/+}$ (456 ± 22 axons). *Gcn2*$^{KO/KO}$;*Gars*$^{P278KY/+}$ axon counts are no longer statistically significant from *Gcn2*$^{+/+,+/KO,\ or\ KO/KO}$;*Gars*$^{+/+}$ mice (550 ± 24 axons). (C) The relative frequency of larger fiber axons is increased in 16 week old *Gcn2*$^{KO/KO}$;*Gars*$^{P278KY/+}$ mice compared to *Gcn2*$^{+/+\ or\ +/KO}$;*Gars*$^{P278KY/+}$, as shown by the shift of the red trace towards the right of the blue trace. (D) A greater percentage of NMJs are fully innervated in 16 week old *Gcn2*$^{KO/KO}$;*Gars*$^{P278KY/+}$ (75.2% ± 14.2) mice compared to (33.6% ± 11.4) *Gcn2*$^{+/+\ or\ +/KO}$;*Gars*$^{P278KY/+}$. A smaller percentage of partially innervated (20.2% ± 12.7) and denervated (4.7% ± 2.9) NMJs are observed in *Gcn2*$^{KO/KO}$;*Gars*$^{P278KY/+}$ mice compared to *Gcn2*$^{+/+\ or\ +/KO}$;*Gars*$^{P278KY/+}$ (43.4% ± 9.1 and 23% ± 15.4).

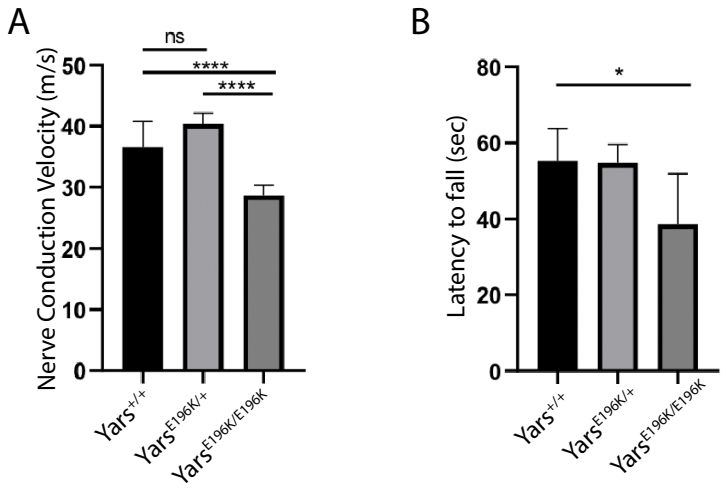

Figure 22: *Yars*$^{E196K/YarsE196K}$ mice show signs of neuropathy at 7 months of age. (A) At 7 months of age *Yars*$^{+/+}$ mice have a sciatic nerve conduction velocity of 36.6 ± 4.2m/s. *Yars*$^{E196K/+}$ mice have a conduction velocity well in the wild-type range at 40.3 ± 1.9 m/s, but *Yars*$^{E196K/YarsE196K}$ mice have a reduced conduction velocity of 28.7 ± 1.7m/s. (B) *Yars*$^{E196K/E196K}$ have impaired motor function at 7 months of age, as demonstrated by decreased latency to fall on the wire hang test. *Yars*$^{+/+}$ mice hang on to an inverted grid for an average of 55.3 ± 8.5 seconds, *Yars*$^{E196K/+}$ for an average of 54.7 ± 5.0 seconds, and *Yars*$^{E196K/YarsE196K}$ for an average of 38.6 ± 13.3 seconds. Nerve conduction analysis was performed with 6-10 animals per genotype. Wire hang analysis was performed with 3-9 animals per genotype. Values in A and B are mean ± SD. *= p<.05; ****=p<.0001.

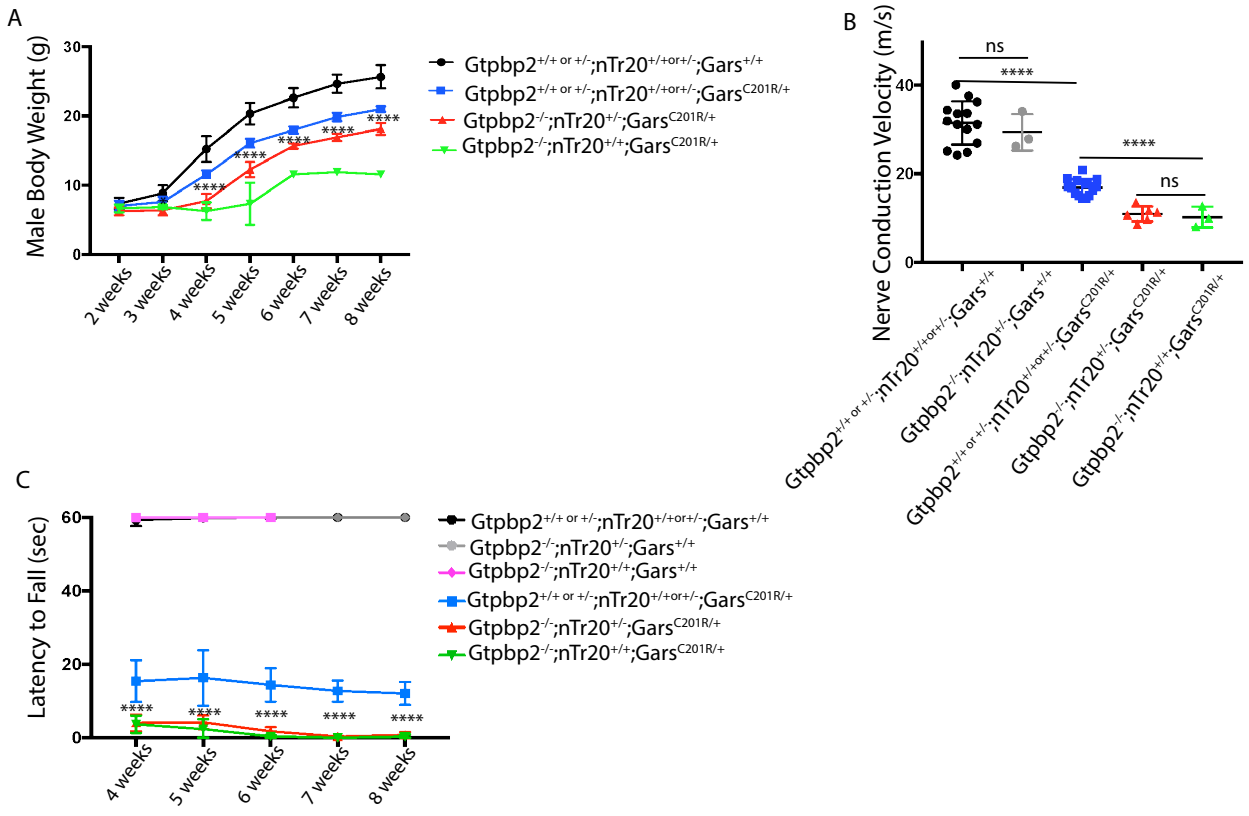

Figure 23: Mutations in the ribosome recycling factor, Gtpbp2, exacerbate *Gars$^{C201R/+}$* neuropathy. (A) *Gtpbp2$^{-/-}$;nTr20$^{+/-}$;Gars$^{C201R/+}$* mice have reduced body weight compared to *Gtpbp2$^{+/+\ or\ +/-}$;nTr20$^{+/-}$;Gars$^{C201R/+}$* mice starting at 3 weeks of age. Preliminary measurements in *Gtpbp2$^{-/-}$;nTr20$^{+/+}$;Gars$^{C201R/+}$* mice suggest that body weight will be further decreased by the developing cerebellar ataxia around 6 weeks of age. Analysis performed with 1-22 mice per genotype. (B) Conduction velocity of the sciatic nerve is decreased in *Gtpbp2$^{+/+\ or\ +/-}$;nTr20$^{+/-}$;Gars$^{C201R/+}$* (10.92 m/s ± 1.7) mice at 8 weeks of age compared to *Gtpbp2$^{-/-}$;nTr20$^{+/-}$;Gars$^{C201R/+}$* (31.44m/s ± 4.88), but not further reduced in *Gtpbp2$^{-/-}$;nTr20$^{+/+}$;Gars$^{C201R/+}$* mice (10.2m/s ± 2.4). Analysis performed with 3-14 mice per genotype. (C) *Gtpbp2$^{-/-}$;nTr20$^{+/-}$;Gars$^{C201R/+}$* and *Gtpbp2$^{-/-}$;nTr20$^{+/+}$;Gars$^{C201R/+}$* mice have decreased latency to fall compared to *Gtpbp2$^{+/+\ or\ +/-}$;nTr20$^{+/-}$;Gars$^{C201R/+}$*. Analysis performed with 1-22 mice per genotype. Values in A and C are mean ± SD. *= p<.05; ****= p<.0001.

APPENDIX C: CHAPTER 3: MATERIALS & METHODS

Mice: The mice used in these experiments were obtained from research colonies maintained at The Jackson Laboratory (Bar Harbor, ME). The two strains of *Gars* mutant mice are established models of CMT2D and are described in several previous publications (Achilli et al. 2009b; Motley et al. 2011a; Seburn et al. 2006; Stum et al.). Briefly, one strain of mice (CAST;B6-*Gars*^{Nmf249}/JRwb; Stock# 17540 (Seburn et al. 2006) carry a spontaneous dominant mutation (insertion) that results in a P to KY substitutions at amino acid 278 of the GlyRS protein. These mice hereafter referred to as *Gars*^{P278KY}; develop overt disease symptoms by 2-3 weeks of age. A second strain of mice (C3H.C-*Gars*^{C201R}/H) (Achilli et al. 2009b, 2009a) carry an ENU-induced dominant point mutation that causes a cysteine to arginine substitution at residue 201 of the GlyRS protein. These mice (hereafter *Gars*^{C201R}) have a qualitatively similar, but generally milder CMT2D phenotype. Both *Gars*^{P278KY} and *Gars*^{C201R} mutant strains are routinely maintained by mating heterozygous male mutant mice to female wild-type mice. *GarsdelETAQ* mice contain a 12 base pair deletion in exon 8 of the Gars gene that results in a four amino acid deletion. The phenotype of these mice is similar the the previously described *Gars* models and intermediate in severity. Other mice used include the ChAT-IRES-Cre knock-in mice (B6;129S6-Chat<tm2(cre)Lowl>/J;Stock# 006410), the RiboTag mice (B6N.129-Rpl22<tm1.1Psam>/J;Stock# 011029), the FUNCAT mice (C57BL/6-Gt(ROSA)26Sor<tm1(CAG-GFP,-Mars*L274G)Esm/J;Stock# 028071, the nmf205 mutant mouse (C57BL/6J-Gtpbp2<nmf205>/J; Stock#004823) (Ishimura et al. 2014), the nTr20 congenic mouse (B6J.B6N-n-Trtct5<C57BL/6N/SlacCx; private colony) (Ishimura et al. 2014), GCN2 knockout mice (B6.129S6-Eif2ak4<tm1.2Dron>/J; Stock# 008240), and YarsE196K mice (private colony; submitted manuscript). All mice were maintained in the same vivarium on a 12:12 light/dark cycle and were provided food and water *ad libitum*. Care and procedures were reviewed for compliance and approved by the Animal Care and Use Committee of The Jackson Laboratory

Fluorescent non-canonical amino acid-tagging (FUNCAT): Mice were injected intraperitoneally with 400mg/kg body weight ANL (Jena Bioscience) dissolved in deionized water and made fresh on the day of use. After 8 hours mice were anesthetized and perfused with cold 4% paraformaldehyde-4% sucrose. The entire spinal column was removed and post-fixed on ice for 1 hour. Columns were moved to phosphate buffered saline (PBS) and kept at 4^{o}C until dissection. Spinal cords were dissected free from vertebrae, embedded in optimum cutting temperature (OCT) (VWR), frozen in cold 2-methyl butane, and kept at -80^{o}C until sectioning. 12um cryosections were dried for 1 hour and blocked in B Block (Tom Dieck et al. 2012) for 1.5 hours at room temperature. After washing with the slides PBS, the FUNCAT reaction was assembled (5ml freshly diluted PBS, pH7.8; 5ul 200uM Tris[(1-benzyl-1H-1,2,3 triazol-4-yl) methyl] amine (TBTA) (Sigma); 5ul 500mM Tris (2-carboxyethyl) phosphine hydrochloride (TCEP) (Sigma); 1ul 2mM alkyne-conjugated Alexa 594 (Thermo Fisher); and 5ul 200mM $CuSO_4$ (Sigma)) and quickly applied to the slides. Slides were incubated in the reaction mix overnight at room temperature with gentle agitation and protection from light. Slides were washed with FUNCAT wash buffer (Tom Dieck et al. 2012) and then PBS, and cover slips were mounted using DAKO fluorescent media (Agilent). Single plane images of both ventral horns from at least 3 sections of each region of the spinal cord per mouse were taken at 20x magnification on either a Leica SP5 confocal microscope or a Nikon Eclipse 600 with DIC-Nomarski optics. Fluorescence intensity was measured in Fiji/ImageJ. Using a circle of constant area that would fit within all sizes of motor neurons, intensity of every motor neuron per section was measured and the background fluorescence from 3 adjacent spots was subtracted. The average fluorescence intensity of each region of the spinal cord per mouse was calculated. To avoid arbitrary pair-wise comparisons, total fluorescence from all mice was summed for each region of the spinal cord.

Puromycin labeling: Mice were injected intraperitoneally with freshly opened Puromycin dihydrochoride (Life Technologies) at a dose of 60mg/kg body weight. Untreated controls were injected with HEPES buffer. After 1 hour mice were euthanized and tissues were snap frozen in liquid nitrogen. Tissues were homogenized in PBS;1% NP40 with Complete protease inhibitor (Sigma). Samples were sonicated for 20 seconds at 18 Watts, spun down at 15,000g for 10 minutes at 4°C, and the resulting supernatant was diluted 1:1 in Laemmli buffer. Samples were gently boiled for 30 seconds to denature native IgG. After electrophoretic protein separation using 4-15% Mini-Protean TGX Precast Gels (Bio-Rad) and transfer to an Invitrolon & Immobilon-P PVDF membrane, the membrane was blocked in Tris Buffered Saline with Tween 20 (TBST) containing 5% nonfat dry milk for 30 minutes at room temperature. Mouse anti-puromycin clone 12D10 (Millipore MABE343) was applied at a concentration of 1:5000 in milk overnight at 4°C. The membrane was washed in 3 times for 10 minutes each in TBST and anti-mouse IgG Veriblot HRP (Abcam, ab131368) secondary anitbody was applied at a concentration of 1:1000 in milk for 1 hour at room temperature. The membrane was washed in 3 times for 10 minutes each in TBST and developed using Pierce ECL Western Blotting Substrate (Thermo Scientific). Blots were then stripped and re-probed with 1:1000 rabbit anti-mouse GAPDH (Sigma). Relative intensities of puromycin-labeled protein smears were measured in Fiji/ImageJ and scaled to GAPDH. Because some untreated animals showed significant non-specific signals at 100kDa and above, only the portion of the smear below 100kDa was used for the analysis.

Ribosome-tagging: Our protocol was adapted from the University of Washington McKnight Lab Protocol (http://depts.washington.edu/mcklab/RiboTag.html). All buffer recipes can be found here and were made fresh on the day of use. All equipment used was made RNAse-free by spraying with RNase-Zap RNase decontamination solution (Thermo Fisher) and rinsing with diethyl pyrocarbonate (DEPC) (Sigma)-treated water. All reagents were made RNAse-free by

treating with 1:1000 DEPC overnight and autoclaving. Mice were euthanized and spinal cords were removed within 1-2 minutes and snap frozen in liquid nitrogen. Samples were stored at -80°C until use. Spinal cords were homogenized on dry ice using the Cryogrinder (POS Diagnostics) until a fine powder. Powder was then transferred to a 2ml dounce homogenizer on ice and homogenized further in 1ml supplemented homogenization buffer. Sample was transferred to a 1.5ml tube, sonicated for 20 seconds at 18 Watts, and centrifuged at 4°C at 10,000 g for 10 minutes. Supernatant was transferred to a new 1.5ml tube and 50ul of washed Protein G Sepharose 4 Fast Flow beads (GE Life Sciences) were added and incubated for 1 hour at 4°C with continuous mixing. Samples were centrifuged at 5,000 g for 30 seconds at room temperature to pellet beads. Supernatant was removed and added to 50ul of supplemented homogenization buffer containing 2ul Rabbit anti-HA antibody (4ul if first diluted in glycerol) (Sigma H6908). Samples were continuously mixed at 4°C for 4 hours. Magnetic Protein G Dynabeads (Thermo Fisher) were washed in supplemented homogenization buffer for 15 minutes at 4°C with continuous mixing. Wash was removed and antibody-tissue homogenates were added to the Dynabeads and allowed to incubate at 4°C overnight with continuous mixing. The following day beads are washed with 800ul of high salt buffer 3 times for 10 minutes each at 4°C with continuous mixing. 350ul lysis buffer was added to the samples immediately after the final high salt wash and vortexed for 30 seconds. Samples were placed on a magnetic rack and supernatant transferred to a new tube. Directions in the RNeasy Micro kit (Qiagen) were then followed exactly, starting with adding 350ul 70% ethanol to each sample. RNA was eluted in 14ul RNase-free water and stored at -80°C until sequencing.

Sequencing was analyzed using our standard Mouse Paired End RNASeq Analysis pipeline. The pipeline uses RSEM which aligns input reads against a reference transcriptome with Bowtie and calculates expression values using the alignments and summarizes the alignment metrics along with gene names and normalization values. We then loaded the short reads into R using the Rsamtools package and counted the number of reads overlapping an annotated collection

of genes. Once transformed, the number of reads were counted that overlap genes, in each experimental condition, for each replicate. Next we combined them into a table of counts. We then chose to use the scaling factor normalization method in edgeR as it preserves the count nature of the data and has been shown to be an effective means of improving DE detection. We calculated the normalization factors using the TMM method and then created a DGE object used by edgeR. The scaling factor calculated using the TMM method is incorporated into the statistical test by weighting the library sizes by the normalization factors (which are then used as an offset in the statistical model). To perform the statistical test for significance, we first estimated the common dispersion parameter. Finally, we calculated the p-values for genes being DE tested=exactTest(disp). Constrained Regression Recalibration (ConReg-R) was used to recalibrate the empirical p-values by modeling their distribution to improve the FDR estimates.

Unilateral sciatic nerve crush surgeries: Mice were anesthetized with isofluorane and placed on a heating pad to maintain body temperature. Opthalmic ointment was placed over the eyes and .5mg/ml carprofen was administered through subcutaneous injection at a dose of .1ul/10g body weight. Hair was removed from the leg and the mouse was moved to a sterile surgical area. The area of skin to be cut was cleaned with 70% ethanol and chlorhexidine diluted 1:256 in water. A 1-2mm incision was made in the skin directly below the femur. Connective tissue is gently cleared away with forceps and the sciatic nerve is identified. The nerve was crushed with forceps for 10 seconds, released, and crushed once more for 10 seconds. The incision site is sutured and 1-2 drops of 2.5 mg/ml bupivacaine is administered to the wound site. Mouse is placed in a warmed cage and monitored until it returns to consciousness.

RNA sequencing: Mice were euthanized and spinal cords were immediately removed and snap frozen in liquid nitrogen. See RiboTagging protocol for analysis methods.

RNAscope in situ hybridization: Spinal cord: Mice were euthanized with CO2 and decapitated. Spinal cords were removed immediately with hydraulic extrusion. Spinal cords were trimmed and a few millimeters of lumbar spinal cord was frozen on aluminum foil on dry ice. Dorsal root ganglia: Mice were euthanized using cervical dislocation and the entire vertebral column was excised. The column was cut open and lumbar ganglia were removed and immediately frozen on aluminum foil on dry ice. Spinal cord pieces or dorsal root ganglia were placed in a cryomold filled with OCT and frozen on dry ice. Blocks were kept in an air-tight plastic bag at -80°C until sectioning. 12um cryosections were taken using a new box of Colorfrost Plus Slides (Fisher Scientific) and kept in an air tight bag at -80°C until further use. From this point, instructions in the RNAscope user manual for fresh frozen tissue (document number 320513) and then for the Fluorescent Multiplex Reagent Kit (document number 320291) were followed exactly. As many as three transcripts were multiplexed at one time, and probe sequences were designed by RNAscope. Single plane images were taken on a Zeiss 2 Axioimager at 20x magnification and fluorescence was quantified as described above for FUNCAT experiments.

NMJ immunohistochemistry and analysis of innervation status: The entire gastrocnemius muscle was removed and placed in 4% paraformaldehyde for 1 hour and then rinsed once in PBS. The soleus and plantaris muscles were then dissected free, flattened between two slides for 30 minutes in blocking solution (2% BSA in PBST), and blocked for an additional hour at room temperature. To visualize postsynaptic acetylcholine receptors (AChRs) on the muscle cell surface, muscles were incubated with α-bungarotoxin conjugated with Alexa Fluor 594 (NMJ only) (1: 1000) (Molecular Probes) in blocking solution for 1 hour at room temperature. To visualize the nerves, the tissue was treated with a cocktail of the following antibodies: 1:500 mouse anti-neurofilament (Sigma) and 1:250 mouse anti-SV2 (DSHB) in block overnight at 4◦C. Muscles were then viewed at 40x magnification on a Nikon Eclipse 600 with DIC- Nomarski

optics. In each muscle 100 NMJs were randomly viewed and classified as described previously (e.g (Seburn et al. 2006)). Junctions where the nerve completely overlapped the AChRs on the muscle were defined as fully occupied, those with a portion of receptors clearly vacated by the presynaptic nerve were defined as partially occupied, and those with AChR plaques that had no associated nerve were defined as denervated.

Axon Histology: The femoral nerves, which include both a motor and sensory branch (Scherer et al., 2005) were dissected free and fixed by immersion in 2% paraformaldehyde, 2% glutaraldehyde in 0.1M cacodylate buffer for 12 hours. Nerves were then plastic embedded, sectioned at 0.5 microns thickness, and stained with Toluidine Blue. Images were collected at 40X magnification on a Nikon Eclipse 600 microscope with DIC- Nomarski optics. Images were analyzed for axon number using an automated method in Fiji/ImageJ that was manually confirmed by visual inspection of images for mis- identified axons. Axon diameter and myelin thickness were measured in Fiji/ImageJ with the Measure & Label Plug-in.

Nerve conduction velocity: Nerve conduction velocity of motor and sensory axons of the sciatic nerve was measured. Mice were anaesthetized with 2% isofluorane and placed on a thermostatically regulated heating pad to maintain body temperature. Action potentials were produced by placing stimuli proximally at the sciatic notch and a pair distally at the ankle. When the proximal node was stimulated, the impulse traveled down the motor branch to the muscle. Compound motor action potential (CMAP), which is the summation of action potentials from a group of stimulated muscle fibers, was measured, as well as latency for the impulse to reach both proximal and distal stimuli. NCV was calculated as [conduction distance/(proximal latency-distal latency)] (Seburn et al., 2006).

Wire Hang Test: A variation on the wire-hang test (Gomez et al. 1997; Rafael et al. 2000) was used to assess motor function starting at 4 weeks of age. Briefly, mice were placed on a 6”x 9”

piece of wire mesh and then the mesh was inverted and held ~6” above a box filled with shavings. The latency (seconds) to a fall was timed and recorded, up to a maximum of 1 minute. Each mouse performed 3 trials in a given session and a rest period of at least 30 s was given between individual trials.

Statistics: All averaged numbers are reported at mean ± standard deviation (SD). For all experiments except for RiboTagging or RNA sequencing, all pairs of genotypes were tested using a Students *t*-test. In all cases the statistical cutoff for declaring a significant difference was $p<.05$.

BIOGRAPHY OF THE AUTHOR

Emily Louisa Spaulding was born in Rockport, Maine on September 14th, 1983. She was raised in Rockland, Maine and graduated from Rockland District High School in 2001. She attended Gordon College in Wenham, Massachusetts and graduated in 2005 with a Bachelor of Science in Biology. After finishing her degree, she enrolled in a Master of Secondary Science Education program at Gordon College and taught high school biology at Hamilton-Wenham Regional High School. She continued taking classes towards her Master's degree while teaching high school biology, chemistry, and physics at Bangor Christian Schools in Bangor, Maine. She received her Master of Secondary Science Education degree in 2010 and enrolled in the University of Maine Graduate School of Biomedical Sciences and Engineering in 2013. She performed her thesis research at The Jackson Laboratory under the mentorship of Dr. Robert Burgess. She is a candidate for the Doctorate of Philosophy degree in Biomedical Science from the University of Maine in December 2019.